Journal of Baku Engineering University Physics

BAKU ENGINEERING UNIVERSITY

ISSN 2521-6368

Volume 2
Number 2
2018

Journal of Baku Engineering University

PHYSICS

Journal is published twice a year
Number - 1. June, Number - 2. December

An International Journal

http://journal.beu.edu.az

Contact address

Journal of Baku Engineering University
AZ0102, Khirdalan city, Hasan Aliyev str. 120, Absheron, Baku, Azerbaijan
***Tel:** 00 994 12 - 349 99 95 **Fax:** 00 994 12 349-99-90/91*

e-mail: *jr-phisics@beu.edu.az*
web: *http://journal.beu.edu.az*
facebook: *Journal Of Baku Engineering University*

ISSN 2521-6368

ISSN 2521-6368

Journal of Baku Engineering University

PHYSICS

Baku - AZERBAIJAN

Journal of Baku Engineering University

PHYSICS

2018. Volume 2, Number 2

CONTENTS

JOURNAL OF BAKU ENGINEERING UNIVERSITY - PHYSICS
2018. Volume 2, Number 2 *Pages 87-94*

UOT: 538.97;539.216.2;539.23
PACS: 73.61.W; 78.66.T; 81.15; 61.16.B; 84.37

CHARACTERIZATION OF Co_3O_4 THIN FILMS SYNTHESIZED BY SILAR METHOD

S.J. MAMMADYAROVA[A*], M.B. MURADOV[A], A.M. MAHARRAMOV[B], G.M. EYVAZOVA[A], Z.A. AGHAMALIYEV[A], O.O. BALAYEVA[B]

[a] Department of Physics, Baku State University, Z.Khalilov str.,23, AZ-1148 Baku, AZERBAIJAN

[b] Department of Chemistry, Baku State University, Z.Khalilov str.,23, AZ-1148 Baku, AZERBAIJAN

[*]*Corresponding author: Sevinc.memmedyarova@inbox.ru (S.J.Mammadyarova).*

ABSTRACT

Co_3O_4 thin films were synthesized on glass and silica substrates for various cycles by using a simple chemical method-successive ionic layer adsorption reaction (SILAR). The reaction was carried out at room temperature. Thin films were prepared using cobalt acetate tetrahydrate [$Co(CH_3COO)_2{\cdot}4H_2O$] as a cobalt ion source and hydrogen peroxide (H_2O_2) as anionic precursor. The synthesized samples were characterized by X-ray diffraction (XRD), energy dispersive X-ray analysis (EDAX), Fourier transform infrared spectroscopy (FTIR), Scanning electron microscopy (SEM) and UV-Visible spectroscopy. It has been determined that as-synthesized films were cobalt oxyhydroxide [CoO(OH)]. Cobalt oxide (Co_3O_4) is formed after thermal annealing of CoO(OH) thin film at 300ºC.

Keywords: cobalt oxide, thin film, optical band gap.

SİLAR METODU İLƏ SINTEZ OLUNMUŞ CO_3O_4 NAZIK TƏBƏQƏLƏRININ XARAKTERISTIKASI.

XÜLASƏ

Kobalt oksid nazik təbəqələri şüşə və silisium altlıqlar üzərində sadə üsulla- ardıcıl ion layının adsorbsiyası və reaksiyası ilə müxtəlif saylı tsikllərdə sintez olunmuşdur. Reaksiya otaq temperaturunda həyata keçirilmiş və kobalt duzu mənbəyi kimi kobalt asetat tetrahidratdan [$Co(CH_3COO)_2{\cdot}4H_2O$], anion prekursor kimi isə hidrogen peroksiddən (H_2O_2) istifadə olunmuşdur. Alınan təbəqələr rentgen difraksiya, enerji dispersləşdirici rentgen spektroskopiya (EDS), infraqırmızı spektroskopiya (İQ), skanedici elektron mikroskopu (SEM) və ultrabənövşəyi spektroskopiya (UB) metodları ilə tədqiq olunmuşdur. Müəyyən edilmişdir ki, çökdürülən zaman təbəqələr kobalt oksihidroksiddən [CoO(OH)] ibarət olmuşdur. [CoO(OH)] nazik təbəqələrinin 300ºC-də termiki emalından sonra isə kobalt oksid formalaşmışdır.

Açar sözlər: kobalt oksid, nazik təbəqə, qadağan olunmuş zonanın eni.

ХАРАКТЕРИСТИКА ТОНКИХ ПЛЕНОК CO_3O_4 ПОЛУЧЕННЫХ МЕТОДОМ SİLAR.

РЕЗЮМЕ

Методом последовательной адсорбции и реакции ионного слоя на стеклянной и кремний подложки были синтезированы тонкие пленки оксида кобальта с различными циклами формирования. Реакцию проводили при комнатной температуре и как прекурсор кобальта использовали тетрагидрат ацетата кобальта [$Co(CH_3COO)_2{\cdot}4H_2O$], а как прекурсор аниона перекись водорода (H_2O_2). Пленки исследовались с помощью рентгеновской дифрактометрии, энергодисперсионной рентгеновской спектроскопии, инфракрасный спектроскопии, сканирующий электронный микроскоп и ультрафиолетовой спектроскопии. Установлено, что при осаждении полученные пленки представляют собой метагидроксида кобальта [CoO(OH)]. Оксид кобальта (Co_3O_4) образуется после термического отжига тонкой пленки CoO(OH) при 300 °C.

Ключевые слова: оксид кобальта, тонкий слой, ширина запрещенной зоны.

1. Introduction

In recent years, nanostructured metal oxides have been widely used in various fields. Among transition metal oxides cobalt oxide is of great importance due to its electronic, chemical and magnetic properties. Cobalt oxide is a p-type antiferromagnetic oxide semiconductor

Manuscript receved 08.07.2018

with two band gaps. It has two different modifications namely as CoO and Co_3O_4. Co_3O_4 is mixed valence compound (CoO and Co_2O_3) and adopts the normal spinel crystal structure. It is a promising candidate for diverse applications like gas sensors [1], supercapacitors [2], lithium-ion batteries [3], catalysts [4], electrochromic devices [5], solar absorbing material [6], magnetic materials [7] and etc. To date, Co_3O_4 thin films were synthesized on polycrystalline or amorphous substrates by different methods such as chemical bath deposition [8, 9], reactive electron beam evaporation [10], spray pyrolysis [11, 12], pulsed laser deposition [13], radio frequency (RF) magnetron sputtering [14], electrodeposition [15], sol–gel spin coating technique [16] and SILAR [17]. Cobalt oxide with different morphologies such as wires, cubes, fibers, tubes, sheets, flowers [18-23] have been reported in literature. It is possible to change properties of the particles by control size and morphology. Kung et al. [24] synthesized Co_3O_4 thin films with different morphologies depending on the anions of the cobalt sources used and the electrodes with these films were applied for the detection of acetaminophen. Wang et al. [25] prepared Co_3O_4 nanoparticles by using $Co(NO_3)_3{\cdot}6H_2O$, NaOH as starting materials and cetyltrimethylammonium bromide (CTAB) as surfactant. Moreover, a single step solution precursor plasma spray technique was proposed to deposite Co_3O_4 films for supercapacitor applications by Tummala et al.[26]. Cobalt oxyhydroxide [CoO(OH)] is a nonstoichiometric oxyhydroxide and it is known as catalysts for the oxygen evolution reaction [27]. Liu et al. [28] synthesized CoO(OH) film by electrochemical oxidation of $Co(OH)_2$ at 95ºC in 1 M KOH. Nanostructured CoO(OH) film was also applied as supercapacitor [29]. SILAR is a very simple method among the synthesis methods of metal oxide nanoparticles. It is possible to control the thickness of films and nanoparticle sizes by using this method [30]. For this reason, we selected this method.

In the present work, cobalt oxide thin films have been deposited by SILAR method on glass and silicon wafer substrates. The effect of different substrates, various cycles and concentration of oxidizing agent on the structural and optical properties have been investigated.

2. Experimental

Before the growth process, the glass substrate were cleaned in dilute HCl solution for 10 min and then rinsed in distilled water. Then the substrates were rinsed in ethanol acetone (1:1) mixture, distilled water and finally dried in oven at 100°C. The silicon substrate was etched in hydrofluoric acid (HF) solution for 10 min to remove native silicon dioxide from wafers, then washed thoroughly with distilled water. Cobalt oxide films were deposited from the cationic precursor of 0.5 M cobalt acetate [Co $(CH_3COO)_2{\cdot}4H_2O$] complex with 1 M sodium hydroxide solution to make pH ~12 and H_2O_2 (1% and 3%) was used as anionic precursor. Previously cleaned substrates were immersed vertically in the alkaline cobalt acetate solution for 30 s, where cobalt complex adsorbed on the substrate. Then substrates with the cobalt complex are then immersed in H_2O_2 for 30 s and the reaction occurred on the surface forming cobalt oxyhydroxide. This process forms one cycle and was repeated 60 times in order to increase the film thickness. Finally, the deposited films were annealed in air at 300°C for 3 h to transform the oxyhydroxide phase to the oxide.

The structural analysis of the synthesized oxide thin films was analyzed by Rigaku Mini Flex 600 X-ray diffractometer (λ = 1.54060 Å) using Ni-filtered Cu Ka radiation. Optical properties of the films were investigated by Specord 250 Plus UV-vis Spectrophotometer using Integrating Sphere. FTIR measurement has been conducted within 400-4000 cm^{-1} region on a

Varian 3600 FTIR spectrometer. The morphology and element composition spectra of samples were obtained on JEOL JSM- 7600F scanning electron microscopy (SEM) and Xmax 50 energy-dispersive X-ray spectroscopy (EDX), respectively.

3. Results

3.1 Thin film formation

At room temperature dipping the substrates in the beaker containing cobalt acetate and sodium hydroxide solution for 30 s causes a cobalt hydroxide to adsorb on the substrate due to attractive forces between ions in the solution and surface of the substrates. The chemical reactions can be represented with the following equations [9, 17]:

$$[Co(H_2O)_6]^{2+} + 2NaOH \rightarrow Co(OH)_2 + 2Na^+ + 6H_2O \quad (1)$$

The substrates is then immediately immersed in a H_2O_2 solution and at this time cobalt hydroxide converts into cobalt oxyhydroxide by the reaction (2):

$$2Co(OH)_2 + H_2O_2 \rightarrow 2CoO(OH)\cdot H_2O \quad (2)$$

After annealing in air at 300ºC, the brown color of the cobalt oxyhydroxide turned into black, indicating that the oxide is formed.

$$12CoO(OH) \rightarrow 4Co_3O_4 + O_2 + 6H_2O \quad (3)$$

3.2 Structural analysis

Fig.1 and Fig.2 show the XRD patterns of as-prepared and annealed films deposited on glass substrate for different deposition cycles.

Fig.1. XRD patterns of CoO(OH) (a) and Co_3O_4 films (b) deposited on glass substrates using 1% H_2O_2. 1- 40 cycles; 2 – 60 cycles ; 3 – 80 cycles ; 4-100 cycles; 5 – 120 cycles

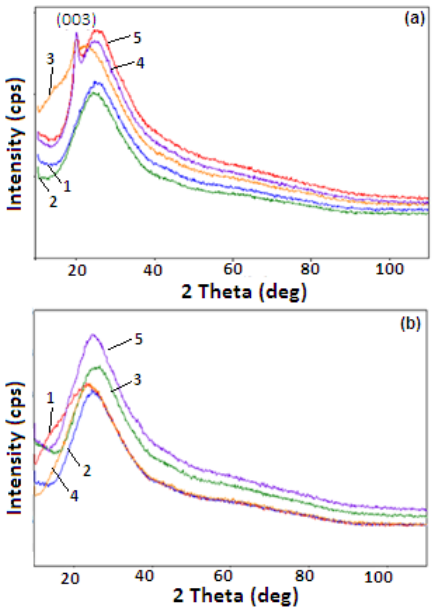

The diffraction peak at 2θ equal to 20º corresponds to (003) plane as compared with standard X-ray diffraction data file JCPDS (file No.14-0673). This revealed that as-synthesized films are consist of polycrystalline cobalt oxyhydroxide [CoO(OH)] particles. The broad hump originates from the diffraction of amorphous glass substrate. No peaks corresponding

to cobalt oxide were observed after annealing in air at 300ºC. It means that the cobalt oxide film showed amorphous nature, similar to S.G. Kandalkar et.al [17]. They synthesized Co_3O_4 thin film on copper substrate with amorphous nature by SILAR method using $CoCl_2 \cdot 6H_2O$ as a cobalt salt source. In other studies [9], they synthesized the amorphous cobalt oxyhydroxide films on glass and copper substrates using chemical bath deposition method, after thermal treatment at 350°C, they obtained low crystalline Co_3O_4 films. Fig.3 shows the XRD patterns of as-prepared and annealed films deposited on silicon substrates for 60 cycles. The several peaks observed in the diffractograms. The peaks observed at 2θ=14.37º, 17.17º, 28.44º for as-prepared samples using 3% H_2O_2 corresponds to silicon substrate. The peak was also observed at 2θ=20.02º (for sample using 3% H_2O_2) and 2θ=20.22º (for sample using 1% H_2O_2) similar to results of samples synthesized on glass substrates. The low intensity peaks appeared at 2θ=19.26º, 36.98º and at 2θ=39.546º, 59.16º after thermal annealing of samples prepared on silicon substrate using 1% and 3% H_2O_2, respectively. This result is consistent with the respective JCPDS (card No. 65-3103). It shows that the formed Co_3O_4 is low cristalline. This can be explained by the fact that the glass is amorphous and amorphous oxide is formed on it.

Fig. 2. XRD patterns of CoO(OH) (a) and Co_3O_4 films (b) deposited on glass substrates using 3% H_2O_2. 1- 40 cycles; 2 – 60 cycles ; 3 – 80 cycles ; 4-100 cycles; 5 – 120 cycles

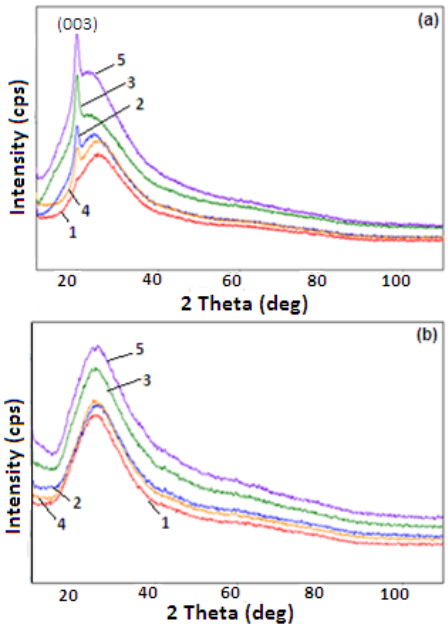

Fig. 3. XRD patterns of CoO(OH) (1) and Co_3O_4 (2) films deposited on silicon substrates using (a) 3% H_2O_2 and (b) 1% H_2O_2

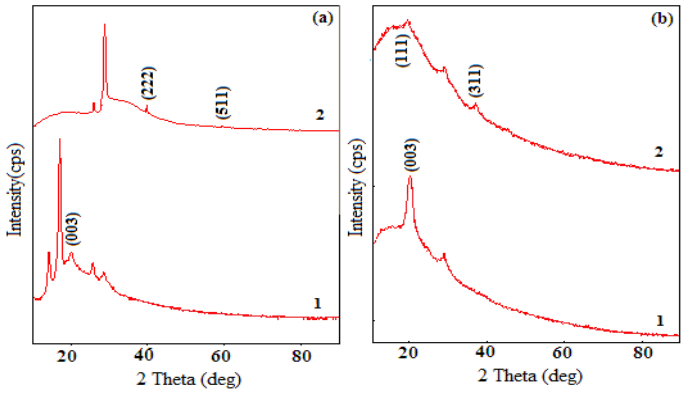

3.3 Optical properties

The Co_3O_4 thin films on glass substrate were used to study the optical absorption. The optical absorption of Co_3O_4 thin films in the wavelength range of 300 nm-800 nm has been investigated. Extrapolation of the linear portion to zero absorption coefficients gives the values of the optical band gap energy. The optical band gap can be calculated by the following equation:

$$\alpha h\nu = B\,(h\nu - E_g)^n \quad (4)$$

where, α is the absorption coefficient, $h\nu$ is the photon energy, B is a constant relative to the material, E_g is the band gap, and n is either 2 for an indirect transition or 1/2 for a direct transition. Fig. 4 shows the variation of $(ah\nu)^2$ versus $(h\nu)$ for samples. The direct optical band gaps of Co_3O_4 samples synthesized on glass substrate by using 1% H_2O_2 for 60 and 120 cycles are 2.1 eV and 3,26 eV; 1.94 eV and 2.50 eV respectively. The band gaps of Co_3O_4 samples synthesized by using 3% H_2O_2 for 60 and 120 cycles are 1.89 eV and 3.24 eV; 1.90 eV and 2.17 eV respectively. The presence of two band gaps can be attributed ligand–metal charge transfer events: $O^{2-} \rightarrow Co^{3+}$ (E_{g1}) and $O^{2-} \rightarrow Co^{2+}$ (E_{g2}). [23, 31, 32] The decrease in E_g with increasing of concentration of oxidizing agent could be due to increase in particle size. For samples synthesized on silicon substrate by using 1% and 3% H_2O_2 (60 cycles) band gap energy was calculated as 1.38 and 1.63 eV. The optical band gaps of Co_3O_4 nanorods synthesized by hydrothermal method have been determined as 1.28 and 2.34eV by Wang et al. [31]

Fig. 4 $(ah\nu)^2$ versus $(h\nu)$ for Co_3O_4 thin films on glass substrate synthesized by using 1% H_2O_2 (60 cycles (a1) and 120 cycles (b1)); 3% H_2O_2 (60 cycles (a2) and 120 cycles (b2)); and films synthesized on silicon substrate for 60 cycles by using (c1)-1% H_2O_2, (c2)-3% H_2O_2

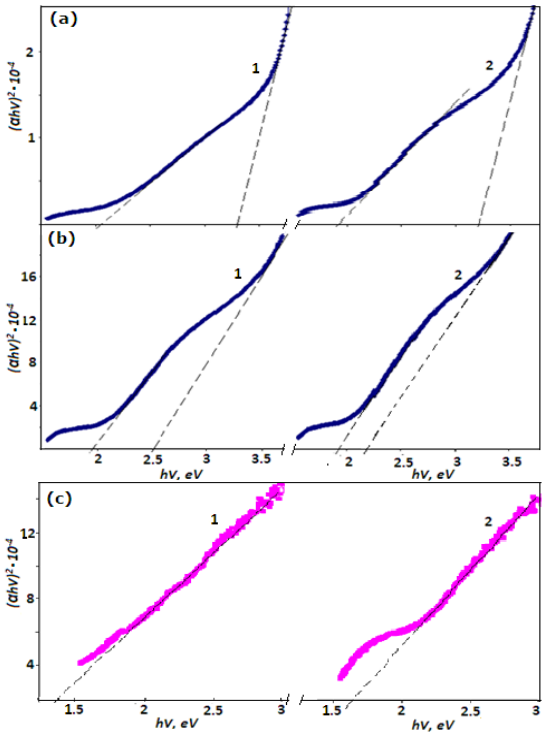

3.4 FT-IR studies

The IR transmittance spectrum of cobalt oxide thin films in the range 400–4000 cm^{-1} is shown in Fig. 5. The bands at 546.402 and 669.951 cm^{-1} for sample synthesized on glass substrate, 556.980 and 658.509 cm^{-1} for sample synthesized on silicon substrate using 3% H_2O_2 (60 cycles). The band

at about 669.951 and 658.509 cm^{-1} is attributed to the stretching vibration mode of metal-oxygen, in which Co is Co^{2+} and is tetrahedral coordinated. The bands observed at 546.402 and 556.980 cm^{-1} can be characteristic to Co-O of octahedral coordinated Co^{3+}. [21]

Fig. 5 FT-IR spectrum of Co_3O_4 thin films synthesized on (1) glass and (2) silicon substrates using 3% H_2O_2

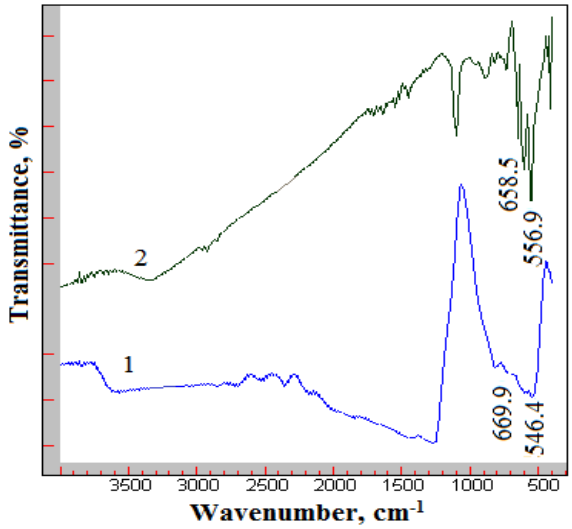

3.5 SEM and EDX

The surface morphology of the thin films was studied by scanning electron microscopy technique. Fig. 6 shows the SEM image of Co_3O_4 film synthesized on glass substrate for 120 cycles using 3% H_2O_2 at low magnification (× 10.000). It is seen that thin film consists of fine elongated particles with some pores among particles. Porous structure among the particles indicates that synthesized thin films can be applied as supercapacitor.

Energy dispersive X-ray spectrometry (EDX) analysis was employed to determine the composition of the Co_3O_4. EDX spectrum of sample synthesized on glass substrate for 120 cycles using 3% H_2O_2 shows that the experimental atomic percentages of Co, O and Si are found to be 14%, 58% and 19.5% respectively. If we take into account the oxygen contained in the glass (SiO_2), it is near to the theoretical ratio (3:4) of Co_3O_4.

Fig. 6 SEM image of Co_3O_4 film synthesized on glass substrate using 3% H_2O_2 (120 cycles).

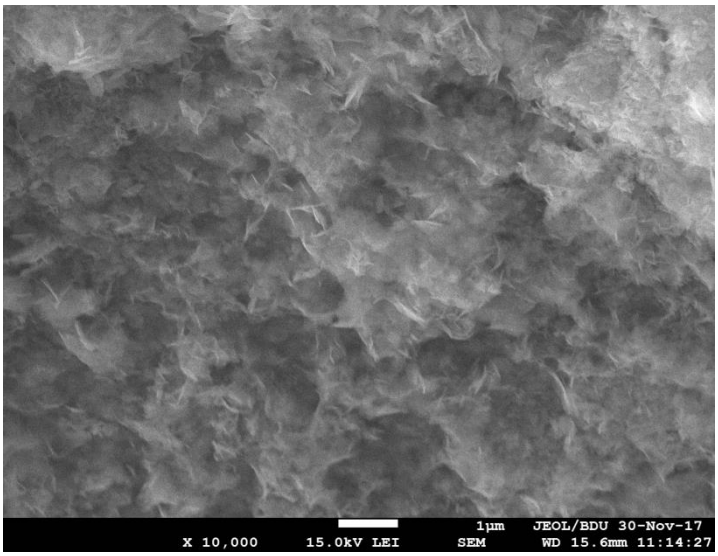

Fig. 7 EDX spectrum of deposited Co_3O_4 film synthesized on glass substrate using 3% H_2O_2 (120 cycles).

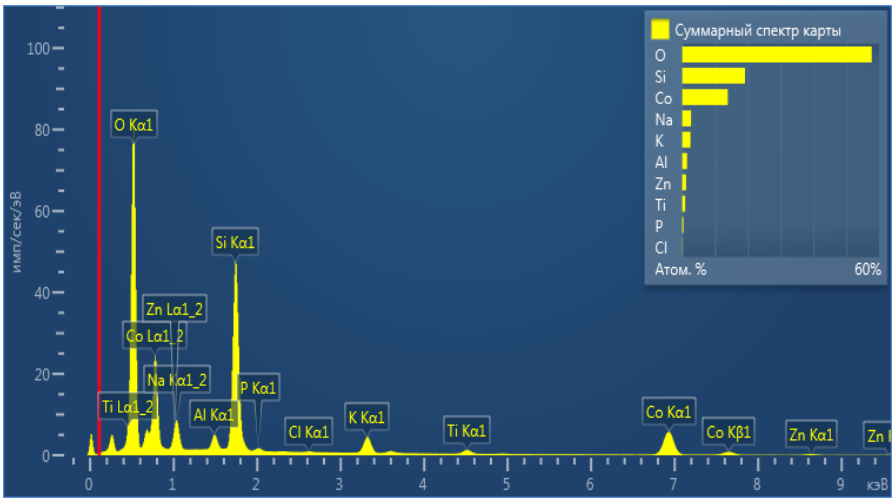

Conclusions

In the present study, Co_3O_4 thin films were synthesized by SILAR method and the effect of different substrates, various cycles and concentration of oxidizing agent on growth process have been investigated. It has been determined that in the initial stage CoO(OH) is formed, after the samples are subjected to thermal treatment at 300°C CoO (OH) is converted to Co_3O_4. EDX and FT-IR analysis also confirm that the composition of the film is Co_3O_4. It is observed two band gaps from optical studies for thin films synthesized on glass substrates. It is explained with the structure of cobalt oxide. For samples synthesized on glass substrates the band gap energy decreases with increasing of concentration of oxidizing agent due to increase in particle size.

REFERENCES

[1] S.Vetter, S.Haffer, T.Wagner, M.Tiemann. *Nanostructured Co_3O_4 as a CO gas sensor: Temperature-dependent behavior*, Sensors and Actuators B: Chemical, Vol.206, p.133-138, 2015

[2] M. Vezvaie, P. Kalisvaart, H. Fritzsche and et al., *The Penetration Depth of Chemical Reactions in a Thin-Film Co_3O_4 Supercapacitor Electrode*, Journal of The Electrochemical Society, Vol.161, No.5, p.A798-A802, 2014

[3] M.Xu, F.Wang, M.Zhao and et al., *Molten hydroxides synthesis of hierarchical cobalt oxide nanostructure and its application as anode material for lithium ion batteries,* Electrochimica Acta, Vol.56, p.4876–4881, 2011

[4] B.Ronan, C.Gregory, V. Sabine. *Sonochemical oxidation of vanillyl alcohol to vanillin in the presence of a cobalt oxide catalyst under mild conditions*, Ultrasonics Sonochemistry, Vol.36, p.27–35, 2017

[5] L. Wang, X.C. Song, Y.F. Zheng. *Electrochromic properties of nanoporous Co_3O_4 thin films prepared by electrodeposition method*, Micro & Nano Letters, IET, Vol.7, p.1026-1029, 2012

[6] J. Moon, T.Kim, B.VanSaders and et al., *Black oxide nanoparticles as durable solar absorbing material for high-temperature concentrating solar power system*, Solar Energy Materials&Solar Cells, Vol.134, p.417–424, 2015

[7] A. M. Salah. *Magnetic properties of Co_3O_4 nanoparticles*, Journal of Magnetism and Magnetic Materials, Vol.246, p.184–190, 2002

[8] Y. Li, K. Huang, Z. Yao, S. Liu, and et al., *Co_3O_4 thin film prepared by a chemical bath deposition for electrochemical capacitors*, Electrochimica Acta, Vol.56, p.2140–2144, 2011

[9] S.G.Kandalkar, J.L.Gunjakar, C.D.Lokhande, and et al., *Synthesis of cobalt oxide interconnected flacks and nano-worms structures using low temperature chemical bath deposition*, Journal of Alloys and Compounds, Vol.478, p.594–598, 2009

[10] J. Wöllenstein, M. Burgmair, G. Plescher and et al., *Cobalt Oxide Based Gas Sensors on Silicon Substrate for Operation at Low Temperatures*, Sensors and Actuators B, Vol.93, p.442–448, 2003

[11] A.Louardi, A.Rmili, T.Chtouki, and et al., *Effect of annealing treatment on Co_3O_4 thin films properties prepared by spray pyrolysis*, JMES, Vol.8, p.485-493, 2017

[12] V.R.Shinde, S.B.Mahadik, T.P.Gujar, and et al., *Supercapacitive cobalt oxide (Co_3O_4) thin films by spray pyrolysis*, Applied Surface Science, Vol.252, p.7487–7492, 2006

[13] Z.Fu, Y.Wang, Y.Zhang, Q.Qin. *Electrochemical reaction of nanocrystalline Co_3O_4 thin film with Lithium*, Solid State Ionics, Vol.170, p.105–109, 2004

[14] C.L. Liao, Y.H. Lee, S.T. Chang, K.Z. Fung. *Structural characterization and electrochemical properties of RF-sputtered nanocrystalline Co_3O_4 thin-film anode*, Journal of Power Sources, Vol.158, p.1379–1385, 2006

[15] I.G. Casella. *Electrodeposition of cobalt oxide films from carbonate solutions containing Co (II)–tartrate complexes*, J. Electroanal. Chem., Vol. 520, p.119-125, 2002

[16] S.Valanarasu, V.Dhanasekaran, M.Karunakaran, and et al., *Role of solution pH on the microstructural properties of spin coated cobalt oxide thin films*, Journal of Nanoscience and Nanotechnology, Vol.14, p.4286–4291, 2014

[17] S.G.Kandalkar, J.L.Gunjakar, C.D.Lokhande. *Preparation of cobalt oxide thin films and its use in supercapacitor application*, Applied Surface Science, Vol.254, p.5540–5544, 2008

[18] X.Shi, S.Han, R.J. Sanedrin, F.Zhou and et al., *Synthesis of Cobalt Oxide Nanotubes from Colloidal Particles Modified with a Co(III)-Cysteinato Precursor*, Chem. Mater., Vol.14, p.1897-1902, 2002

[19] Y.Ding, Y.Wang, L.Su. *Electrospun Co_3O_4 nanofibers for sensitive and selective glucose detection*, Biosensors and Bioelectronics, Vol.26, p.542–548, 2010

[20] D. Vickers, L.A. Archer, T. Floyd-Smith. *Synthesis and characterization of cubic cobalt oxide nanocomposite fluids*, Colloids and Surfaces A: Physicochem. Eng. Aspects, Vol. 348, p.39–44, 2009

[21] T.Ozkaya, A.Baykal, M.S.Toprak and et al., *Reflux synthesis of Co_3O_4 nanoparticles and its magnetic characterization*, Journal of Magnetism and Magnetic Materials, Vol.321, p.2145–2149, 2009

[22] K.D.Bhatte, B.M.Bhanage, *Synthesis of cobalt oxide nanowires using a glycerol thermal route*, Materials Letters, Vol. 96, p.60–62, 2013

[23] Y.Zhang, Y.Chen, T.Wang and et al., *Synthesis and magnetic properties of nanoporous Co_3O_4 nanoflowers*, Microporous and Mesoporous Materials, Vol.114, p.257–261, 2008

[24] C.Kung, C.Lin, R. Vittal, K.Ho, *Synthesis of cobalt oxide thin films in the presence of various anions and their application for the detection of acetaminophen*, Sensors and Actuators B, Vol.182, p.429– 438, 2013

[25] Y.Wang, J.Shi, J.Cao, G.Sun, Z.Zhang, *Synthesis of Co_3O_4 nanoparticles via the CTAB-assisted method,* Materials Letters, Vol.65, p.222–224, 2011

[26] R.Tummala, R.K.Guduru, P.S.Mohanty. *Nanostructured Co_3O_4 electrodes for supercapacitor applications from plasma spray technique*, Journal of Power Sources, Vol. 209, p.44– 51, 2012

[27] Z.Chen, C.X. Kronawitter, Y.Yeh. *Activity of pure and transition metal-modified CoOOH for the oxygen evolution reaction in an alkaline medium*, J. Mater. Chem. A, Vol.5, p.842-850, 2017

[28] Y.Liu, J.A. Koza, J.A. Switzer. *Conversion of electrodeposited $Co(OH)_2$to CoOOH and Co_3O_4, andcomparison of their catalytic activity for the oxygen evolution reaction,* Electrochimica Acta, Vol.140, p.359–365, 2014

[29] M.Wang, W.Ren, Y.Zhao and et al., *Synthesis of nanostructured CoOOH film with high electrochemical performance for application in supercapacitor*, J Nanopart Res., Vol.16, p.1-7, 2014

[30] M.B.Muradov, G.M.Eyvazova, E.Y.Malikov, O.O.Balayeva. *Formation of the copper sulfide nanoparticles by ion exchange from electrolyte solutions*, IJISET - International Journal of Innovative Science, Engineering & Technology, Vol.1, p.352-360, 2014

[31] W.Guoxiu, Sh.Xiaoping, H.Josip and et al., *Hydrothermal Synthesis and Optical, Magnetic, and Supercapacitance Properties of Nanoporous Cobalt Oxide Nanorods*, J. Phys. Chem. C, Vol.113, p.4357–4361, 2009

[32] S.A.Makhlouf, Z.H.Bakr, K.I.Aly and et al., *Structural, electrical and optical properties of Co_3O_4 nanoparticles*, Superlattices and Microstructures, Vol.64, p.107–117, 2013

JOURNAL OF BAKU ENGINEERING UNIVERSITY - PHYSICS
2018. Volume 2, Number 2 *Pages 95-102*

UOT:534
PACS:71.23.-k

RADIATION OF A SEMICONDUCTOR WITH DEEP TRAPS IN AN EXTERNAL ELECTRIC FIELD

[1.2] E.R.GASANOV, [2]R.K.MUSTAFAEVA, [1]V.M.HAJIEVA, [1]E.B.MAHARRAMOV

Institute of Physics of the National Academy of Sciences of Azerbaijan
Baku, AZ-1143, G. Javid Ave, 131
Baku State UniversityAZ-1148, Z. Khalilov 23
vefa86haciyeva@gmail.com

ABSTRACT

In semiconductors with specific deep traps, proven, that oscillations of charge carrier and electric field concentrations are excited, in the presence of an external constant electric field. Analytical expressions for the electric field and for the current oscillation frequency are determined in all cases. It is proved that the injection of minority charge carriers through the contacts of the crystal enhances the radiation of the specified semiconductor. Possible occurrence and inductive resistance and capacitance with the same injection of non-primary charge carriers. In all cases, the circuit has a capacitive or inductive resistance. In the above two cases, inductive and capacitive resistance may occur.

Key words: trap, frequency, oscillations, impurity, generation, recombination.

ИЗЛУЧЕНИЕ ПОЛУПРОВОДНИКА С ГЛУБОКИМИ ЛОВУШКАМИ ВО ВНЕШНЕМ ЭЛЕКТРИЧЕСКОМ ПОЛЕ

РЕЗЮМЕ

В полупроводниках с конкретными глубокими ловушками, доказано, что возбуждается колебания концентраций носителей заряда и электрического поля, при наличии внешнего постоянного электрического поля. Определены во всех случаях аналитические выражения для электрического поля и для частоты колебания тока. Доказано, что инжекция неосновных носителей заряда через контактов кристалла усиливает излучение указанного полупроводника. Возможно возникновение и индуктивного сопротивления и емкостного сопротивления при одной и той же инжекции не основных носителей заряда. Во-всех случаях в цепи возникает сопротивление емкостного характера или индуктивного характера. В двух вышеуказанных случаях возможно возникновения сопротивление индуктивного характера и емкостного характера.

Ключевые слова: ловушка, частота, колебания, примесь, генерация, рекомбинация.

XARİCİ ELEKTRİK SAHƏSİNDƏ YERLƏŞƏN DƏRİN TƏLƏLİ YARIMKEÇİRİCİLƏRİN ŞÜALANMASI

XÜLASƏ

Müəyyən dərin tələli yarımkeçiricilərdə elektrik yüklərinin və elektrik sahəsinin rəqslərinin yaranması isbat olunmuşdur. Dörd halda elektrik sahəsinin və rəqsin tezliyinin analitik ifadələri hesablanmışdır. İsbat olunmuşdur ki, qeyri əsas yük daşıyıcıların injeksiyası şüalanmanı gücləndirir. Elektron və deşiklərin konsentrasiyaları şüalanmada müxtəlif nisbətdə iştirak edir. Şüalanma zamanı dövrədə induktiv və tutum xarakterli müqavimət yaranır. İnjeksiyanın eyni qiymətində həm induktiv, həm də tutum müqaviməti yarana bilər. Bütün hallarda, dövrə içində bir capacitive təbiətin və ya induktiv təbiətin müqaviməti var.Yuxarıda göstərilən iki halda, induktiv və kapasitiv müqavimət ola bilər.

Açar sözlər: tələ, tezlik, dalğa, qarışıq, qenerasiya, rekombinasiya.

Many hundreds of papers are devoted to oscillatory phenomena in semiconductors. The appearance of such a large number of works is connected with the possibility of practical application of the phenomenon of current instability in semiconductors to create high-frequency generators, amplifiers and various converters. Various semiconductors are used in the works to explain the various causes of instabilities. In these works it is noted that, the appearance of current oscillations requires the injection of minority charge carriers. However, for current oscillation in

Manuscript receved 19.08.2018

semiconductors, an external electric field effect on charge carriers is necessary. Gann effect has become very popular, due to the special structure of the conduction band of some semiconductor compounds. Appearances in semiconductors of various instabilities, which lead to current fluctuation, bound by impurities in semiconductors. The rate of capture of electrons (or holes) by an impurity center in a semiconductor, depends on the electron energy. The presence of an electric field can increase the energy of electrons, therefore, the capture rate should inflate from the electric field. Consequently, the stationary concentration of electrons in the conduction band may change with increasing electric field. By increasing the electron capture rate with the field, decreases the electron concentration in the conduction band. If the lattice temperature remains constant and there is no impact ionization, then the generation rate does not change with the field and the only result is the drop in electron density. Current oscillations of different origin were observed experimentally with the value of the electric field. Some impurities in the semiconductor create centers, which are able to be in several states (once, twice, etc. positively or negatively charged). For example, gold atoms in germanium can, except the neutral state to be once positively charged and once, twice and three times negatively charged centers. Such impurity centers correspond to several energy levels in the band gap. These energy levels are located at different distances from the bottom of the conduction band (or from the upper edge of the valence band). Depending on the removal of these levels of the valence band (or conduction band), they are called deep. These deep levels can capture electrons or holes, depending on their charge states. As a result of this capture, the number of electrons in the conduction band, the number of holes in the valence band change, and of course, the semiconductor's electrical conductivity also changes. Under various experimental conditions, these deep levels are more or less active. For example, in the experiment [7], active traps were once and twice negatively charged gold centers in germanium. In the presence of an external electric field, electrons (and also holes) receive energy from the electric field of the order of ***eEL***. (e- positive elementary charge). ***E***-value of the electric field, ***l***-length of the electron free path). Therefore, electrons can overcome the Coulomb barrier of a once charged center and become trapped. In addition, due to thermal transfer, electrons can be generated in the conduction band. These generations and recombination's change the number of electrons in the conduction band (and the number of holes in the valence band). In the above listed works in semiconductors with deep traps and with two types of charge carriers (electrons n_-, holes n_+) the conditions for the occurrence of current oscillations were theoretically investigated and the values of frequency and electric field when a current oscillated in an electric circuit was found. We in this theoretical work will indicate that the parameters $\beta_{\pm}^{\gamma}$ depending on the frequency values current oscillations and on the value of the external electric field vary greatly and the conditions for the occurrence of current oscillations depend on the numerical values of the parameters $\beta_{\pm}^{\gamma}$. Thus, several conditions are obtained for radiation above the specified semiconductor.

A model of a semiconductor and the basic equations of the problem

Consider a semiconductor with carriers of both signs, those. electrons n_- and holes n_+ . In addition, in the semiconductor there are negatively charged deep traps with a concentration of N_0 . Of which part N concentration of once negatively charged traps but, N_- concentration of doubly negatively charged traps.

$$N_0 = N + N_0 \quad (1)$$

The continuity equation for electrons in this semiconductor will be:

$$\frac{\partial n_-}{\partial t} + div\vec{j}_- = j_-(0)n_{1_-}N_- - \gamma_-(E)n_-N = \left(\frac{\partial n_-}{\partial t}\right)_{рек} \quad (2)$$

Hereinafter $\vec{j}_{\mp}$ density of electron and hole fluxes $\vec{j}_-(0)$ electron emission coefficient of double negatively charged traps in the absence of an electric field. It is sometimes called the heat generation coefficient, $\gamma_-(E)-$ the electron capture coefficient of singly negatively charged traps in the presence of an electric field. With

E=0, $\gamma_-(E) = \gamma_-(0)$ (3)

Concentration is defined as follows. From the stationarity condition i.

$$\left(\frac{\partial n_-}{\partial t}\right)_{рек} = 0 \text{ will get } n_{1_-} = \frac{n_-^0 N_0}{N_-^0} \quad (4)$$

Flux density j_- (without magnetic field and temperature gradient) is determined by the expression

$$\vec{j}_- = -n_-\mu_-(E)\vec{E} - D_-\nabla n_- \quad (5)$$

Where $\mu_-(E)-$ electron mobility D_- – electron diffusion coefficient. We assume that there is a Einstein relation $D_{\pm} = \frac{T}{e}\mu_{\pm}$ (T-temperature in eras)

The continuity equation for holes will be:

$$\frac{\partial n_+}{\partial t} + div\vec{j}_+ = \gamma_+(E)n_{1_+}N - \gamma_+(0)n_+N_- = \left(\frac{\partial n_+}{\partial t}\right)_{rek} \quad (6)$$

$\gamma_+(E)-$ hole emission coefficient of singly negatively charged traps in the presence of an electric field. $\gamma_+(0)-$ hole capture coefficient of doubly negatively charged traps in the absence of an electric field. In stationary conditions

$$n_{1_+} = \frac{n_+^0 N_-^0}{N_0} \quad (7)$$

The change with time of twice negatively charged traps determines the change of once negatively charged traps. Therefore:

$$\frac{\partial N_-}{\partial t} = \left(\frac{\partial n_+}{\partial t}\right)_{rek} - \left(\frac{\partial n_-}{\partial t}\right)_{rek} \quad (8)$$

In the presence of recombination and generation of current carriers, the quasineutrality condition means that the total current. Does not depend on the coordinates, but depends on the time.

$$div\vec{J} = ediv(\vec{j}_+ - \vec{j}_-) \quad (9)$$

e- elementary positive charge. $\mathcal{J}$- full current.

Under the influence of an external electric field inside the semiconductor, fluctuations in the concentrations of charge carriers and the electric field occur. These vibrations can go out into the

external circuit, i.e. Current oscillations appear in the external circuit and the semiconductor radiation begins. At the beginning of radiation, the wave vector becomes a complex value, and the frequency of oscillation is a real value. To determine the oscillation frequency, it is necessary to calculate the crystal impedance. From the condition that the impedance of the circuit is zero, the frequency of current oscillation in the circuit is determined. To determine the impedance of the crystal, we must determine the electric field from the equations (2,5,7,8). Putting $n_{\pm} = n_{\pm}^0 + \Delta n_{\pm}$, $N_- = N_-^0 + \Delta N_-$, $E = E_0 + \Delta E$ and considering that $\Delta n_{\pm} << n_{\pm}^0$, $N_- << N_-^0$; $\Delta E << E_0$ we linearize (2,5,7,8) and enter below the specified characteristic frequencies, $\nu_- = \gamma_-(E_0)N_0 -$ the frequency of electron capture by single-charged traps, $\nu_+^E = \gamma_+(E_0)N_0 -$ hole emission frequency of double charged traps

$\nu_+^{'} = \gamma_+(0)n_+^0 + \gamma_+(E_0)n_{1_+}$, $\nu_-^{'} = \gamma_-(0)n_{1_-} + \gamma_-(E_0)n_-^0$ -combined frequencies.

$\beta_-^{\gamma} = 2\dfrac{d\ln\gamma_-(E_0)}{d\ln(E_0^2)}$; $\beta_+^{\gamma} = 2\dfrac{d\ln\gamma_+(E_0)}{d\ln(E_0^2)}$; $\beta_{\pm}^{\mu} = 1 + 2\dfrac{d\ln\mu_{\pm}}{d\ln(E_0^2)}$;

Besides $\Delta J \sim e^{-i\omega t}$, $\Delta n_{\pm} = \Delta n_{\pm}^{/} e^{-i\omega t} + \Delta n_{\pm}^{"} e^{i(kx-\omega t)}$, $\Delta E^0 = \Delta E^{/} + \Delta E^{"}$

From linearization we get two systems of equations

$$\begin{aligned} &A_-\Delta n_-^{"} + B_-\Delta E^{"} + C_-\Delta N_-^{"} = 0 \\ &A_+\Delta n_+^{"} + B_+\Delta E^{"} + C_+\Delta N_-^{"} = 0 \end{aligned} \qquad (10).$$

$$\begin{aligned} &\Delta N_-^{"} = R_-\Delta n_-^{"} + R_+\Delta n_+^{"} + r\Delta E^{"} \\ &\Delta E^{"} = \phi_-\Delta n_-^{"} + \phi_+\Delta n_+^{"} \end{aligned} \qquad (11)$$

$$\begin{aligned} &a_-\Delta n_-^{/} + b_-\Delta E^{/} + d_-\Delta N_-^{/} = 0 \\ &a_+\Delta n_+^{/} + b_+\Delta E^{/} + d_+\Delta N_-^{/} = 0 \end{aligned} \qquad (12)$$

$$\begin{aligned} &\Delta N_-^{/} = \varphi_-\Delta n_-^{/} + \varphi_+\Delta E^{/} + \alpha_+\Delta n_+^{/} \\ &\Delta E^{/} = \frac{1}{\sigma}\left(\Delta J - e\vartheta_-\Delta n_-^{/} - e\vartheta_+\Delta n_+^{/}\right) \end{aligned} \qquad (13)$$

Constant coefficients are easily obtained by linear zing the equations (2,5,7,8) and therefore we do not write them out. Substituting $\Delta N_-^{\prime}\ u\ \Delta E^{\prime\prime}$ from (11) to (10) we obtain dispersion equation for determining the wave vector k and deviations from equilibrium values of the concentrations of electrons and holes.

$$\begin{aligned} &\Delta n_+(x,t) = M_1^+ e^{ik_1 x} + M_2^+ e^{ik_2 x} + M_+\Delta I \\ &\Delta n_-(x,t) = M_1^- e^{ik_1 x} + M_2^- e^{ik_2 x} + M_-\Delta I \end{aligned} \qquad (14)$$

Due to the cumbersome expressions $M_{\pm}, u\ k_1, k_2$ we did not write out their explicit form. To define a constant $M_1^{\pm}\ u\ M_2^{\pm}$ we have to use boundary conditions for $\Delta n_{\pm}(x,t)$ The contacts of the crystal are injecting i.

$$\Delta n_{\pm} = \delta_{\pm}\Delta I \qquad (15)$$

Conditions (15) has the form:

$\Delta n_+(0) = \delta_+^0\Delta I$, $\Delta n_+(L) = \delta_+^L\Delta I$, or $\Delta n_-(0) = \delta_-^0\Delta I$, $\Delta n_-(L) = \delta_-^L\Delta I$, Substituting conditions (15) into (14) we define $M_1^{\pm}\ u\ M_2^{\pm}$ and substituting their values in (12) we obtain the expressions for the alternating electric field. The impedance of the crystal is determined by the integral

$$Z = \frac{1}{\Delta I S}\int_0^L \Delta E(x,t)dx \tag{16}$$

S is the crystal cross section. However, equation (16) in its general form is extremely cumbersome, and therefore we will consider its solutions in two limiting cases.

1) High frequency case

$$\omega >> \nu_{\pm},\ \nu_{+}^{E}, \nu_{\pm}' \qquad \nu_{\pm}' << \nu_{\pm}, \nu_{+}^{E} \tag{17}$$

In obtaining the values of the wave vectors k1 and k2, we used small parameters

$$\frac{\nu_{\pm}'}{\nu_{\pm}'} << 1,\ \frac{T\nu_{\pm}}{eE_0\vartheta_{\pm}^0} << 1,\ \frac{T}{eE_0 L} << 1 \tag{18}$$

L is the sample length, $\vartheta_{\pm}^0 = \mu_{\pm}(E_0)E_0$ drift velocities of holes and electrons**.** **T**o determine the frequency of current oscillations in the circuit and the electric field in the case of (17) from (16), we consider four cases of crystals, differing in electron and hole concentrations and injection conditions, on one of the crystal contacts.

If there are identical recombination's and electron and hole generations at the crystal contacts, the probability of injection may be the same. However, recombination and generation in our semiconductor is not the same and therefore the cases indicated below are more likely.

1) $n_{-}^0 >> n_{+}^0$, set δ_{+}^0

$$\frac{\mathrm{Re}\, z}{Z_0} 1 - \left(\frac{2\nu_{-}\beta_{-}^{\gamma}}{\omega}\right)^2 - \frac{E_0}{E_1} - \frac{E_0^2}{E_2^2}\left(\frac{3\nu_{-}\beta_{-}^{\gamma}}{\omega}\sin\theta + \cos\theta\right), \theta = \frac{\omega L}{\vartheta_{+}}$$

$$\frac{\mathrm{Im}\, z}{Z_0} = \left(\frac{2\nu_{-}\beta_{-}^{\gamma}}{\omega}\right)^2 - \frac{6\nu_{-}\beta_{-}^{\gamma}}{\omega}\frac{E_0}{E_1} - \frac{E_0^2}{E_2^2}\left(\sin\theta - \frac{3\nu_{-}}{\omega}\cos\theta\right) \tag{19}$$

$$\vartheta_{+}^0 >> L\nu_{-}\beta_{-}^{\gamma}$$

$$\frac{1}{E_1} = \frac{8\nu_{+}^{E}\nu_{-}^2\mu_{+}\beta_{+}^{\gamma}(\beta_{-}^{\gamma})^2}{L\omega^4}\frac{n_{+}^0}{n_{-}^0};\ \frac{1}{E_2^2} = \frac{4\nu_{-}\mu_{-}\mu_{+}e\delta_{+}^0\beta_{+}^{\gamma}}{L\omega^2}$$

To determine the oscillation frequency and the electric field from (19), we must solve the following equations

$$\mathrm{Re}\, z + R = 0 \text{ и } \mathrm{Im}\, z + R_1 = 0 \tag{20}$$

Here, R is the total positive ohmic resistance in the circuit, R1 is the inductive or capacitive resistance in the circuit. From solution (20) it is easy to get:

$$\omega = \nu_{-}\cdot\frac{R}{3R_1};\ R >> 3R_1,\ E_0 >> E_2\left(\frac{R_1}{Z_0}\right)^{1/2};\ R_1 > 0,\ \beta_{-}^{\gamma} = \frac{5}{12}\frac{\omega}{\nu_{-}}$$

2) $n^0 >> n_{+}^0$, set δ_{-}^0

$$\frac{\mathrm{Re}\, z}{Z_0} 1 - \left(\frac{2\nu_{-}\beta_{-}^{\gamma}}{\omega}\right)^2 - \left(\frac{E_0}{E_2}\right)^2\left(2 + \frac{\omega}{\nu_{-}}\sin\theta - \cos\theta\right),$$

$$\frac{\mathrm{Im}\, z}{Z_0} = \frac{\vartheta_{+}^0\vartheta_{-}^0 e\delta_{-}^0}{L\omega}\left(\frac{\nu_{-}\beta_{-}^{\gamma}}{\omega}\sin\theta + \cos\theta - 1\right) - \left(\frac{2\nu_{-}\beta_{-}^{\gamma}}{\omega}\right)^2 \tag{21}$$

Solution (20) in case (21) with $R_1 > 0$

$$\beta_-^\gamma = \left(\frac{R_1}{R}\right)^2 \frac{Z_0}{R};\ \omega = \nu_- \frac{R_1}{R};\ R_1 >> R; \qquad E_0 = \left(\frac{L\omega}{\mu_-\mu_+ e\delta_-^0}\right)^{1/2} \text{ and at } R_1 < 0\ \ \omega = \nu_- \frac{R_-}{Z_0};$$

$$R >> Z_0 = \frac{L}{\sigma_0 S};\ \ \sigma_0 = e(n_-^0\mu_-^0 n_+^0\mu_+^0); \qquad E = \left(\frac{L\omega}{\mu_-\mu_+ e\delta_-^0}\right)^{1/2} \frac{R^2}{|R_1|Z_0};\ \ \beta_-^\gamma = \frac{|R_1|}{R}\frac{\omega}{\nu_-}$$

3) $n_-^0 << n_+^0$, set δ_-^L

$$\frac{\mathrm{Re}\, z}{Z_0} = 1 + \frac{E_0}{E_1}\cos\theta - \left(\frac{E_0}{E_2}\right)^2\left[\frac{\mu\omega}{\mu_+\nu_-}\sin\theta + \left(1 + \frac{4n_-^0\mu_-\beta_-^\gamma}{n_+^0\mu_+}\right)\cos\theta\right]$$

$$\frac{\mathrm{Im}\, z}{Z_0} = \frac{E_0}{E_1}\left(\sin\theta - \frac{\nu_-}{\omega}\cos\right) - \left(\frac{E_0}{E_2}\right)^2\left(\sin\theta - \frac{4\omega\mu_-}{\nu_-\mu_+}\cos\theta\right)$$

$$\theta = \frac{\omega L}{\vartheta_-};\ \ \vartheta_- >> \frac{L\nu_- n_-^0\beta_-^\gamma}{n_+};\ \ \frac{1}{E_1} = \frac{n_-^0\mu_-^2\nu_-\beta_-^\gamma}{n_+^0\mu_+ L\omega^2};\ \ \frac{1}{E_2} = \left(\frac{\mu_-\mu_+\nu_- e\delta_-^L}{L\omega^2}\right)^{1/2}$$

From the solution (21) taking into account (20) we get

$$\beta_-^\gamma = \left(1 + \frac{R}{Z_0}\right)\left(\frac{n_+\mu_+}{n_-\mu_-}\right)^3 \cdot \frac{L\omega^2 e\delta_-^L}{4\nu_-}\frac{\mu_+}{\mu_-}; \qquad E_0 = E_1\frac{\mu_+}{4\mu_-}\left(\frac{\nu_-}{\omega}\right)^2;\quad R_1 > 0,\ \ |R_1| < Z_0$$

$$\omega = 2\left[\frac{\beta_-^\gamma\nu_-}{Le\delta\left(1 + \frac{R}{Z_0}\right)}\right]^{1/2} \cdot \left(\frac{n_-}{n_+}\right)^{3/2}\left(\frac{\mu_-}{\mu_+}\right)^2 \text{ and at } R_1 < 0 \quad \omega = \nu_-\frac{n_-}{n_+}\beta_-^\gamma\frac{|R_1|}{Z_0}\cdot\frac{1}{1 + \frac{R}{Z_0}}$$

$$\beta_-^\gamma > \frac{n_+}{n_-}\left(\frac{Z_0}{|R_1|} + \frac{R}{|R_1|}\right);\quad E_0 = \left(\frac{\mu_+}{2\mu_-}\right)^2\frac{L\nu_-}{\mu_-}\cdot\frac{1}{\beta_-^\gamma}\cdot\frac{1}{\beta_-^\gamma}$$

4) $n_-^0 << n_+^0$; set δ_+^L

$$\frac{\mathrm{Re}\, z}{Z_0} = 1 + \frac{E_0}{E_1}\left[\left(\frac{n_-\beta_-^\gamma}{n_+} - \frac{\mu_-}{\mu_+}\right)\sin\theta + \frac{\mu_-\omega}{\mu_+\nu_-}\cos\theta\right] + \left(\frac{E_0}{E_2}\right)^2\left[\frac{\mu_-\omega}{\mu_+\nu_-}\sin\theta + \left(1 - \frac{n_-\beta_-^\gamma}{n_+}\right)\cos\theta\right]$$

$$\frac{\mathrm{Im}\, z}{Z_0} = \frac{\nu_-}{\omega}\cdot\frac{E_0}{E_1}\left[\left(\frac{n_-\beta_-^\gamma}{n_+} - 1\right)\sin\theta - \frac{\omega}{\nu_-}\cos\theta\right] + \left(\frac{E_0}{E_2}\right)^2\left[\left(1 - \frac{n_-\beta_-^\gamma}{n_+}\right)\sin\theta + \frac{\mu_-\omega}{\mu_+\nu_-}\cos\theta\right];\ \theta = \frac{\omega L}{\vartheta_-} \qquad (22).$$

From solution (20) in case (22) we get:

$$E_0 = \left(\frac{\mu_+}{\mu_-}\right)^{1/2}\frac{L\omega}{\mu_-}\left(\frac{\omega}{\nu_-}\right)^2;\quad \omega >> \nu_-;\quad \beta_+^\gamma = \frac{R}{|R_1|}\left(\frac{\mu_+}{\mu_-}\right)^{1/2}\frac{\nu_-}{\nu_+^E};\quad R_1 < 0$$

Low frequency case $\omega << \nu_\pm, \nu_+^E, \nu_\pm'$

1) $n_-^0 << n_+^0$, set δ_+^0

$$\frac{\mathrm{Re}\, z}{Z_0} = 1 - \frac{E_0}{E_1}\left(\frac{4\omega}{\nu_+}\sin\theta + \cos\theta\right) - \left(\frac{E_0}{E_2}\right)^2\left(\frac{\omega}{\nu_+}\sin\theta + \cos\theta\right);\quad \theta = \frac{\omega L}{\vartheta_+^0\beta_-^\gamma};\ \vartheta_+^0 >> \frac{L\nu_+}{\beta_-^\gamma}$$

$$\frac{\operatorname{Im} z}{Z_0}=\frac{E_0}{E_1}\left[\left(\frac{4\omega}{\nu_+}\cos\theta-\sin\theta\right)-\frac{\omega}{\nu_+}\right]+\left(\frac{E_0}{E_2}\right)^2\left(2\sin\theta-\frac{\omega}{\nu_+}\cos\theta\right)$$

$$\frac{1}{E_1}=\frac{n_+\nu_+^E\mu_+^2\beta_+^\gamma}{L\nu_+^2\mu_-n_-};\ \frac{1}{E_2^2}=\frac{\mu_+^2\beta_+^\gamma e\delta_+}{L\nu_+}$$

$$R_1>0,\ E_0\frac{E_2^4}{2E_1^2}\left(1+\frac{R_1}{Z_0}\frac{E_1^2}{E_2^2}\right),\ \omega=\frac{\nu_+}{16}\qquad \beta_+^\gamma=\left(\frac{n_-\mu_-\nu_+}{n_+\mu_+\nu_+^E}\right)^{1/2}L\nu_+e\delta_+$$

2) $n_-<<n_+$, set δ_-^0

$$\frac{\operatorname{Re} z}{Z_0}=1+\frac{E_0}{E_1}\left(\frac{3\omega}{\nu_+}\sin\theta+\cos\theta-1\right)-\left(\frac{E_0}{E_2}\right)^2\left(\frac{\omega}{\nu_+}\sin\theta+\cos\theta\right);$$

$$\frac{\operatorname{Im} z}{Z_0}=\frac{E_0}{E_1}\left[\left(\frac{3\omega}{\nu_+}\sin\theta+3\cos\theta\right)-\frac{\omega}{\nu_+}\right]+\left(\frac{E_0}{E_2}\right)^2\left(\sin\theta+\frac{\omega}{\nu_+}\cos\theta\right)$$

$$\frac{1}{E_1}=\frac{\mu_+\beta_+^\gamma}{L\nu_+};\ \frac{1}{E_2^2}=\frac{\mu_+\mu_-\beta_-^\gamma e\delta_-^0}{L\nu_+};\qquad R=2Z_0,\ E_0=E_1,\ R_1<<3Z_0,\quad \omega=\nu_+\frac{R_1}{3Z_0}\quad R_1>0, R_1<0$$

3) $n_-<<n_+$ set δ_-^L

$$\frac{\operatorname{Re} z}{Z_0}=1-\left(\frac{\nu_+^E\beta_+^\gamma}{\nu_+}+\frac{\mu_-n_-\beta_-^\gamma}{\mu_+n_+}\right)-\left(\frac{E_0}{E_1}\right)^2\left[\frac{\omega}{\nu_+}(\sin\theta-\cos\theta)+1\right]$$

$$\frac{\operatorname{Im} z}{Z_0}=\left(\frac{\mu_-n_-\nu_-}{\mu_+n_+\nu_+}-\frac{\nu_+^E\beta_+^\gamma}{\nu_+\beta_-^\gamma}\right)\frac{\omega}{\nu_-}\left(\beta_-^\gamma\right)^2-\left(\frac{E_0}{E_1}\right)^2\left(\frac{\omega}{\nu_+}-\sin\theta-\frac{\omega}{\nu_+}\cos\theta\right)$$

$$\frac{1}{E_1^2}=\frac{\mu_+\mu_-n_-\beta_-^\gamma e\delta_-^L}{L\nu_+n_+}$$

$$\beta_-^\gamma=\frac{\mu_+n_+}{2\mu_-n_-}\left(\sqrt{1+\left(\frac{2\mu_-n_-}{\mu_+n_+}\right)^2\frac{\nu_-}{\nu_+}}+1\right);\ R_1<0,\ R<<|R_1|,\ \omega=\frac{R}{R_1}\nu_+;\qquad E_0=E_1\frac{\nu_+R}{\omega Z_0}$$

4) $n_-<<n_+$, set δ_+^L

$$\frac{\operatorname{Re} z}{Z_0}=1-\left(\frac{\nu_+^E\beta_+^\gamma}{\nu_+}+\frac{\mu_-n_-\beta_-^\gamma}{\mu_+n_+}\right)-\left(\frac{E_0}{E_1}\right)^2(1+\sin\theta-\cos\theta)+\frac{E_0}{E_1}(\sin\theta+\cos\theta)$$

$$\frac{\operatorname{Im} z}{Z_0}=\left(\frac{\mu_-n_-\nu_-}{\mu_+n_+\nu_+}-\frac{\nu_+^E\beta_+^\gamma}{\nu_+\beta_-^\gamma}\right)\frac{\omega}{\nu_-}\left(\beta_-^\gamma\right)^2-\frac{E_0}{E_1}\left(\sin\theta+\frac{2\omega}{\nu_+}\cos\theta\right);\ \theta=\frac{\omega Ln_+}{\vartheta n_-\beta_-^\gamma}$$

$$\frac{1}{E_1}=\frac{n_-\mu_-\beta_-^\gamma e\delta_-^L\nu_+^E}{L\nu_+^2};\ \frac{1}{E_1^2}=\frac{\mu_+\mu_-n_-\beta_-^\gamma e\delta_+^L}{L\nu_+n_+^0};\qquad E_0=E_1;\qquad \omega=\frac{2\nu_+}{1+\frac{\nu_+^E}{\nu_+}\beta_+\gamma},$$

$$\beta_-^\gamma=\frac{2\nu_-}{\nu_+^E\beta_+^\gamma};\qquad a=\frac{\nu_+^E\beta_+^\gamma}{\nu_+}+\frac{\mu_-n_-\beta_-^\gamma}{\mu_+n_+},\qquad \beta_-^\gamma=\left(1+\frac{R}{Z_0}\right)\frac{\nu_-}{\nu_+}\frac{1}{a}$$

The Discussion of the Results

Thus, in the above-mentioned semiconductors, oscillations of carrier concentration and electric field oscillations in the high-frequency and low-frequency cases are possible. The injection of crystal contacts plays a major role in the excitation of current oscillations. There are four excitation options in the high-frequency and in the low-frequency case. Main charge carriers

n_+^0 and n_-^0 depending on the injection of contacts (i.e., the arrival and departure of charge carriers through contacts) basically changes the values of the critical electric field at which the radiation begins. Constants $\beta_\pm^\gamma$ in each case have a specific meaning. High frequency spacing electric field and constants $\beta_\pm^\gamma$ may well be measured experimentally. In the low-frequency case of the constant $\beta_\pm^\gamma$ mainly expressed by resistances and. In the above two cases, inductive and capacitive resistance may occur.

REFERENCES

1. E.R.Hasanov, R.N.Hosseyn, A.Z.Panahov A.İ.Demirel. *Instability in Semiconductors with Deep Traps in the Presense of Strong* $(\mu_\pm H >> C)$ *External Magnetic Field. and Adv. Studies Theor. Phys.*5,2011,15-30.
2. E.R.Hasanov, A.Z.Panahov and A.İ.Demirel *High Freguenay Energy Radiation of n-Type Semiconductors at Constant Electric and Magnetic Field. Adv. Studies Theor. Phus.*7 (2013) 21,1035-1042.
3. F.F.Aliyev, E.R.Hasanov. *Nonlinear Oscillations of the Charge Curriers Concentration and Electric Fieldin Semiconductors With Deep Traps. 10SR Journal of applied Physics* (10SR-JAP)e-ISSN.2278-4861.10.ISUE 1.II (Jan-Feb 2018) 36-42.
4. E.Z.Panahov, A.İ.Demirel. *The nonlinear Theory of GUNNS Eeffect Progress of Theoretical Physice* N03 (March 2009) 121
5. E.R.Hasanov, R.K.Gasimova, A.Z.Panahov, A.İ.Demirel. *Ultrahigh Fredueney Generationin GaAS-tupe TWO-Valley Semiconductors Adv. Studies Theor. Phys,*3(2009) 8,293-298.
6. I.B.Gunn. *From book Proc.I.nt. Conf. Phys. Semiconductors kyoto* (1966) 505.
7. М.Н.Иглицын, Э.Г.Пель, *Л.*Я.Первова, В.Г.Фистуль. *Неустойчивость электронно-дырочной плазмы полупроводника, обусловленная нелинейности вольтамперных характеристик. ФТТ.*8.12 (1966) 3606-3617.

JOURNAL OF BAKU ENGINEERING UNIVERSITY - PHYSICS
2018. Volume 2, Number 2 *Pages 103-105*

UOT: 530.145;530.12;537.8
PACS: 03.70,+k,11.10-z, 11.30.RD

FINITE SIZE AND TOPOLOGICAL EFFECT IN GAUGED FOUR-FERMION INTERACTION MODEL

Tomohiro INAGAKI[1'2]

[1] Information Media Center, Hiroshima University, Higashi-Hiroshima, 739-8521, Japan, [2]Core of Research for the Energetic Universe, Hiroshima University, Higashi-Hiroshima,

739-8526, Japan, e-mail: *inagaki@hiroshima-u.ac.jp*

Keywords: Quantum field theory, Chiral symmetry, Spontaneous symmetry breaking, Finite size effect, Topological effect.

1. INTRODUCTION

Many models of the particle physics are constructed based on symmetry. In the ground state of the system some symmetry is spontaneously broken. The chiral symmetry plays an important role for the mass generation of fermion fields. The symmetry must be broken for a massive fermion. In QCD the chiral symmetry is dynamically broken by the non-vanishing vacuum expectation value for a composite operator constructed by a quark and an anti-quark.

The symmetry property of the ground state depends on the environment. It is expected that the broken symmetry is restored in some critical environments, small size, high temperature, high density and strong curvature. We often employ a four-fermion interaction model as a low energy effective model of the strong interaction and investigate the symmetry behavior.

In this article we focus on the finite size and topological effect to the chiral symmetry breaking. In Sec. 2 a gauged four-fermion interaction model is introduced as a simple model which induces the chiral symmetry breaking. In Sec. 3 we evaluate the ground state by observing the extremum of the effective potential. Finally, we will give some concluding remarks.

2. FOUR-FERMION INTERACTION MODEL ON $R^{D-1} \otimes S^1$

We start from a gauged four-fermion interaction model defined by the Lagrangian density,

$$L = -\frac{1}{4} F^{\mu\nu} F_{\mu\nu} + \sum_{k=1}^{N} \overline{\psi}_k i\gamma^\mu D_\mu \psi_k + \frac{\lambda_0}{2N} \left(\sum_{k=1}^{N} \overline{\psi}_k \psi_k \right)^2 , \tag{1}$$

Where D_μ represents the covariant derivative, λ_0 is a coupling constant, N is the number of fermion species. This Lagrangian is invariant under the discrete chiral transformation,

$$\psi \to \gamma^5 \psi \tag{2}$$

This Z_2 chiral symmetry prevent the Lagrangian from having a mass term.

In order to investigate the finite size and the topological effect we consider the model on the background, $R^{D-1} \otimes S^1$, where R^{D-1} is a (D — 1)-dimensional flat Minkowski space time and S^1 is the one dimensional sphere. The boundary condition for the compact direction, x^{D-1}, can be determined by the spin structure of the fermion. Here we set the boundary condition,

Manuscript receved 21.09.2018

$$\psi\left(x^0,...,x^{D-2},x^{D-1}+L\right)=e^{i\delta}\psi\left(x^0,...,x^{D-2},x^{D-1}\right), \tag{3}$$

where *L* is the size of the compact direction. It should be noted that the theory is equivalent with the finite temperature field theory for the anti-periodic boundary condition, $\delta=\pi$, [3]. According to the auxiliary field method, the Lagrangian (1) is rewritten as

$$L=-\frac{1}{4}F^{\mu\nu}F_{\mu\nu}\sum_{k=1}^{N}\overline{\psi}_k(i\gamma^\mu D_\mu-\sigma)\psi_k-\frac{N}{\lambda_0}\sigma^2 \tag{4}$$

If the auxiliary field, a, develops a non-vanishing vacuum expectation value, the fermion mass term is dynamically generated and the Z_2 chiral symmetry is spontaneously broken.

3. EFFECTIVE POTENTIAL ANALYSIS

We usually evaluate the vacuum expectation value for the auxiliary field, a, by observing the minimum of the effective potential. As a review, see for example [4]. In the leading order of the 1/N expansion the effective potential is given by

$$\frac{V(\sigma)}{N}=\frac{1}{2\lambda_0}\sigma^2-\frac{1}{\sqrt{2}L}\sum_{n=-\infty}^{\infty}\int\frac{d^{D-1}k}{\left(2\pi^2\right)^{(D-1)/2}}\ln\left[\left(k^2+\sigma^2\right)L^2\right]+O\left(\frac{1}{N}\right) \tag{5}$$

With

$$d^{D-1}k\equiv dk_0...dk_{D-2,}k^2\equiv k_0^2+....+k_{D-2}^2+\omega_n^2,\omega_n\equiv\frac{2n\pi+\delta}{L} \tag{6}$$

In this expression the time component of κ is transformed as $k_0\to -i\omega_n$.

The effective potential (5) contains an ultraviolet divergence. The divergence can be regulated by the dimensional regularization, i.e. computing as an analytic function of the spacetime dimension, *D.* The divergence can be eliminated by renormalizing the coupling constant. We introduce the renormalized coupling, λ, and the renormalization scale μ,

$$\frac{1}{\lambda_0}\equiv\left(\frac{1}{\lambda}-\frac{1}{\lambda_C}\right)\mu^{D-2}\quad\text{with}\quad\frac{1}{\lambda_C}\equiv\frac{1-D}{(2\pi)^{D/2}}\Gamma\left(1-\frac{D}{2}\right) \tag{7}$$

The extremum of the potential satisfies the gap equation,

$$\frac{1}{\lambda}-\frac{1}{\lambda_C}-\frac{\sqrt{2}}{L\mu(2\pi)^{(D-1)/2}}\Gamma\left(\frac{3-D}{2}\right)\sum_{n=-\infty}^{\infty}\left(\frac{\omega_n^2+\sigma^2}{\mu^2}\right)^{(D-3)/2}=0 \tag{8}$$

To calculate the gap equation we perform the integration over $k_0,...k_{D-2}$ in Eq. (5). An existence of a non-vanishing real solution of the gap equation is a necessary condition for the auxiliary field, a, to develop a non-vanishing expectation value at the ground state. In Ref. [1] the solution of the gap equation is evaluated as a function of the phase 5 in a curved spacetime, The broken symmetry can be restored with decreasing the coupling constant through the second order phase transition. The critical value of the coupling, λ_{cr}, is given by the $\sigma\to 0$ limit of the gap equation,

$$\frac{1}{\lambda_{cr}}-\frac{1}{\lambda_c}-\frac{\sqrt{2}(2\pi)^{(D-5)/2}}{(L\mu)^{D-2}}\Gamma\left(\frac{3-D}{2}\right)\left[\xi\left(3-D,\frac{\delta}{2\pi}\right)+\xi\left(3-D,1-\frac{\delta}{2\pi}\right)\right]=0 \tag{9}$$

In order to find a contribution of the boundary condition we transform the fermion as,

$$\psi'(x)\equiv e^{i\theta(x)}\psi(x),\ \text{with}\ \theta\left(x^0,...,x^{D-2},x^{D-1}+L\right)=\theta\left(x^0,...,x^{D-2},x^{D-1}\right)+\eta. \tag{10}$$

The boundary condition for the transformed fermion is given by,

$$\psi'\left(x^0,...,x^{D-2},x^{D-1}+L\right)=e^{i(\delta+\eta)}\psi'\left(x^0,...,x^{D-2},x^{D-1}\right) \tag{11}$$

The transformation (10) changes the kinetic term for the fermion. It can be cancelled by the gauge transformation. Thus, the Lagrangian is invariant under the transformation (10). It means that the phase δ should be fixed to minimize the effective potential.

To find the ground state we numerically evaluate the effective potential (5) with the phase *5* varies. Here we discuss the result for a small coupling case, $\lambda \prec \lambda_{cr}(L,\delta)$. Since the gap equation (8) has no real solution for $\lambda \prec \lambda_{cr}(L,\delta)$, the extremum of the effective potential is found at $\sigma=0$, only. In Fig. 1 shows the effective potential at $\sigma=0$ as a function of the phase δ. The minimum is observed at $\delta=\pi$. For a non-vanishing δ the fermion has to depend on the co-ordinate of the compact direction, x^{D-1}, to satisfy the boundary condition (3). We cannot avoid to consider the inhomogeneous distribution of the fermion.

FIGURE 1. 5-dependence of the effective potential at $\sigma=0$ for D = 2.0 (bottom at $\delta=\pi$), 2.5,3.0 and 3.5 (top at $\delta=\pi$).

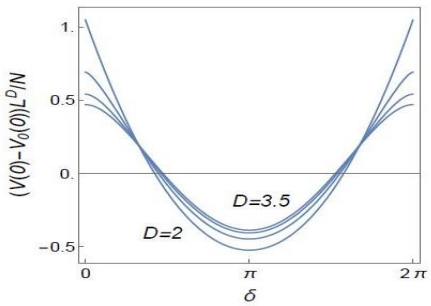

4. CONCLUSION

The effective potential of the gauged four-fermion interaction model has been investigated on the background $R^{D-1}\otimes S^1$. If the coupling constant is smaller than the critical one, the minimum of the effective potential is found at the anti-periodic boundary condition, $\delta=\pi$.

In the effective potential analysis, we assume that the configuration of the auxiliary field, a, is constant. In Ref. [2] it is pointed out that an inhomogeneous configuration of the auxiliary field can be realized at the ground state for a four-fermion interaction model in two dimensions. To evaluate the inhomogeneous configuration of the auxiliary field we need to extend the analysis for the gauged four-fermion interaction model in arbitrary dimensions. This will be discussed elsewhere.

AMS Subject Classification: 70S10, 81Txx

REFERENCES

[1] Flachi A., Dual Fermion Condensates in Curved Space, *Phys. Rev. D,* Vol.88, No.8, 2013, pp.085011.

[2] Flachi A., Nitta M., Takada S. and Yoshii R., Sign Flip in the Casimir Force for Interacting Fermion Systems, *Phys. Rev. Lett.,* Vo.119, No.3, 2017, pp.031601.

[3] Inagaki T., Kouno T. and Muta T., Phase structure of four fermion theories at finite temperature and chemical potential in arbitrary dimensions, *Int. J. Mod. Phys. A,* Vol.10, 1995, pp.2241-2268.

[4] Inagaki T., Muta T. and Odintsov S. D., Dynamical symmetry breaking in curved space-time: Four fermion interactions, *Prog. Theor. Phys. Suppl.,* Vol.127, 1997, pp.93-193.

JOURNAL OF BAKU ENGINEERING UNIVERSITY - PHYSICS
2018. Volume 2, Number 2 *Pages 106-110*

PACS: 72.40. +w
УДК: 621.315.592

CURRENT PASSING MECHANISM AND ELECTRICAL PARAMETERS OF InSe

V. M. SALMANOV[1], A. G. GUSEINOV[1], R. M. MAMEDOV[1], A. SALMANOVA[2], N.D. DASHDAMIROVA[1]

[1]Baku State University, Baku, AZ1148 Azerbaijan

[2] Azerbaijan State University of Oil and Industry, Baku, Azerbaijan

**e-mail: vagif_salmanov@yahoo.com*

ABSTRACT

The temperature dependences of the electrical conductivity, concentration and mobility of current carriers in InSe crystals grown in different modes of the process are investigated. From the temperature dependence of the electrical conductivity, the activation energy of the impurity level was determined to be 48 meV. It has been established that, in the temperature range below 70K, scattering by impurity ions dominates in the mechanism of charge carrier scattering, and above acoustic oscillations of the lattice, above 70K. It has been shown that in some fairly pure samples, the mobility value reaches ~ 9100 $cm^2/V \cdot sec$.

Keywords: Indium selenide, mobility, absorption, acoustic phonons.

МЕХАНИЗМЫ ТОКОПРОХОЖДЕНИЯ И ЭЛЕКТРИЧЕСКИЕ ПАРАМЕТРЫ InSe

АННОТАЦИЯ

Исследованы температурные зависимости электропроводности, концентрации и подвижности носителей тока в кристаллах InSe, выращенных в разных режимах технологического процесса. Из температурной зависимости электропроводности определена энергия активации примесного уровня, равная 48 мэВ. Установлено, что в области температур ниже 70K в механизме рассеяния носителей заряда преобладает рассеяния на ионах примеси, а выше 70 K – на акустических колебаниях решетки. Показано, что в некоторых довольно чистых образцах значение подвижности достигает ~ 9100 $см^2/В \cdot сек$.

Ключевые слова: Селенид индия, подвижность, поглощение, акустические фононы.

İnSe-NİN ELEKTRİK PARAMETRLƏRİ VƏ CƏRƏYANKEÇİRMƏ MEXANİZMİ

XÜLASƏ

Texnoloji prosesin müxtəlif rejimlərində yetişdirilmiş İnSe kristalında elektrik keçiriciliyinin, yükdaşıyıcıların konsentrasiyasının və yürüklüyünün temperatur asılılıqları tədqiq olunmuşdurlar. Elektrik keçiriciliyinin temperatur asılılıqlarından aşqar səviyyənin yerləşmə dərinliyinin 48 meV olduğu müəyyən edilmişdir. 70K temperaturdan aşağıda yükdaşıyıcıların səpilmə mexanizmi ionlaşmış aşqarlardan, 70K-dən yuxarıda isə akustik fononlardan səpilmədən ibarət olduğu müəyyən edilmişdir. Göstərilmişdir ki, kifayət qədər təmiz kristallarda yükdaşıyıcıların yürüklüyü ~ 9100 $sm^2/V \cdot s$ qiymətini alır.

Açar sözlər: İndium selen, yürüklük, udma, akustik fononlar.

I. Introduction

Among 2D crystals, indium selenide is most vulnerable to a wide range of researchers because of the simplicity and large variety of technology for producing ultrathin films. InSe crystals belong to A^3B^6 type layered semiconductor compounds. The ionic - covalent bond between the atoms in the layers and the weak van der Waals interaction between the layers make it possible to mechanically obtain films consisting of 2 to 20 monolayers. The layered structure of the InSe crystal structure causes a strong anisotropy of their physical properties and is the main reason for observing a number of effects that are not typical of other anisotro-

Manuscript receved 16.06.2018

pic semiconductors. Due to the presence of a low density of surface states (less than 10^{10} cm^{-2}), these crystals respond well to intercalation with various substances, they can easily be cleaved, and exfoliated surfaces turn out to be specular. Different methods of mechanical and chemical processing allow to produce samples one micron thick and less [1-3]. The ultrathin layers of indium monoselenide have unique properties that qualitatively distinguish it from the other two-dimensional crystals. In two-dimensional samples of indium monoselenide, electron mobility is the highest. This material parameter is extremely important from the point of view of improving the speed of devices that can be created on its basis. According to scientists, indium monoselenide has wide prospects for further practical use, because its nanolayers combined with graphene and some other functional two-dimensional crystals have every chance to compete with silicon (Si) as the main material of modern electronics [4-6]. The perfection of technological equipment and the improvement of the accuracy of measuring instruments stimulate anew and more thoroughly examine the previously studied properties of crystals. Studies of the electrical properties of layered A^3B^6 type crystals have shown that they contain uncontrolled structural defects, which are caused by the displacement of the monolayers relative to each other on an atomic scale. Such defects significantly affect the electrical and photoelectric properties of the crystal. However, obtaining and studying 2D crystals of A^3B^6 compounds and comparing the results with the results of similar modern studies of large crystals, will accelerate the innovation of new ideas.

This work is devoted to the experimental study of the electrical and optical parameters of thin films of indium selenide obtained in different conditions of the technological process.

II. Samples and Experimental Technique

The investigated InSe single crystals were grown by the Bridgman–Stockbarger method. The whole process of growing was carried out in automatic mode, which allowed to obtain perfect single crystals with a natural mirror surface. Samples with a thickness of 100–200 μm and an area of ~ 1 cm^2 were made by cleaving large ingots. An ohmic contact of In was deposited on the freshly cleaved surface of the sample by thermal evaporation in vacuum. In the study of the absorption spectra, an automated monochromator with double dispersion M833 (spectral resolution ~ 0.024 nm at a wavelength of 600 nm) with computer control and a detector recording radiation in the wavelength range of 350-2000 nm was used. The electrical parameters were determined by the standard Hall effect method. The magnetic field strength was ~ 11000 Gauss. The measurements were carried out in the temperature range of 4.2-300 K for two directions, parallel and perpendicular to the optical axis "c".

III. Experimental results and discussion

All the grown crystals had n-type conductivity, the specific conductivities of the samples cut from the crystals in the form of a rectangle are presented in Table 1. The absorption spectrum of sample 4, with an InSe film thickness of 85 μm, is shown in Fig. 1. As can be seen from the figure, the edge of the absorption band is located in the near infrared region of the spectrum. The band gap in InSe, determined from the $\alpha^2 \sim f(h\nu)$ dependence, turned out to be equal to E_g=1.32 eV. It should be noted that the values we found for E_g are comparable with the data given in [7, 8, 9].

Based on Hall measurements, the main electrical parameters, Hall constant (R), resistivity (ρ), current carrier concentration (n), mobility (μ), conductivity type of thin InSe films in the direction parallel and perpendicular to the optical axis "c" were determined.

Fig. 1. Absorption spectra of thin InSe films.

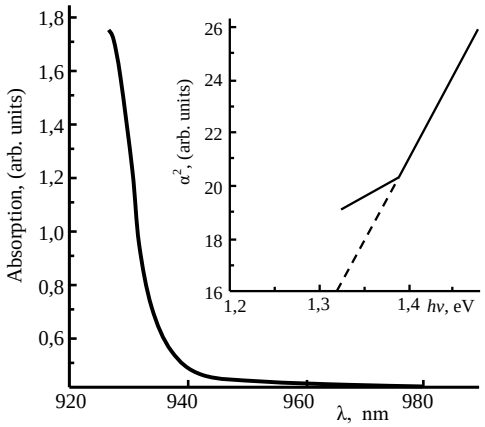

The data for six samples in the direction perpendicular to the optical axis-s at 300 K and 77 K are shown in Table 1. As can be seen from the table, these parameters in InSe vary widely for samples obtained from different ingots. It was not possible to determine any regularities for the dependence of mobility on the specific resistance of the crystal. The reason for this, in our opinion, is the complexity of the behavior of defects in crystals. A rather large value of mobility (~ 9000 $cm^2/V{\cdot}sec$) for sample №1 at 77 K should be noted, which is a very important parameter for the manufacture of high-speed detectors of laser radiation.

Table 1. Electrical parameters of thin InSe films in the direction perpendicular to the optical axis "c"

300 K						77 K				
crystal №	d μm	ρ Om·cm	R Om	μ $cm^2/V{\cdot}s$	concen. cm^{-3}	ρ Om·cm	R Om	μ $cm^2/V{\cdot}s$	con. cm^{-3}	type
1.InSe	65	0,12	337	278	$1.8{\cdot}10^{15}$	0.8	1688	9100	$3.7{\cdot}10^{15}$	n
2.InSe	55	0.52	334	638	$1.8{\cdot}10^{15}$	0.68	1578	2321	$3.99{\cdot}10^{15}$	n
3.InSe	75	1.63	281	172	$3.6{\cdot}10^{16}$	1.45	1309	901	$4.7{\cdot}10^{15}$	n
4.InSe	85	1.83	305	16.6	$2.0{\cdot}10^{15}$	2.80	2256	805	$2.86{\cdot}10^{15}$	n
5.InSe	45	2.67	708	265	$1.8{\cdot}10^{15}$	2.02	9290	1134	$6.2{\cdot}10^{15}$	n
6.InSe	87	3.13	725	231	$1.9{\cdot}10^{15}$	3.78	4140	1095	$1.5{\cdot}10^{15}$	n

In table 2, for comparison, the same data from one of the studied samples for two directions, parallel and perpendicular to the optical axis "c", is given. As can be seen from the table, the resistivity and mobility of current carriers depend on the orientation of current contacts, which indicates the presence of strong mechanical anisotropy in InSe.

Table 2. Comparison of the electrical parameters of InSe thin films in a direction parallel and perpendicular to the optical axis "c".

crystal №	$\rho_\perp$ Om·cm	con. cm^{-3}	$\mu_\perp$ $cm^2/V{\cdot}s$	con. cm^{-3}	$\rho_\parallel$ Om·cm	$\mu_\parallel$ $cm^2/V{\cdot}s$
InSe	5.2	$9.3{\cdot}10^{15}$	130	$9.3{\cdot}10^{15}$	$3.7{\cdot}10^{2}$	4.2

The temperature dependences of the resistivity and carrier concentration in a wide range of temperatures, from 4.2 K to 300 K are presented in Fig.2. As follows from the figure, the resistivity in the temperature range of 100–300 K remains almost constant, and the electron concentration increases with increasing temperature. From the dependence ϱ (T) in the range of 20–100 K, the activation energy of the impurity level is determined to be 48 meV.

Fig. 2. Dependences of resistivity (1) and concentration (2) on the temperature of thin InSe films.

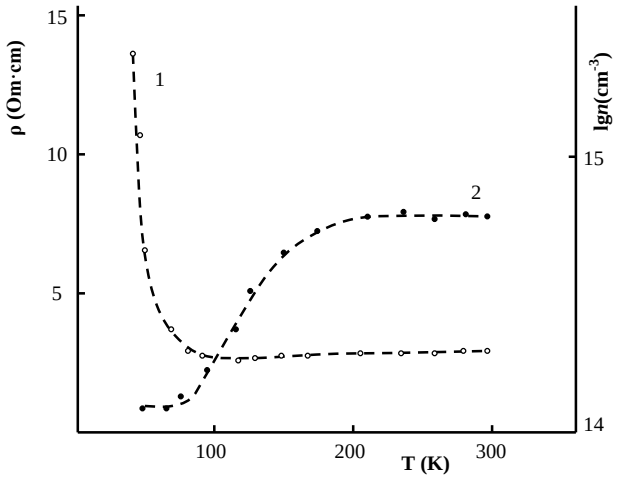

Figure 3 shows the dependence of the mobility of InSe on temperature. We see that basically, there are two trends in the change of mobility. At first, up to 70 K, an increase in mobility is observed, and then, starting from this value, it decreases. The change in the Hall mobility of current carriers with temperature obeys the laws $\mu \sim T^{3/2}$ (<70K) and $\mu \sim T^{-3/2}$ (>70K), which corresponds to carrier scattering on impurity ions and on acoustic lattice vibrations.

Fig. 3. Dependence of InSe mobility on temperature.

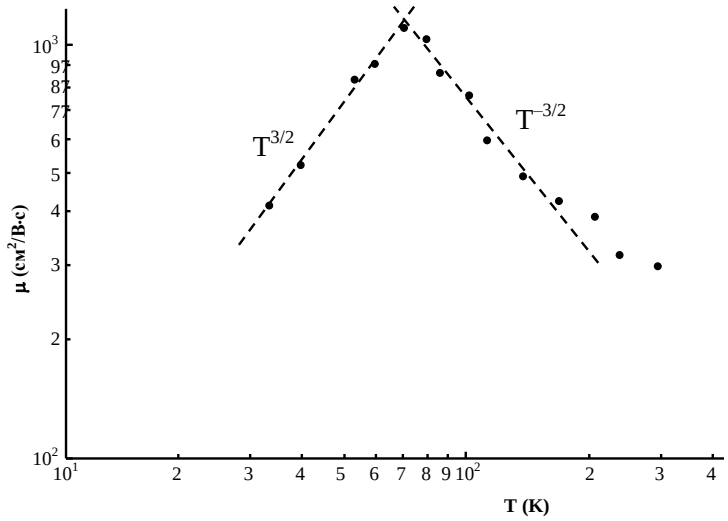

IV. Conclusion

The main electrical parameters of InSe thin films were determined by an experimental method: resistivity, mobility, conductivity type, current carrier concentration. It has been shown that in some fairly pure samples, the mobility value reaches ~ 9100 $cm^2/V \cdot sec$.

It was revealed that, depending on the orientation, a significant anisotropy is observed in the values of mobility and resistance. It has been shown that in most of the n-InSe samples that were selected as objects for further research, the mobility reaches ~700 $cm^2/V \cdot s$, and the carrier concentration is $10^{16}\ cm^{-3}$.

This work was supported by the Science Development Foundation under the President of the Republic of Azerbaijan **- Grant № EİF/ MQM/ Elm-Tehsil-1-2016-1(26)-71/01/1.**

REFERENCES

1. A. Segura, F. Pomer, A. Cantarero, W. Krause, and A. Chevy. Electron scattering mechanisms inn-type indium selenide. Phys. Rev. B 29, 5708 – Published 15 May 1984.
2. H.M. Pathan, S.S. Kulkarni, R.S. Mane, C.D. Lokhande. Preparation and characterization of indium selenide thin films from a chemical route. Materials Chemistry and Physics, volume 93, Issue 1, 2005, Pages 16-20.
3. Jin-Ho Park, Mohammad Afzaal, Madeleine Helliwell, Mohmmad A. Malik, Paul O'Brien, Jim Rafters. Chemical Vapor Deposition of Indium Selenide and Gallium Selenide Thin Films from Mixed Alkyl/Dialkyl seleno phosphoryl amides. Chem. Mater., 2003, 15 (22), pp 4205–4210, DOI: 10.1021/cm0310420.
4. A.F. Qasrawi. Temperature dependence of the band gap, refractive index and single-oscillator parameters of amorphous indium selenide thin films. Optical Materials, Volume 29, Issue 12, 2007, Pages 1751-1755.
5. M.Di. Giulioab, D. Manno, R. Rella, P. Siciliano, A. Tepore. Effects of thermal annealing on optical absorption of amorphous indium selenide thin films. Solar Energy Materials, Volume 15, Issue 3, 1987, Pages 209-218.
6. Aytunç Ateş, Mutlu Kundakçı, Aykut Astam, Muhammet Yıldırım. Annealing and light effect on optical and electrical properties of evaporated indium selenide thin films. Physica E: Low-dimensional Systems and Nanostructures, Volume 40, Issue 8, 2008, Pages 2709-2713.
7. Atakishiev S., Akhundov G.A. Band structure and optical properties of graphite and the layer compounds GaS and GaSe. Phys. Stat. Sol., 1969, v. 32, p. k39-k43.
8. Fivaz R, Mooser E. Mobility of charge carriers in semiconducting layer structures. Phys. Rev., 1967, v. 163, № 3, p. 743-747.
9. Ottoviani G., Canali C., Nava F., Schmid Ph., Mooser E., Minder R., Zschokke I. Comparison of nonlinear optical properties of sulfide glasses in bulk and thin film form. Solid. Stat. Comm., 1974, v.14, p.933-936.

JOURNAL OF BAKU ENGINEERING UNIVERSITY - PHYSICS
2018. Volume 2, Number 2 *Pages 111-114*

***UOT:** 532*
PACS: 77.22.Ej, 64.75 Bc, 31.70. Dk, 61.70 Og

RHEOLOGICAL INVESTIGATIONS OF REPRESENTATIVE SOLVENTS OF AGAROSE

A.H. ASADOVA, V.V. PRUDKO, E.A. MASIMOV

aynuramrahova@gmail.com, masimovspektr@rambler.ru

ABSTRACT

In the present work the temperature dependence of the intrinsic viscosity of liquid solutions in water of agarose one of the classical representative of polysaccharides which is obtained from the red seaweed and Huggins constant (20 ˚-70 ˚C temperature interval) was investigated. It was absorbed that if we added salts to such a systems (agarose-water) the structure of system and the parameters which is characterized this system will changed as a result of different types of interaction between salt, agarose and water molecules. It is clear that at the results of this interactions there will be some changes in the properties of solution, structure and also in values of intrinsic viscosity depending on the temperature.

Key words: agarose, polymer gels, aqueous solution, Huggins constant, intrinsic viscosity, sodium salt of lemon acid.

AQAROZANIN SUDA DURU MƏHLULLARININ REOLOJI XASSƏLƏRI

XÜLASƏ

İşdə geləmələgətirən polisaxaridlərin tipik nümayəndəsi olan və qırmızı dəniz yosunlarında alınmış aqarozanın suda duru məhlullarının xarakteristik özlülüyü -[η] və Xaqqins sabitinin temperatur aslılığı (20˚C÷ 70˚C) həm saf halda, həm də limon turşusunun natrim duzu ilə təsir etdikdən sonra təyin edilmişdir.Tədqiq olunan məhlulların struktur dəyişikliyini xarakterizə edən bu parametrləri qiyməti artan temperaturla artır.Alınan nəticələr göstərir ki, aqaroza-su sistemi həllolmanın yüksək kritik temperaturuna(HYKT) malkdir.Bu işdə limon turşusunun natrium duzununyuxarıdakı parametrlərdəki dəyişikliklərin təbiətinə təsirini öyrənmişik.

Açar sözlər:aqaroza,polimer gellər, Haqqins sabiti, xarakteristik özlülük,limon turşusunun natrium duzu, sulu məhlullar.

РЕОЛОГИЧЕСКИЕ ИССЛЕДОВАНИЯ ВИДНЫХ РАСТВОРОВ АГАРОЗЫ

АННОТАЦИЯ

В работе исследовано температурная зависимости (от 20°C до 70°C) характеристическиявязкости- [η]и постоеннойХаккинса видных растворов одного из классических представителей полисахаридов полученных из красных водорослей агарозы. Значение этих параметров, характеризующая структурная изменение в исследованные растворах, увеличивается с ростом температуры. Полученные результаты показывают, что система агароза- вода имеет высшую критическую температура растворения (ВКТР).В работе изучена такие влияние натриевой соли лимонной кислоты на характер измененияевышеупомянутых параметров.

Ключевые слова: агароза, полимерные гели, водные растворы, постоянная Хаккинса, характеристическая вязкость,

Introduction

It`s kwon that, viscosity is the main parameter which is determine the structure of liquid solutions, characterised the force of friction between molecules in systems. High molecular compounds have a specific properties and also they have high viscosity than low molecular compounds. At the same time viscosity depends on the flow rate of liquid, molecular mass of polymer in such systems and the dependence on concentration is described in nonlinear expressions. Although polymer was widely used for many years, the specific characteristics

which is observed on physical and chemical properties still is completely has not been studied yet. According to the existing imaginations [1] in the solutions of macromolecules their long flexibility molecules are twisted and turned into a statistical flake. This statistical flake keeps particular solvents inside and moves together with solvent. This Motion can be chaotic (Brownian motion) or directional (diffusion). During the laminar flow the different parts of macromolecular flake in definite price of speed gradient it is exposed different fast displacement in fast and slow zones of flow. At this time, the macromolecule is under the influence of the double force that oblige it to rotate. During the rotational motion of this macromolecule in liquid fluid there happens the process which is characterized with the friction (interaction) of molecule of solvent and macromolecule`s segments and its mean that the viscosity of solution macroscopically increases than the viscosity of solvent. The increasing of viscosity as a result of rotational motion of separate molecules is estimated with the increasing of intrinsic viscosity. In some cases we can explain the decreasing of viscosity with the increasing of speed gradient or tension, as opening of flake [2,3] (macromolecule) getting conformation [14] of stick and with the orientation to the direction of liquid flood. It is known that the specific viscosity ($\eta_{sp} = \frac{\eta_{solution}-\eta_{solvent}}{\eta_{solvent}}$) of high molecule compound`s liquids goes beyond the line dependence over the concentration and the reduced viscosity ($\eta_{re}=\frac{\eta_{sp}}{c}$) doesn`t remain to a constant in many cases depends on the concentration as linearity and described with following expression

$$\frac{\eta_{sp}}{c} = \left(\frac{\eta_{sp}}{c}\right)_{c\to 0} + k` \left(\frac{\eta_{sp}}{c}\right)^2 c + \cdots \quad (1)$$

Here k`- Huggins constant [4;5]. The penetration of solvent into the statistical flake characterized the degree of resistance which is shown. The price of reduced viscosity from extrapolation of the concentration to zero is named as intrinsic viscosity or viscosity number and characterized the resistance to liquid flood by macroscopic flake at low concentrations.

2. Experimental section

2.1. Materials and methods

In the present work the temperature dependence of the intrinsic viscosity [6] of liquid solutions in water of agarose one of the classical representative of polysaccharides which is obtained from the red seaweed and Huggins constant [7] (20 ˚-70 ˚C temperature interval) was investigated. (we use the agarose of CONDA company and average molecular mass is 120000 g/mol)

Figure.1 The dependence of intrinsic viscosity and Huggins constant of aqueous solution of agarose on temperature

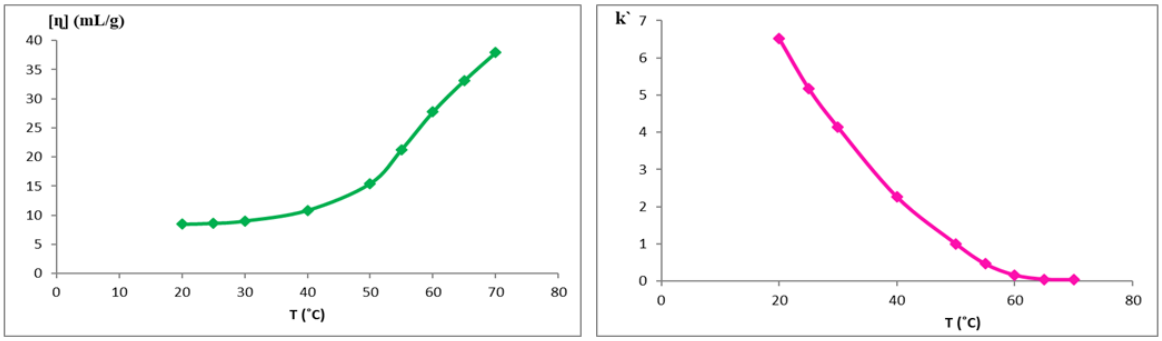

The obtaining results were shown in figure.1. As seen from the figure intrinsic viscosity increase as monotonously and the value of Huggins constant decreases in this temperature

interval. This dependence is related to the affinity of water to agarose increase with the increasing of temperature interval in agarose- water systems, so the thermodynamic quality improves (second virial coefficient A_2 increase) and the penetration of water into the statistical flake which is created by agarose macromolecule. And this process increases the volume of flake (flake swells more) its resistance to liquid flood and also increases the value of intrinsic viscosity which is determined from the experiment. It is natural that as stated above the quantity which is characterized the penetration of solvent into statistically flake is a coefficient k degreases monotonously with the increasing of temperature. Let`s note that the coefficient k`-receives rather high prices in chemical compounds with rigid molecules as the result of resistance is higher for the penetration of solvent to macromolecule. But in compounds which have flexible molecules k`-receives rather low prices fig.1. It is necessary to emphasize that with the increasing of temperature the increasing of quality of solvent it`s affinity to polymer second virial coefficient and also increasing of solution belongs to the systems which have high critical temperature of solution (HCTS). In such a systems the heat is absorbed during the solution. To prevent the increasing of temperature (Le- Chatelier`s principle) the solution process should be increased so that heat can be absorbed and the temperature increases. We absorbed that if we added salts to such a systems (agarose-water) the structure of system and the parameters which is characterized this system will changed as a result of different types of interaction between salt, agarose and water molecules. For explore this changes we determine the intrinsic viscosity [8,9,10] and coefficient-k` of agarose –water- sodium salt of lemon acid system has been studied experimentally.

3. Results

Figure.2 The dependence of intrinsic viscosity of aqueous solution of agarose+ sodium salt of lemon acid system on temperature

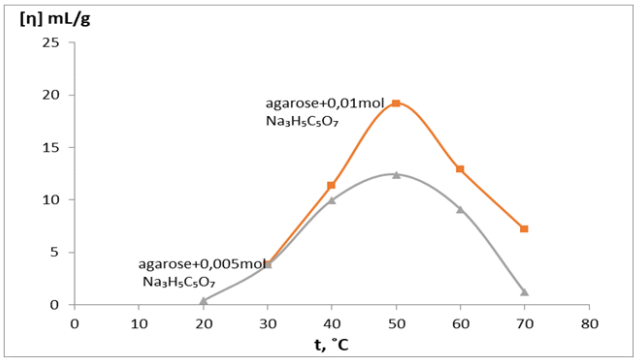

The obtaining results were shown in pictures. We can explain the obtaining results as follows. If salt is added to the agarose-water system there is different interactions between salt molecules and agarose also salt molecules and water molecules. It is clear that at the results of this interactions there will be some changes in the properties of solution, structure and also in values of intrinsic viscosity depending on the temperature [11,12].

It is well known that, the salt molecule is dissolved in the aqueous environment and separated into ions and there is formed hydrate layer around these ions. Among the molecules which are penetrated to the flake there are sodium ions (the probability of the penetration to the flake is less according to the higher sizes of salt`s onions) with its hydrate layer along with the water molecule (the number of hydrating ions define with the degree of dissociation depending on temperature). As a result of the relative decreasing the number of free water molecules

which is penetrating to the flake the increase in size is weakening and the increase of intensity of [η] gets decrease.

Let`s note that as a result of sodium ions accumulation there will be positive overload inside of flake and these ions will prevent the next sodium ions with hydrate and water to enter inside of flake and the increasing of flake`s sizes weakened and consequently the increasing of [η] weakened too.

It should be noted that Na ions will generate complex with oxygen which is in agarose molecule so hydration will be strengthened and the number of water molecules which is entering inside of flake will be decrease. As a result the flake will get narrow an [η] will be decrease. Huggins constant will be increased accordingly depending on the temperature. The processes (interactions) which is stated above [η] –T and k`-T dependencies incur to a quantitative changes.

Figure. The dependence of Huggins constant of aqueous solution of agarose+ sodium salt of lemon acid system on temperature

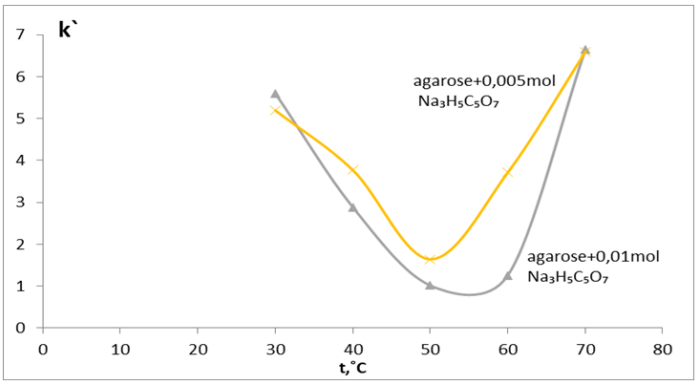

REFERENCES

[1] Уветков В.Н.,Эскин В.Е.,Френкел С.Я.//Структура макромолекул в растворах//Наука, 1964, 719с

[2] Тагер А.А., Вишвков С.А., Андреева В.М., Секачева Т.В. //Высокомолекулярная соединения.1974.Т.16.А,№1,с. 9

[3] Усков И.А., Цылляева А.М., Кленин В.И., Раевский В.С. // Высокомолекулярная соединения. 1976. Т.18.А, №1, с. 243

[4] Сибилева М.А., Тарасова Э.А. // Жур. физ. химии. 2004, т.78, №7, с. 1240-1244

[5] Boucher E.A., Hines P.M. // J.Polym.Sci. phys. Ed. 1976, V. 14. p.2241.

[6] Martin Alberto Masuelli, "Mark-Houwink Parameters for Aqueous-Soluble Polymers and Biopolymers at Various Temperatures." Journal of Polymer and Biopolymer Physics Chemistry, vol. 2, no. 2 (2014): 37-43. doi: 10.12691/jpbpc-2-2-2

[7] J. P. Holman Heat Transfer, McGraw-Hill, 2002 ISBN 0071226214 Frank P. Incropera, David P. DeWitt, Fundamentals of Heat and Mass Transfer, Wiley, N 2007, 0471457280

[8] Harding, Stephen E. The Viscosity Intrinsic of Biological Macromolecules. Progress in Measurement, Interpretation and Application to Structure in Dilute Solution. Progress in Biophysical Molecules Biological 1997; 68: 207-262.

[9] Harding, Stephen E. The Viscosity Intrinsic of Biological Macromolecules. Progress in Measurement, Interpretation and Application to Structure in Dilute Solution. Progress in Biophysical Molecules Biological 1997; 68: 207-262.

[10] Bailery F.E., Callard R.W. // J. Appl Polym. Sci 1959, V 1, p.56, 373

[11] Масимов Э.А., Пашаев Б.Г., Гасанов Г.Ш., Мусаева С.И. // Жур. физ. Химии, 2013, т.87, №12, с. 2151-2153

[12] Рафиков С.Р., Будтов В.П., Монаков Ю.Б. // Под ред. В.В. Коршака. Введение в физико-химию растворов полимеров. М. Наука, 1978. 328с

JOURNAL OF BAKU ENGINEERING UNIVERSITY - PHYSICS
2018. Volume 2, Number 2 *Pages 115-123*

UOT: 530.145
PACS No: 12.40.Yx, 12.40.Nn

THE AXIAL VECTOR MESON NUCLEON COUPLING CONSTANT g_{a_1NN} IN THE FRAMEWORK OF A SOFT-WALL MODEL ADS/QCD

N.J. HUSEYNOVA[1]

[1]Institute for Physical Problems of BSU

Baku / AZERBAIJAN

nerminh236@gmail.com

ABSTRACT

In the present paper, the interaction of the axial vector meson with nucleons is investigated in the framework of a soft-wall model AdS/QCD. Inside the Anti-de Sitter space (AdS), axial vector fields are defined by gauge fields with left and right chiral symmetries. In addition, a pseudoscalar field is introduced into the space AdS for breaking the chiral symmetry. Inside the AdS space, the Lagrangian for these fields is introduced and profile functions are found which are solutions of the equation of motion. According to AdS/CFT, the interaction constant for the axial vector meson with nucleons is obtained as an integral in the additional measurement. Our main idea is to find the numerical value of the interaction constant of the axial vector meson with nucleons in the framework of the soft wall model AdS/QCD. With the help of the computer program "Mathematics 7", these values are determined. As a result, a comparison of the theoretical and experimental data revealed significant correlations of the results.

Keywords: Anti-de Sitter space, axial vector meson, nucleon, profile function.

КОНСТАНТА ВЗАИМОДЕЙСТВИЯ g_{a_1NN} -АКСИАЛЬНОГО ВЕКТОР-МЕЗОНА С НУКЛОНАМИ В МОДЕЛИ МЯГКОЙ СТЕНЫ АДС/ КХД

РЕЗЮМЕ

В предлагаемой работе исследуется взаимодействие аксиального вектор-мезона с нуклонами в модели мягкой стены АдС / КХД. Внутри пространства Анти-де-Ситтера (АдС) с помощью калибровочных полей с левой и правой киральными симметриями определены аксиальные векторные поля. Дополни-тельно во внутры пространства АдС введено псевдоскалярное поле для нарушения киральной симметрии. Внутри пространства АдС введен Лагранжиан для этих полей и найдены профильные функции, которые являются решениями уравнения движения. Согласно АдС/КТП получено соответствие константы взаимо-действия аксиального вектор-мезона с нуклонами в качестве интеграла по дополнительному измерению. Основной задачей работы является нахождение числынных значений константы взаимодействия аксиального вектор-мезона с нуклонами в модели мягкой стены АдС/КХД. С помощъю компъютерной программы “Математика 7” определены эти значения. В результате, сопоставления теоретических и експериментaлъных данных были выявлены существенные соответствия резулътатов.

Ключевые слова: пространство Анти-де Ситтера, аксиальный вектор мезон, нуклон, профильная функция.

AdS/KXD-NİN YUMŞAQ DİVAR MODELİ ÇƏRÇİVƏSİNDƏ g_{a_1NN} AKSİAL VEKTOR MEZON-NUKLON QARŞILIQLI TƏSİR SABİTİ

XÜLASƏ

Təqdim edilən işdə a_1-aksial-vektor mezon ilə nuklonların qarşılıqlı təsiri AdS/KXD-nin yumşaq divar modeli çərçivəsində araşdırılmışdır. Anti de Sitter (AdS) fəzasının daxilində sol və sağ kiral simmetriyaya malik olan kalibrləşmə sahələri vasitəsilə aksial vektor sahə təyin olunmuşdur. Bunlardan əlavə kiral simmetriyanı pozmaq üçün psevdoskalyar X sahəsi daxil edilmişdir. Bu sahələr üçün AdS fəzasının daxilində qarşılıqlı təsir Laqranjianı yazılmış, hərəkət tənlikləri alınmış və bu hərəkət tənliklərinin həlli olan profil funksiyaları tapılmışdır. AdS/KSN uyğunluğundan və daxili AdS fəzasında yazılmış qarşılıqlı təsir Lagranjianından istifadə edərək a_1-aksial vektor mezon-nuklon qarşılıqlı təsir sabiti g_{a_1NN} üçün AdS/KXD-nin yumşaq divar modeli əsasında əlavə ölçü üzrə integral ifadə alınmışdır. İşin əsas məqsədi a_1-aksial vektor mezon-nuklon qarşılıqlı təsir sabitinin ədədi qiymətini

Manuscript receved 28.03.2018

AdS / KXD-nin yumşaq divar modeli çərçivəsində tapmaqdır. "Matematika7"proqramının köməyi ilə a_1-aksial vektor mezon-nuklon qarşılıqlı təsir sabiti g_{a_1NN} üçün ədədi qiymət alınmışdır. Nəticədə, alınmış nəticələrin məlum nəzəri və eksperimental nəticələrlə müqayisəsindən onlar arasında əhəmiyyətli uyğunluq olduğu göstərilmişdir.

Açar sözlər: Anti de Sitter fəzası, aksial vektor mezon, nuklon, profil funksiya.

I. The actuality of the subject

The study of the coupling constants and form-factors of elementary particles are the important problems in recently theoretical physics. The newly created AdS/QCD models is based on the principle of the AdS/CFT and is considered to be very effective method in the calculation of this quantity. The string theory created a connection between a gauge theory in d-dimensional space-time to a gravity theory in a (d + 1)-dimensional space-time, so, is called the theory of holographic principle of duality. An example of this duality is the most widely studied AdS/CFT correspondence principle. At the end of the last century, this principle has been successfully applied in various areas of modern theoretical physics.

Holographic principle of duality has particular significance for solving QCD problems-gauge theory of strong interactions. Since, in QCD the strong coupling constant get a high value in a small value of the transmitted momentum. So, direct application of the perturbati-ve methods to solve phenomenological problems of strong interactions impossible. Pheno-menological problems of strong interactions are coupling and decay constants, form-factors and mass spectrum. Since, application perturbative methods solving this problems impossib-le, so that this constants, form-factors and etc. calculate with the non-perturbative methods. In other side, the non-perturbative methods gives difference between calculating and experimental values of the quantity. Unlike quantum field theory AdS/QCD models, based on the principle of AdS/CFT are not occur such difficulties and shall be used to solve problems of the strong interaction without restrictions to the region energy and momentum transferred. For this reason, AdS/QCD models are being successfully applied to the study of strongly interacting quark-qluon plasma and strong interaction constants and form-factors as well [1-7].

AdS/QCD models are constructed by adding an extra direction in a original 4-dimen-sional space, which includes non-perturbative aspects such as chiral symmetry breaking and confinement. These models show that non-perturbative properties provides with a simple way. AdS/QCD models contain from the soft-wall and hard-wall models.

ϱ-vector meson-nucleon, π-meson-nucleon and a_1-axial vector meson-nucleon coup-lings constants and form-factors can be measured in practice. These constants and form-fac-tors also calculated in the framework of chiral quark model and QCD sum rules. After the establishment of AdS/QCD models these form-factors and constants are calculated in the fra-mework of these models and were compared to the results from other theoretical and experi-mental values. As part of these studies, calculation of these constants and form-factors in the framework of AdS/QCD models is advisable. Also, according to the results obtained in the framework of these models, one can say opinions about the effectiveness of the models.

In this paper, working in the framework of the soft-wall model, we calculate g_{a_1NN} the axial vector meson nucleon coupling constant in vacuum. Note, that this coupling constant has been calculated in the framework both – soft-wall and hard-wall models and for this constant there is empirical data as well, that give possibility to stand comparison with it.

The present paper was organized as follow. In **section II** we briefly present AdS/CFT correspondence principle, metrics of AdS space, equation of motions and profile functions for a_1-meson and nucleons in the framework soft-wall model AdS/QCD. In section **III,** in the framework of the soft-wall model is written the explicit form of action from the interaction lagrangian between the axial vector, psevdoscalar and fermion fields in the bulk of AdS spa-ce. Then we calculate g_{a_1NN} the axial vector meson nucleon coupling constant in vacuum in the framework of soft-wall model AdS/QCD.

II. The soft-wall model of AdS/QCD.

With $\eta_{\mu\nu} = diag(1,-1,-1,-1)$ Minkowski metrics in (x^μ, z) coordinates the d+1 dimensional AdS_5 space is written as follow:

$$ds^2 = g_{MN}dx^M dx^N = e^{2A(z)}\left(dz^2 + \eta_{\mu\nu}dx^\mu dx^\nu\right) =$$

$$= \frac{1}{z^2}\left(-dz^2 + \eta_{\mu\nu}dx^\mu dx^\nu\right)\mu,\nu = 0,1,2,\dots,d-1, \quad (1)$$

where

$$g_{MN} = \frac{R^2}{z^2}\begin{pmatrix} 1 & 0 & 0 & 0 & 0 \\ 0 & -1 & 0 & 0 & 0 \\ 0 & 0 & -1 & 0 & 0 \\ 0 & 0 & 0 & -1 & 0 \\ 0 & 0 & 0 & 0 & -1 \end{pmatrix} = \frac{R^2}{z^2}\eta_{MN}\ , \quad (2)$$

is the metric of AdS space and $\eta_{\mu\nu} = diag(1,-1,-1,-1)$- is 4-dimensional Minkowski metrics.

Axial-vector isovector current in QCD.

The vector and axial-vector currents of nucleons is occur in β-decay of nuclears and neytrons $n \to p + e^- + \tilde{\nu}_e$ and μ-capture $\mu^- + p \to \nu_\mu + n$ proceses. In such proseses there is form-factor in the interaction vertex, which is named nucleons axial-vector isovector form-factors [10].

As we know, in Quantum Chromodinamics the axial-vector isovector current is constructed with $\gamma^\mu\gamma^5$ pseudovector matrix. Thus, in QCD the axial-vector isovector current with three components is defined as follows:

$$j^{\mu,a}(x) = \bar{\psi}(x)\gamma^\mu\gamma^5\frac{\tau^a}{2}\psi(x), a = 1,2,3\ . \quad (3)$$

$j^{\mu,a}(x)$ the axial-vector isovector current operates has such propers:

1. Hermiticity requirement: $j^{\mu,a\dagger}(x) = j^{\mu,a}(x)$
2. Anticommutation requirement: $[Q_V^a(t), j^{\mu,b}(t,\vec{x})] = i\epsilon^{abc}\, j^{\mu,c}(t,\vec{x})$
3. Space inversion: $j^{\mu,a}(x) \to -j_\mu^a(\tilde{x})$, $\tilde{x}^\mu = \tilde{x}_\mu$
4. Charge conjugation: when a=1,3, $j^{\mu,a}(x) \to j^{\mu,a}(x)$ and when a=2, $j^{\mu,2}(x) \to -j^{\mu,2}(x)$.
5. The axial-vector isovector current is a partially conserved in a weak interaction: $\partial_\mu j^{\mu,a}(x) = i\bar{\psi}(x)\gamma^5\{\frac{\tau^a}{2}, \mu\}\psi(x)$, where $\psi = \begin{pmatrix} u \\ d \end{pmatrix}$ is a doublet of a u and d quark, μ is a mass matrix of a u and d quark : $\mu = diag(m_u, m_d)$.

In $m_u = m_d = m$ a exact isospin symmetry case μ matrix has a diagonal form and in one-nucleon states a matrix element of the axial-vector isovector current is defined with such structure:

$$\langle N(p')|j^{\mu,a}(0)|N(p)\rangle = \bar{u}(p')\left[\gamma^{\mu}\gamma^{5}G_A(q^2) + \frac{q^{\mu}}{2m_N}\gamma^{5}G_P(q^2)\right]\frac{\tau^a}{2}u(p), \quad (4)$$

where $q_\mu = p'_\mu - p_\mu$ is a total momentum in an interaction , m_N-is a nucleon mass. $G_A(q^2)$ and $G_P(q^2)$ respectively are called axial-vector and effective pseudoscalar form-factors.

Similarly to vector mesons and according to AdS/CFT correspondence the axial vector mesons conformity to the UV boundary value of KK modes of axial-vector gauge field. In other side, although the axial vector field include two components as $A = A_\perp + A_\parallel$, only longitudinal components has physical meaning related with pion field as follow: $A^a_{M\parallel}(x,z) = \partial_M \psi^a(x,z)$. The $A_\perp$ component is fixed with $A_5 = 0$ condition. The general action for the all fields in the bulk of AdS/QCD is written as follow [1-7] :

$$S = \int_0^\infty d^5x\,\sqrt{g}\,e^{-\Phi(z)}\,Tr\left\{|DX|^2 + 3|X|^2 - \frac{1}{4g_5^2}Tr[F_V^2 + F_A^2]\right\}, \quad (5)$$

where $X(x,z) = v(z)\frac{U(x,z)}{2}$ is a scalar field in the bulk of AdS space, $g_5^2 = \frac{12\pi^2}{N_r}$, $U(x,z) = \exp(2it^a\pi^a(x,z))$ is a chiral field term and $v(z) = \frac{1}{2}m_q z + \frac{1}{2}\sigma z^3$. The values of m_q and σ are found from the UV and IR boundary values of the solution of equations of motion for X field [1-7]:

$$S_{AdS}^{aksial} = \int_0^\infty d^5x\,\sqrt{g}\,e^{-\Phi(z)}\,Tr\left\{-\frac{1}{4g_5^2 z}A^{MN}A_{MN} + \frac{v^2(z)}{2z^3}(A_M^a - \partial_M\pi^a)^2\right\}. \quad (6)$$

Thus, according to the Higgs model the axial vector gauge symmetry is broken by including mass term depending on z to the lagrangian. After the Fourier transformation the equation of motion for the same $A^a_{\perp\mu}(x,z)$ component is find from the (6):

$$\left[z^3\partial_z\left(\frac{1}{z}e^{-k^2z^2}\partial_z\tilde{A}^a_\mu(p,z)\right) + p^2z^2e^{-k^2z^2}\tilde{A}^a_\mu(p,z) - g_5^2v^2e^{-k^2z^2}\,\tilde{A}^a_\mu(p,z)\right]_\perp = 0, \quad (7)$$

where $\tilde{A}^a_{\perp\mu}(p,z) = A(p,z)A^a_\mu(p)$ and $A(p,0) = 1$ and $A'(p,z_0) = 0$ are boundary conditions. The equation of motion for $A_n(z)$ the n-th Kaluza-Kleyn modes is written as follow [7]:

$$\left[-\frac{p^2}{z} - \partial_z\left(\frac{1}{z}\right)\partial_z + \frac{2g_5^2v^2}{z^3}\right]A_n(z) = 0. \quad (8)$$

$A(p,z) = \sum_{n=0}^\infty A_n(z)\,f_n(p)$ for $A_n(z)$ the n-th Kaluza-Kleyn modes $m_n^2 = p^2$, so the equation of motion (8) will be as follow:

$$\partial_z\left(e^{-B(z)}\,\partial_z A_n\right) + m_n^2e^{-B(z)}A_n = 0. \quad (9)$$

where $B(z) = \Phi(z) - A(z) = k^2z^2 + \ln z$ and $A_n(z)$ denoted as follow:

$$A_n(z) = e^{B(z)/2}\psi_n(z). \quad (10)$$

Thus the solution of motion for $\psi_n(z)$ is written as follow:

$$\psi_n(z) = e^{-k^2z^2/2}(kz)^{m+1/2}\sqrt{\frac{2n!}{(m+n)!}}L_n^m(k^2z^2)\,. \quad (11)$$

For a_1-meson $m = 1$ and (11) will be like this :

$$A_n(z) = k^2z^2\sqrt{\frac{2}{(1+n)}}L_n^1(\mathrm{k}^2z^2). \quad (12)$$

Thus, (12) is a expression for the profile function of the axial vector meson in the framework of soft-wall model of AdS/QCD .

Nucleons in the framework of soft-wall model of AdS/QCD

According to 4-dimensional AdS space action for a fermion fields in a 5-dimensional AdS space is written as follow[1-7] :

$$S_{s.w.} = \int d^5x\, e^{-\phi(z)}\sqrt{g}(i\bar{N}_1 e_A^M \Gamma^A D_M N_1 - (M+\phi(z))\bar{N}_1 N_1) \quad (13)$$

where the interaction between $\phi(z)$ scalar Dilaton field and spinor field is include in the last term. After the variation from the action (13):

$$\delta S_{s.w.} = \int d^5x \sqrt{g}(i\delta\bar{N}_1 e_A^M \Gamma^A D_M N_1 + i\bar{N}_1 e_A^M \Gamma^A D_M \delta N_1 - (M+\phi(z))\delta\bar{N}_1 N_1 - (M+\phi(z))\bar{N}_1 \delta N_1). \quad (14)$$

and from the (14) the equation of motion for the nucleons in the framework of the soft-wall model of AdS/QCD is written as follow:

$$ie_A^M \Gamma^A D_M N_1 - (M+\phi(z))N_1 = 0. \quad (15)$$

where $e_A^M = z\eta_A^M = z\, diag(1,1,1,1,-1)$, $\Gamma^A = (\gamma^\mu, -i\gamma^5)$, $D_M = \partial_M - \frac{i}{4}\omega_{M\,BC}\Sigma^{BC}$

$$ie_A^M \Gamma^A \left(\partial_M - \frac{i}{4}\omega_{M\,BC}\Sigma^{BC}\right)N_1 - \left(M+\phi(z)\right)N_1 = 0. \quad (16)$$

Here $\omega_{M\,BC}$ is a spin connection and its non-zero components are:

$$\omega_\mu^{5A} = -\omega_\mu^{A5} = \frac{1}{z}\delta_\mu^A \ (\mu = 0,1,2,3). \quad (17)$$

thus, from (16) equation of motion for 5D spinors was written as follow:

$$(z\gamma^5\partial_z + iz\eth - 2\gamma^5)N_1 - \left(M+\phi(z)\right)N_1 = 0. \quad (18)$$

After the writing spinors in a momentum space:

$$N_1(x,z) = \frac{1}{2\pi}\int d^4p\, e^{-ipx}[F_{1L}(p,z)\psi_{1L}(p) + F_{1R}(p,z)\psi_{1R}(p)], \quad (19)'$$

and substitution (19) in (18) one can get equation of motion for nucleons as follow:

$$\begin{matrix}\left(\partial_z^2 - \frac{4}{z}\partial_z + \frac{(6+m_5-m_5^2)}{z^2}\right)F_{1L} = -|P|^2 F_{1L} \\ \left(\partial_z^2 - \frac{4}{z}\partial_z + \frac{(6-m_5-m_5^2)}{z^2}\right)F_{1R} = -|P|^2 F_{1R}\end{matrix}. \quad (20)$$

By solving (20) equations of motions the expression for profile functions of nucleons was found with the Lager polinoms as follow[4, 6]:

$$F_{1L}^n(z) = n_{1L}\,(kz)^{2\alpha}L_n^{(\alpha)}(kz),$$
$$F_{1R}^n(z) = n_{1R}\,(kz)^{2\alpha-1}L_n^{(\alpha-1)}(kz). \quad (21)$$

There is a connection between α parameter and 5D mass: $\alpha = M + \frac{1}{2}$. α parameter also con-nect m_n mass of the n-th Kaluza-Kleyn modes with the number of modes:

$$m_n^2 = 4k^2(n+\alpha). \quad (22)$$

$n_{L,R}$ constants was found from the

$$\int_0^\infty dz \frac{e^{-k^2z^2}}{z^{2M}} F_{1L}^n F_{1L}^m = \delta_{nm}, \quad (23)$$

normalization condition and is written with the gamma functions as follow [4, 6] :

$$n_{1L} = \frac{1}{k^{\alpha-1}}\sqrt{\frac{2\Gamma(n+1)}{\Gamma(\alpha+n+1)}},$$
$$n_{1R} = n_{1L}\sqrt{\alpha+n}\,. \quad (24)$$

III. a_1-meson–nucleon coupling constant in the framework of AdS/QCD. Action for the bulk fields in AdS

In this section was calculated g_{a_1NN} the axial vector meson nucleon coupling constant in vacuum in the framework of soft-wall model AdS/QCD. After using profile functions for a_1-mesons and nucleons, the interaction lagrangian for axial-vector field, and "Mathematics"

program the numerical value for this constant was calculated in the framework of soft-wall model AdS/QCD .

For this aim we use from the expression (3) for the axial-vector current and from the action between axial-vector field and fermion fields in the bulk of AdS. In the framework of soft-wall model AdS/QCD the action is expressed with Lagrang function as follow:

$$S_{q/t}(A(q,z)) = \int_0^\infty d^4x\, dz \sqrt{g}\, e^{-\Phi(z)} \mathcal{L}_{q/t}\,, \quad (25)$$

where $\mathcal{L}_{q/t}$-is a interaction Lagrangian between axial-vector field and fermion fields in the bulk of AdS.

According to AdS/CFT similarly the vector field the expression of generating function for axial vector field in CFT will be as follow:

$$Z_{KXD}(A_\mu^a) = e^{iS_{q/t}(\tilde{A}_\mu(q,z))}. \quad (26)$$

where $\tilde{A}_\mu^a(q,z)$ is a vector field in a 5-dimensional AdS space, $\tilde{A}_\mu^a = \tilde{A}_\mu(q,z=0) = A_\mu(q)$ is $(A(q,z=0)=1)$ a ultraviolet boundary value of $\tilde{A}_\mu^a(q,z) = A_\mu^a(q)A(q,z)$ axial-vector field in a 5-dimensional space.

In other side 4-dimensional axial-vector current of nucleons in the bulk of AdS space equal by taking variation from the gravity functional generating function for the vacuum expectation value of the axial vector field:

$$< J_\mu^a >= -i \frac{\delta Z_{KXD}}{\delta \tilde{A}_\mu^a}|_{\tilde{A}_\mu^0=0}\,, \quad (27)$$

where J_μ^a - is a axial vector current for nucleons and expressed with the a_1-axial vector izo-vector form-factors as follow: $J_\mu^a(p',p) = G_A \bar{u}(p')\gamma^5\gamma_\mu \frac{\tau^a}{2} u(p)$. $\tilde{A}_\mu^a$ is a source for J_μ^a current.

Let us define the explicit form of $\mathcal{L}_{q/t}$ interaction lagrangian including (25) to calculate g_{a_1NN} the axial vector meson nucleon coupling constant. As we know, the interaction Lagrangian is contructed basing on the gauge invariance of the model. Depending on the interaction between gauge, scalar and spinor fields in the bulk of AdS, the several interaction terms in a different literature.

The total interaction lagrangian consist of the terms contributing to both vector and axial vector currents in the β-decay of nuclears and neytrons $n \to p + e^- + \tilde{\nu}_e$ and μ-capture $\mu^- + p \to \nu_\mu + n$ proceses. In our case we use only in the interaction terms producing axial-vector $\bar{\psi}(x)\gamma^\mu\gamma^5\frac{\tau^a}{2}\psi(x)$ structure in the action. We use from three interaction terms between A_M-gauge, X-scalar və $\Psi_{1,2}$ –fermion fields, which are give the contribution to the g_{a_1NN} a_1-meson-nucleon coupling as follow:

1) A minimal coupling constant term $L^{(1)}$:

$$L^{(1)} = \bar{\Psi}_1 \Gamma^M (A_L)_M \Psi_1 - \bar{\Psi}_2 \Gamma^M (A_R)_M \Psi_2 = \frac{1}{2}(\bar{\Psi}_1 \Gamma^M A_M \Psi_1 - \bar{\Psi}_2 \Gamma^M A_M \Psi_2). \quad (28)$$

These term was introduced in [5] by Hong and expressed interaction between axial vector field with the current of fermions. This interaction Lagrangian is constructed basing on the gauge invariance of the model.

2) A magnetic gauge coupling term $L^{(2)}$, expressed interaction between axial vector field with the 5-dimensional spinors in a bulk of AdS space:

$$L^{(2)} = ik_1\{\bar{\Psi}_1\Gamma^{MN}(F_L)_{MN}\Psi_1 - \bar{\Psi}_2\Gamma^{MN}(F_R)_{MN}\Psi_2\} = = \frac{i}{2}k_1\{\bar{\Psi}_1\Gamma^{MN}F_{MN}\Psi_1 + \bar{\Psi}_2\Gamma^{MN}F_{MN}\Psi_2\}. \quad (29)$$

where $F_{MN} = \partial_M A_N - \partial_N A_M$, A_M-is a field stress tenzor of a axial vector field.

These Pauli term was introduced in [1-7] by Ahn, Hong and others at first and expressed interaction between axial vector field with the magnetic moment of fermions. This interaction Lagrangian is also constructed basing on the gauge invariance of the model.

3) In [10] was introduced $L^{(3)}$term by Mamedov:

$$L^{(3)} = \frac{g_Y}{2}\{\bar{\Psi}_1 X\Gamma^M(A_L)_M\Psi_2 - \bar{\Psi}_2 X^+\Gamma^M(A_R)_M\Psi_1\} = g_Y\{\bar{\Psi}_1 X\Gamma^M A_M\Psi_2 + \bar{\Psi}_2 X^+\Gamma^M A_M\Psi_1\}, \quad (30)$$

$L^{(3)}$ is also a triple interaction of the bulk fields and hermitian and parity invariant.

Thus, axial vector current for the spinor field in the bulk of AdS space is found from the interaction lagrangian as we list above.

The 5-dimensional action is the 5D space integrals of the total $L^{(i)}$ lagrangians. The 4-dimensional integrals in Fourier components gives the δ function of energy-momentum conser vation $q = p' - p$ in a interaction vertex. Thus, the expression for the 5D current is constructed from this lagrangians as follow:

$$j^{5\mu}(p', p) = \bar{u}(p')\gamma^5\gamma^\mu\frac{\tau^a}{2}u(p). \quad (31)$$

Let us substitute the expressions of Lagrang function (28), (29) and (30) in the formula for action (25). Then after the writing expressions Fourier components for profile function of 5D spinors, 4D spinors profile functions and 5D gamma matrices in a total expression of a action continue calculating in a momentum space. After the simplicity we get expressions for action as follow:

From the minimal interaction lagrangian term $L^{(1)}$ we get $S^{(1)}$:

$$S^{(1)y/d}_{a_1NN} =$$
$$\frac{1}{2}\int d^4x\int_0^\infty dz\,\sqrt{G}\,e^{-k^2z^2}(\bar{\Psi}_1\Gamma^\mu A_\mu\Psi_1 - \bar{\Psi}_2\Gamma^\mu A_\mu\Psi_2) =$$
$$= \frac{1}{2}\int d^4p\,d^4p' j^{5\mu}(p', p)A^a_\mu(q)\int_0^\infty\frac{dz}{z^4}e^{-k^2z^2}A_n(z)\,[|F_{1R}(mz)|^2 - |F_{1L}(mz)|^2]. \quad (32)$$

From the magnetic gauge coupling term $L^{(2)}$ we get $S^{(2)}$:

$$S^{(2)y/d}_{a_1NN} = \frac{i}{4}k_1\int d^4x\int_0^\infty dz\,\sqrt{G}\,e^{-k^2z^2}(\bar{\Psi}_1[\Gamma^5,\Gamma^\mu]\partial_5 A_\mu\Psi_1 - \bar{\Psi}_2[\Gamma^5,\Gamma^\mu]\partial_5 A_\mu\Psi_2) =$$
$$= \frac{k_1}{2}\int d^4p\,d^4p' j^{5\mu}(p', p)A^a_\mu(q)\int_0^\infty\frac{dz}{z^3}e^{-k^2z^2}\big(\partial_z A_n(z)\big)\,[|F_{1R}(mz)|^2 + |F_{1L}(mz)|^2. \quad (33)$$

From the triple term $L^{(3)}$ we get expression $S^{(3)}$ as follow:

$$S^{(3)y/d}_{a_1NN} =$$
$$g_Y\int d^4x\int_0^\infty dz\,\sqrt{G}\,e^{-k^2z^2}(\bar{\Psi}_1 X\Gamma^\mu A_\mu\Psi_2 + \bar{\Psi}_2 X^+\Gamma^\mu A_\mu\Psi_1) =$$
$$= 2g_Y\int d^4p\,d^4p' j^{5\mu}(p', p)A^a_\mu(q)\int_0^\infty\frac{dz}{z^4}e^{-k^2z^2}A_n(z)\,v(z)F_{1L}(mz)F_{1R}(mz). \quad (34)$$

in (32), (33) and (34) formulas $A_n(z)$ is a profile function of a a_1-mesonun in AdS space and is defined with the formula (12).

According to holography principle, after using the total action expression $S = S^{(1)y/d}_{a_1NN} + S^{(2)y/d}_{a_1NN} + S^{(3)y/d}_{a_1NN}$, we can get integral expression for g_{a_1NN} the axial vector meson nucleon coupling constant for the ground state of nucleons. For this aim, lets take derivatives from the expressions (32), (33) and (34) respectively, $S^{(1)y/d}_{a_1NN}$ minimal interaction action, $S^{(2)y/d}_{a_1NN}$ magnetic type interaction term and $S^{(3)y/d}_{a_1NN}$ Yukava interaction term over $A^a_\mu(q)$.

Thus, we get contribution for the minimal interaction lagrangian term to a_1-meson-nucleon coupling constant $g_{a_1NN}^{(1)y/d}$ as follow:

$$1)\ g_{a_1NN}^{(1)s.w.} = \frac{1}{2}\int_0^\infty \frac{dz}{z^4} e^{-k^2z^2} A_n(z)\,[|F_{1R}(mz)|^2 - |F_{1L}(mz)|^2]. \quad (35)$$

contribution for the magnetic type interaction lagrangian term to a_1-meson-nucleon coupling constant $g_{a_1NN}^{(2)y/d}$ as follow:

$$2)\ g_{a_1NN}^{(2)s.w.} = \frac{k_1}{2}\int_0^\infty \frac{dz}{z^3} e^{-k^2z^2}\left(\partial_z A_n(z)\right)[|F_{1R}(mz)|^2 + |F_{1L}(mz)|^2]\ . \quad (36)$$

and contribution for the Yukawa interaction lagrangian term to a_1-meson-nucleon coupling constant $g_{a_1NN}^{(3)s.w.}$ as follow:

$$3)\ g_{a_1NN}^{(3)y/d} = 2g_Y\int_0^\infty \frac{dz}{z^4} e^{-k^2z^2} A_n(z)\,v(z)F_{1L}(mz)F_{1R}(mz)\ . \quad (37)$$

Thus, total expression for $g_{a_1NN}^{s.w.}$ the axial vector meson nucleon coupling constant for the ground state of nucleons in the framework of soft-wall model AdS/QCD is written as a sum of three expression as follow:

$$g_{a_1NN}^{s.w.} = g_{a_1NN}^{(1)s.w.} + g_{a_1NN}^{(2)s.w.} + g_{a_1NN}^{(3)s.w.} =$$
$$= \frac{1}{2}\int_0^\infty \frac{dz}{z^4} e^{-k^2z^2} A_n(z)\,[|F_{1R}(mz)|^2 - |F_{1L}(mz)|^2] + \frac{k_1}{2}\int_0^\infty \frac{dz}{z^3} e^{-k^2z^2}\left(\partial_z A_n(z)\right)[|F_{1R}(mz)|^2 +$$
$$+2g_Y\int_0^\infty \frac{dz}{z^4} e^{-k^2z^2} A_n(z)\,v(z)F_{1L}(mz)F_{1R}(mz). \quad (38)$$

In order to keep the clarity about each contributions of different terms of lagrangian $g_{a_1NN}^{y/d}$ to axial vector meson nucleon coupling constant in the framework of soft-wall model AdS/QCD, we calculate results for $g_{a_1NN}^{(1)y/d}$, $g_{a_1NN}^{(2)y/d}$, $g_{a_1NN}^{(3)y/d}$ separately. For this aim, we use from the "Mathematica" package. Then we compare obtained results of the values $g_{a_1NN}^{nm}$ coupling constant, with the experimental data for this coupling constant and with the ones obtained in the framework the other theoretical models. During the calculating the numerical values of k, k_1, g_Y, m_q and σ free parameters in this model are fixed. The numerical value of k parameter were determined from matching of the mass spectra of the a_1-meson and nuc-leons which were derived in the framework of soft-wall and hard-wall models with experi-mental values of the masses of these particles and was fixed as $k = 0.389\ GeV$ in [3, 8]. The numerical value of mass of u və d light quarks m_q and σ chiral condensate were taken from [5].For this parameters we use numerical values respectively, $m_q = 0.00234\ Gev$ and $(\sigma)^{1/3} = 0.311\ GeV$. The value for k_1 constant was obtained from the fitting of couplings constants π-meson-nucleon $g_{\pi NN}$ and ρ-meson-nucleon $g_{\rho NN}$ obtained in the framework of hard-wall model with the experimental data[5]. For $k_1$parameter we also use $k_1 = -0.98$ value.

The value of Yukava parameter in [5] was fixed as $g_Y = 9.182$, to get correct nucleon mass in the framework hard-wall model having fixed parameters $m_q = 0.00234\ Gev$,$(\sigma)^{1/3} = 0.311\ GeV$ and $z_m = (0.330\ Gev)^{-1}$.

In literature, there is not data of the direct measurements of the g_{a_1NN} coupling constant. It was determined from other measurements in the experiment. For example, experimental data for g_{a_1NN} coupling constant is $g_{a_1NN}^{exp.} = 4.7 \pm 0.6$, phenomenological dat is $g_{a_1NN}^{pheno.} =$ 1.5~4.5,values in the framework of soft-wall model of AdS/QCD is $g_{a_1NN}^{s.w.}$ =0.14, in the framework of hard-wall model of AdS/QCD is $g_{\rho NN}^{h.w.} = -2.93$ [1-11].

To keep the lucidity about relative different contribution terms of Lagrangian, we present the results for the $g_{a_1NN}^{(0)nm}$, $g_{a_1NN}^{(1)nm}$, $g_{a_1NN}^{(2)nm}$ and $g_{a_1NN}^{our\,r.}$ coupling constants separately in Table 1. From the comparison of the soft-wall model results with the experimental and theo-retical values provided above shows that the soft-wall model gives the results more close to the experimental data than the hard-wall model. In the excited states of nucleons the results increases as the excitation number n increases. Unfortunately, there is no experimental data for this constant for the $n \neq 0$ states, so we can't make a conclusion about which model predicts a best result. Also, from the comparison of results it can be seen that the $g_{a_1NN}^{our\,r.}$ coupling constant is more sensitive to the value of parameters σ and m_q s.

Table 1. The numerical values of $g_{a_1NN}^{(0)nm}$, $g_{a_1NN}^{(1)nm}$, $g_{a_1NN}^{(2)nm}$, $g_{a_1NN}^{y.d.}$ coupling constants for the k=0.383 GeV, $m_\rho^{y.d.} = 1.230\ Gev$, $k_1 = -0.98\ GeV^3$, $g_Y = 9.182\ GeV^3$, $\sigma = (0.311)^3 GeV^3$, $m_q = 0.00234\ GeV$ parameters.

n	m_n (GeV)	$g_{a_1NN}^{(0)nm}$	$g_{a_1NN}^{(1)nm}$	$g_{a_1NN}^{(2)nm}$	$g_{a_1NN}^{our\,r.}$	$g_{a_1NN}^{exp.}$	$g_{a_1NN}^{h.w.}$	$g_{a_1NN}^{s.w.}$
0	0.94	-0.09	-1.588	16.038	14.36	4.7 ± 0.6	1.5~4.5 -2.93 (0.42)	0.14
1	1.44	-0.068	-2.073	64.028	61.888			
2	1.535	-0.056	-2.468	143	141.4			

This work was done under the grant "BSU 50+50", so N.J.Huseynova thanks BSU for this support.

LITERATURE

1. Erlich J., Katz E., Son D.T. and Stephaov M.A. *QCD and a Holographic Model of Hadrons,* Physics Review Letters 95:261602,2005
2. Karch A., Katz E., Son D.T. and Stephanov M. A. *Linear confinement and AdS/QCD*, Physics Review D 74, 015005 (2006)
3. Abidin Z. and Carlson C.*Nucleon electromagnetic and gravitational form factors from holography,* Physics Review D 79, 115003 (2009)
4. Grigoryan H. R. and Radyushkin A. V. *Structure of Vector Mesons in Holographic Model with Linear Confinement*, Physics Review D 76, 095007 (2007)
5. Ahn H.C., Hong D. K., Park C. and Siwach S. *Spin 3/2 Baryons and Form Factors in AdS/QCD*, Physics Review D 80, 054001 (2009)
6. Hong D. K., Inami T. and Yee H. U. *Baryons in AdS/QCD,* Physics Letters B 646:165-171, 2007
7. Gherghetta T., Kapusta J. I. and Kelley T. M. *Chiral symmetry breaking in soft-wall AdS/QCD,* Phys. Rev. D 79:076003 ,2009
8. Huseynova N., Mamedov Sh. *ρ meson-nucleon coupling constant from the Soft-Wall AdS/QCD model,* Int. J. Theor. Phys., 2015, v. 54, №10, p. 3799-3810
9. Mamedov Sh., Huseynova N., Gardashova A., *Condensate dependence of profile function of axial vector meson,* GESJ: Physics, 2016, №2, p. 19-21
10. Mamedov Sh., Sirvanli B., Atayev İ., Huseynova N. *Nucleon's axial-vector form factor in the hard-wall AdS/QCD model*, Int. J. Theor. Phys., 2017, V. 56, №6, p. 1861-1874.
11. Huseynova N. *The axial vector meson-Δ baryon coupling constant from the hard-wall model of AdS/QCD model* İnternational Conference "Modern Trends in Physics" 20-22 April 2017

JOURNAL OF BAKU ENGINEERING UNIVERSITY - PHYSICS
2018. Volume 2, Number 2 *Pages 124-128*

UOT:532
PACS: 77.22.Ej, 64.75 Bc, 31.70. Dk, 61.70 Og

PEQ-LİMON TURŞUSUNUN Na DUZU-SU İKİFAZALI SİSTEMİNİN AYIRDETMƏ QABİLİYYƏTİNİN TƏYİNİ

ŞAHBAZOVA G.M., OCAQVERDİYEVA S.Y., SURXAYLI Ə.E, ŞAHVERDİYEV Y.X., MƏSİMOV E.Ə

Bakı Dövlət Universiteti

shahbazova.gunel@mail.ru

XÜLASƏ

Təqdim olunan işdə polietilenqlikol-limon turşusunun Na duzunun suda məhlulu ikifazalı sisteminin hal diaqramı qurulmuş və bu sistemin ayırdetmə qabiliyyəti (n^*) təyin edilmişdir. Daha sonra bir sıra duzların (natrium sulfat,natrium karbonat) bu sistemin hal diaqramına və ayırdetmə qabiliyyətinin qiymətinə təsiri öyrənilmişdir. Müəyyyən olunmuşdur ki, əlavə olunan duzlar (natrium sulfat,natrium karbonat) polietilenqlikol-limon turşusunun natrium duzu-su ikifazalı sisteminin hal diaqramını koordinant başlanğıcına doğru, heterogen oblastın artması istiqamətində (homogen oblastın azalması istiqamətində) sürüşdürür, yəni ikifazalı sistem komponentlərin daha kiçik konsentrasiyalarında əmələ gəlir. Eyni zamanda əlavə edilən bu duzlar (natrium sulfat,natrium karbonat) PEQ-limon turşusunun natrium duzu-su ikifazalı sisteminin ayırdetmə qabiliyyətinin (n^*) qiymətini artırmışdır.

Açar sözlər: polietilenqlikol, limon turşusunun natrium duzu, ayırdetm qabiliyyəti, natrium sulfat, natrium karbonat.

DETERMINATION OF SEPERATION ABILITY OF POLYETYLENGLICOL-SODIUM SALT OF CITRIC ACID-WATER

ABSTRACT

In this paper, we investigated the effects of some salts (sodium sulphate, sodium carbonate) on the phase diagram of the aqueous two-phase system PEQ-sodium salt of citric acid-water and its separation ability has been studied. Experimental phase diagrams and the influence of sodium sulphate and sodium carbonate to the phase diagram are presented. It was found that the phase diagram of binodals in the presence of this salts (m sulphate, sodium carbonate) are mixed in the direction of increasing the heterogeneous region (decreasing homogeneous region) of the phase diagram.İn other words, the separation of phases process occur at low (high) concentration of polymer and salt which formed phases. At the same time, these salts have increased the value of separation ability of PEQ-sodium salt of citric acid-water.

Keywords: polyetylenglicol, sodium salt of citric acid, separation ability, sodium sulphate, sodium carbonate.

ОПРЕДЕЛЕНИЕ РАЗДЕЛИТЕЛЬНОЙ СПОСОБНОСТИ ПОЛИЭТИЛЕНГЛИКОЛЬ-НАТРИЕВАЯ СОЛЬ ЛИМОННОЙ КИСЛОТЫ-ВОДА

РЕЗЮМЕ

В этой статье мы исследовали влияние некоторых солей (сульфата натрия, карбоната натрия) на фазовую диаграмму водной двухфазной системы ПЭГ-натриевая соль лимонной кислоты-вода и ее разделительную способность. Представлены экспериментальные фазовые диаграммы и влияние сульфата натрия и карбоната натрия на фазовую диаграмму. Было обнаружено, что фазовая диаграмма бинодалей в присутствии этих солей (сульфат натрия, карбонат натрия) смешивается в направлении увеличения гетерогенной области (уменьшение гомогенной области) фазовой диаграммы. Другими словами, разделение фаз протекает при низкой (высокой) концентрации полимера и соли, в которых образуются фазы. В то же время эти соли повысили значение разделяющей способности ПЭГ -натриевой соли лимонной кислоты-воды.

Ключевые слова: полиэтиленгликоль, натриевая соль лимонной кислоты, разделительной способност, сульфат натрия, карбонат натрия.

İkifazalı sulu polimer sistemləri ilk dəfə geniş XIX əsrin ortalarında Isveç tədqiqatçısı P. O.Albertson |1| tərəfindən tədqiq edilmişdir. O, göstərmişdir ki, zülallar, nuklein turşuları və

Manuscript receved 11.04.2018

s. kimi bioloji mənşəli maddələri, hüceyrə, virus və s. kimi bioloji hissəcikləri ikifazalı sistemlərdə həll etdikdə, həmin maddələrin sistemin eyni zamanda tarazlıqda olan fazaları arasında qeyri-bərabər paylanması baş verir ki, bu da həssas və dayanıqsız struktura malik olan bioloji maddələrin hissəciklərini, onların nativ xüsusiyyətlərini saxlamaqla, əldə etməyə imkan verir. Belə ki, ikifazalı sulu sistemlərin hər iki fazasının əsasını su təşkil etdiyindən bu sistemlərdən bioloji hissəcikləri yumşaq ayırmaq məqsədlə istifadə etmək çox əlverişlidir. İkifazalı sistemlərin, eyni zamanda mövcud olan və bir-birindən hidrofobluqlarına görə fərqlənən fazaları arasında bioloji maddələrin paylanmasının araşdırılması, çoxkomponentli, çoxfazalı sistem olan canlı orqanizmdə gedən bir sıra proseslərin o cümlədən maddələr mübadiləsi prosesinin bəzi məqamlarına aydınlıq gətirə bilər. İkifazalı sistemlərin əsas spesifik cəhəti də məhs onların fazalarının tərkiblərinin insan orqanizminin 75-80% ni təşkil edən sudan ibarət olmasıdır.

Məlum olduğu kimi, canlı orqanizmin əsas hissəsini su və yüksəkmolekullu birləşmələr təşkil edir və orqanizmdəki maddələr mübadiləsi əsasən qan vasitəsi ilə həyata keçirilir. Çox komponentli çox fazalı sistem olan canlı orqanizmdə gedən proseslərin ən sadə modelini yaratmaq üçün ikifazalı polimer-polimer-su sistemlərindən istifadə etmək olar. Doğrudan da, ikifazalı polimer-polimer-su sisteminin eyni zamanda tarazlıqda olan fazalarının əsas hissəsini su və polimerlər təşkil edir. Bu fazalar bir-birindən polimer tərkibi ilə fərqləndikləri kimi maddələrin qeyri bərabər paylanmasını təmin edən əsas şərtlərdən biri olan hidrofobluqları ilə də fərqlənirlər. Qeyd edək ki, aparılmış çoxlu sayda tədqiqatlar göstərmişdir ki, |1| tədqiq olunan sistemlər qanda mövcud olan çox cüzi dəyişikliyi (xəstəlik və ya şüalandırma zamanı) hiss edir və bu dəyişikliyin baş vermə səbəblərini keyfiyyətcə izah etmək olur |2,6|. Məlum olduğu kimi,belə sistemlərdə müxtəlif maddələrin qeyri-bərabər paylanması həmin maddələrin sistemin fazalarının su mühitləri ilə hidrofob və hidrofil qarşılıqlı təsirininin müxtəliflikləri ilə əlaqədardır. Əgər həll olunan maddə hidrofob fazaya yığılırsa bu maddə nisbi hidrofob, əks halda isə hidrofil olur. Xarici amillərin təsiri ilə (şüalanma və ya hər hansı patalogiya) paylanma dəyişirsə, onda həmin maddə molekullarında baş vermiş konformasiya dəyişməsi və buna uyğun hidrofob qarşılıqlı təsirin dəyişməsi barədə mülahizələr yürütmək olar. Başqa sözlə, ikifazalı sulu polimer sistemlərində paylanma metodu ilə nəinki, xəstəliyi qeyd etmək, həmçinin, xəstəliyin yaranması mexanizmi barədə müəyyən fikirlər söyləmək olar. Polimer-polimer-su ikifazalı sistemlərində paylanma metodu bioloji hissəciklərin təmizlənməsi üçün effektiv bir metod kimi də geniş istifadə olunur |1|. Böyük məhsuldarlığa və keyfiyyətə malik olan bu metoddan daha geniş və effektiv istifadə etmək üçün yeni sistemlərin axtarışı, tədqiqi və tətbiqi çox vacibdir |4,6|. İkifazalı polimer-su sistemlərində paylanma metodundan zülalların və digər bioloji hissəciklərin səth xassələrini, zülalların quruluşunu və konformasiyasını tədqiq etmək üçün |2,4| analitik metod kimi də istifadə etmək olar. Bu metodun daha səmərəli tətbiqi üçün homogen sistemin (məhlulun) fazalara ayrılmasının və paylanan maddələrin paylanma mexanizmlərinin molekulyar aspektlərinin təhlili də böyük maraq kəsb edir. Aparılmış çoxlu sayda tədqiqat işlərinin nəticələri onu göstərir ki, biomakromolekulların və eləcə də kiçik molekullu birləşmələrin ikifazalı sistemdə paylanması sistemin eyni zamanda mövcud olan fazalarının su mühitinin müxtəliflfyi ilə müəyyən olunur. Ədəbiyyatda |5,7| polimer-polimer-su ikifazalı sistemlərindən dekstran-polietilenqlikol-su, dekstran-fikoll-su və dekstran-polivinilpirrolidon-su sis-temləri, PVP-qeyri-üzvi elektrolit ikifazalı sistemlərinin də bəziləri qismən tədqiq olunmuşdur |5,9|. İkifazalı sistemin eyni zamanda mövcud olan fazalarının su mühitinin strukturunun müxtəlifliyi özünü maddənin bir fazadan digərinə keçməsi zamanı sərbəst enerjinin müxtəlif cür dəyişməsində biruzə verir. Bu enerjilərin kəmiyyətcə qiymətləndirilməsi üçün B.Y.Zaslavski və E.Ə.Məsimov yeni metod işləyib hazırlamışdır |10 |. Bu metodda marker maddələr kimi dinit-

rofenilləşdirilmiş amin turşularının homoloji sırasının paylanması təklif olunmuşdur. Alınan nəticələr göstərmişdir ki, marker maddələrin paylanma əmsalının loqarifmi (K = $\frac{C^I}{C^{II}}$, burada C^I və C^{II} paylanan maddənin ikifazalı sistemin fazalarındakı çəki konsentrasiyalarıdır) markerlərdəki metilen qruplarının sayından (n_{CH_2}) asılılığı aşağıdakı xətti funksiya ilə təsvir olunur:

$$\ln K = C + En_{CH_2} \quad (1)$$

Burada C marker molekulunda dəyişməyən hidrofil qrupunun fazalararası keçid sərbəst enerjisini, E isə metilen qrupununun fazalararası keçidsərbəst enerjisini xarakterizə edən əmsaldır. Belə ki,

$$K = \frac{C^I}{C^{II}} = e^{\frac{G}{RT}} \quad (2)$$

məlum ifadəsini nəzərə alsaq,

$$RT\ln K = \Delta G = RTC + RTEn_{CH_2} \quad (3)$$

yaza bilərik. Burada bütöv marker molekulunun bütövlükdə RTC və $RTEn_{CH_2}$ isə uyğun olaraq markerin dəyişməyən hidrofil qrupunun və bir metilen qrupunun ikifazalı sistemin fazalararası keçid sərbəst enerjisini göstərir.

Şəkil1. Müxtəlif ümumi tərkibli ikifazalı sistemlər üçün $lnK - n_{CH_2}$ asılılığı.

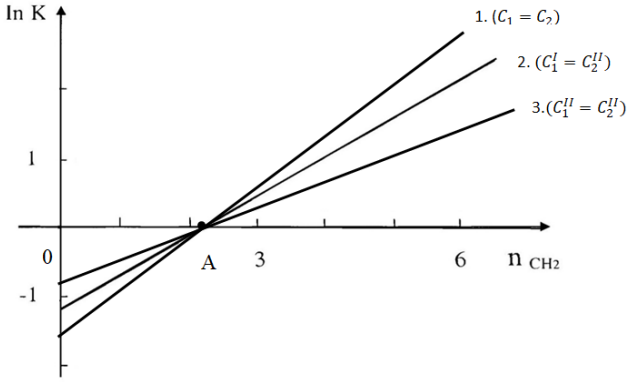

Lakin müəyyən olunmuşdur ki, (3) asılılığındakı həm C, həm E kəmiyyətləri ikifazalı sistemin ümumi tərkibindən (1,2,3 xəttləri) asılıdır. Müxtəlif ümumi tərkibli ikifazalı sistemlər üçün $lnK - n_{CH_2}$ asılılığı şəkil 1-də verilmişdir. Şəkildən göründüyü kimi bu asılılıqlar absis oxunu eyni A nöqtəsində kəsirlər. Bu nöqtədə ($n_{CH_2} = n^*_{CH_2}$) lnK=0, K= $\frac{C^I}{C^{II}}$ = 1; $C^I = C^{II}$ olur, yəni paylanan maddənin konsentrasiyası hər iki fazada eyni olur. Göründüyü kimi, n*- DNF molekulunda metilen qruplarının elə hipotetik sayıdır ki, molekul sistemin fazalarında bərabər paylanır. Bu onu göstərir ki, ion və hidrofob hidratasiyaların (C,E) lnK-ya payları bərabər və əks işarəli olub bir-birini kompensə edirlər. Göründüyü kimi C və E-dən fərqli olaraq $n^* = -\frac{C}{E}$ kəmiyyəti verilmiş ikifazalı sistemi almaq üçün götürülmüş ümumi tərkibdən asılı deyil, yəni, sistemi birqiymətli xarakterizə edə bilər. n* kəmiyyəti müxtəlif ikifazalı sistemləri bir-birləri ilə müqayisə etməyə imkan verir. Bununla yanaşı n* kəmiyyətinin qiymətində paylanan maddə ilə fazaların komponentləri arasında mövcud olan bütün qarşılıqlı təsirlər nəzərə alınır.

n* kəmiyyəti ikifazalı sistemi xarakterizə edən ən vacib parametrlərdən biri olub sistemin ayırma və ya ayırdetmə qabiliyyətinin göstəricisidir. İşdə PEQ-$C_6O_7H_5Na_3$-H_2O ikifazalı sis-

teminin ayırdetmə qabiliyyəti və müxtəlif əlavələrin bu kəmiyyətin qiymətinə təsirləri yuxarıda qeyd olunan metodla təyin edilmişdir. Şəkil 2-də markerlərin DNF amin turşularının PEQ-limon turşusunun Na duzu-su sistemində paylanma əmsallarının loqarifminin markerlərin yan zəncirindəki metilen qruplarının (karbon atomlarının) sayından asılılığı göstərilmişdir. Şəkildən göründüyü kimi, bu asılılıq xəttidir ((1)tənliyinə uyğun olaraq).

Şəkil2. 1)PEQ-$C_6O_7H_5Na_3$-H_2O ikifazalı sistemi üçün amin turşularının paylanma əmsalının loqarifminin yan zəncirdəki metilen qruplarının sayından asılılığı; 2) Na_2SO_4-ün təsiri; 3) Na_2CO_3-ün təsiri

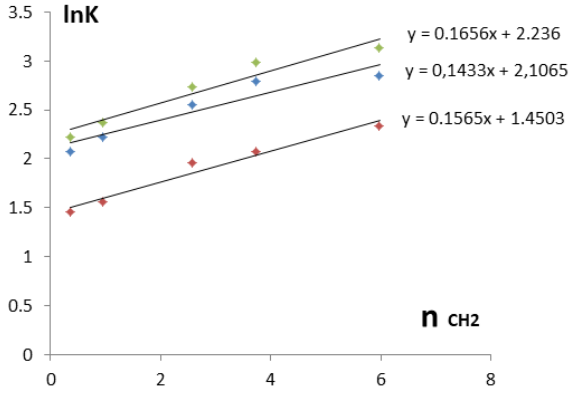

Məlumdur ki, ikifazalı sistemləri tədqiq etmək üçün onların hal diaqramları (binodalları, birləşdirici xəttləri və s.) qurulur. İkifazalı sistemlərin konsentrasiyaları arasındakı asılılığı (C_{PEQ}-$C_{Nalimon}$) xarakterizə edən binodal əyri sistemin homogen (birfazalı) hissəsi ilə heterogen (ikifazalı) oblastlarını bir-birindən ayırır. Tədqiq etdiyimiz PEQ-$C_6O_7H_5Na_3$-H_2O ikifazalı sisteminin hal diaqramı və ona natrium sulfat və natrium karbonat duzlarının təsiri 3-cü şəkildə göstərilmişdir. Ayırdetmə qabiliyyətinin, C və E kəmiyyətlərinin qiymətləri cədvəl1-də göstərilmişdir.

Şəkil3. 1-PEQ-$C_6O_7H_5Na_3$-H_2O ikifazalı sisteminin hal diaqramı ; 3- hal diaqramına Na_2CO_3-ün təsiri (n*=13,5); 2-Na_2SO_4-ün təsiri (n*=14,7)

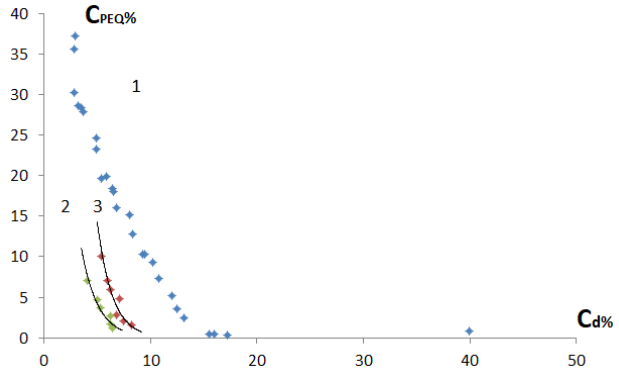

Cədvəl 1

Sistem	n*	C	E
PEQ-limon turşusunun Na duzu-su	9,3	1,461	0,1565
PEQ-Nalimon-su+Na_2CO_3-su	13,5	2,236	0,1656
PEQ-Nalimon-su+Na_2SO_4-su	14,7	2,1124	0,1433

Nəticə. Şəkildən göründüyü kimi, əlavə olunan duzlar (natrium sulfat, natrium karbonat) polietilenqlikol-limon turşusunun natrium duzu-su ikifazalı sisteminin hal diaqramını koordinant başlanğıcına doğru, heterogen oblastın artması istiqamətində (homogen oblastın azal-

ması istiqamətində) sürüşdürür, yəni ikifazalı sistem komponentlərin daha kiçik konsentrasiyalarında əmələ gəlir. Bu o deməkdir ki, baxılan duzlar suyun strukturunu strukturlaşdıran faktor kimi çıxış edir. Nəticədə sərbəst su molekullarının sayı azalır, faza əmələ gətirən komponentlərin həllolması çətinləşir və fazalara ayrılma komponentlərin daha kiçik konsentrasiyalarında baş verir. Eyni zamanda əlavə edilən bu duzlar (natrium sulfat, natrium karbonat) PEQ-limon turşusunun natrium duzu-su ikifazalı sisteminin ayırdetmə qabiliyyətinin (n^*) qiymətini artırmışdır.

Qeyd etmək lazımdır ki, bioloji hissəciklərin «incə» və «kobud» ayrılması nöqteyi nəzərindən bu sistem «incə» ayrılma üçün məqsədə uyğundur. Belə ki, ayırma (ayırdetmə) qabiliyyəti böyük olan ikifazalı sistemdə paylanma metodu vasitəsi ilə bir-birindən hidrofobluqlarına görə kəskin fərqlənən maddələri ayırdıqdan sonra («kobud» ayırma) hidrofobluqlarına görə bir-birindən az fərqlənən maddələri ayırmaq üçün («incə» ayırma) ayırma qabiliyyəti kiçik olan ikifazalı sistemdən istifadə etmək məqsədə uyğundur.

İkifazalı polimer-duz-su sistemlərində də maddələrin qeyri-bərabər paylanması ikifazalı polimer-polimer-su sistemlərində olduğu kimi sistemin eyni zamanda mövcud olan fazalarının müxtəlif hidrofobluğa malik olması ilə əlaqədardır. Bu sistemlərdə paylanılan maddələrin fəza quruluşunda istənilən dəyişiklik özünü həmin maddənin su ilə qarşılıqlı təsirində büruzə verir və maddənin hidrofobluğu kəmiyyətcə dəyişir. Sistemin eyni zamanda mövcud olan fazalarının nisbi hidrofobluqlarını bilməklə paylanılan maddənin hidrofobluğu haqqında mülahizələr yürütmək olar.

Ədəbiyyatdan məlum olduğu kimi polimer-su ikifazalı sistemlərində paylanma metodundan bəzi xəstəliklərin ilkin diaqnozu məqsədi ilə istifadə oluna bilər. Digər tərəfdən bəzi xəstəliklərin yaranması və sağalma mexanizmi haqqında da bəzi mülahizələr yürütmək olar.

ƏDƏBİYYAT

1. Альбертсон П.. Разделение клеточных частиц и макромолекул. - М.: Мир, 1974, 381 с.
2. Zaslavsky B. Aqueous Two-Phase Partitioning: Physical Chemistry and Bioanalytical Applications, Marcel Dekker, New York, 1994, -212 p
3. Məsimov E. Bioloji sistemlərdə suyun rolu. Hidrofobluq, monoqrafiya, Bakı, 2008, 328 s.
4. Masimov E., Bagirov T., Zaslavsky B. Separation ability of aqucous polymer two-phase systems // Journal of Qafqaz Universitety, 2007, № 19, p.26-2
5. Masimov E., Makhmudov A., Bagirov T., Gasanova G. The blood plasma distribution in aqueous two-phase polymer systems / IV Европейскаяконф. Биохроматографияимолек. биология, France, Grand Momne, 1992, p.241.
6. Багиров Т., Масимов Э., Алиева Н. Распределение сыворотки крови онкологических больных в водных двухфазных системах / Fizikanın aktual problemləri, II resp. elmi konf., Bakı, 2001, s. 125.
7. Məsimov E., Bağırov T., Mahmudov A.., Zaslavski B. Maye məhlullarda fazalara ayrılma, Journal of Qafqaz Universitu, 2008 №21, səh.77-88.
8. Bağırov T. İkifazalı sulu polimer sistemləri və onların əsas xarakteristikaları, Bakı, BDU, 2005 56 s.
9. S.Y. Ojagverdieva. Candidate's dissertation, Baku, 2015
10. Заславский Б.Ю., Масимов Э.А., Михеева Л.Б. Способ оценки относительной гидрофобности водных растворов полимеров. ДАН СССР,1981, 261, стр. 657.
11. Bağırov T., Həsənova X., Hüseynli A., Məsimov E. PVP-$C_4O_6H_4Na_2$-H_2O ikifazalı sistemlərinin hal diaqramlarına xarici amillərin təsiri // Bakı Universitetinin Xəbərləri, fizika-riyaziyyat elmləri seriyası, 2005 №1, s.129-133.
12. Məsimov E., Bağırov T. İkifazalı su-polimer sistemlərində paylanma metodu vasitəsilə makromolekulların nisbi hidrofobluqlarının tədqiqi. // AMEA-nın Xəbərləri, fizika-riyaziyyat və texnika elmləri seriyası, fizika və astronomiya, 2006, XXVI cild №5, s.132-140.

JOURNAL OF BAKU ENGINEERING UNIVERSITY - PHYSICS
2018. Volume 2, Number 2 *Pages 129-133*

UOT 669.859.232:539.219.3
PACS: 66.30.Ra;66.30.xj;66.70.Lm

THE DIFFUSION OF BISMUTH ATOMS INTO MONOCRYSTAL RHENIUM

A. K. ORUJOV
Baku State University,
Baku, AZERBAIJAN
orar@mail.ru

ABSTRACT

It was first revealed by thermodesorption spectroscopy that when bismuth atoms diffuse the bismuth atoms through an intermediate graphite layer, they show certain characteristic features. In the Re(1010)–C system at 1400 K <*T* < 1600 K we witness the most strong form of diffusion of bismuth into rhenium. It has been found that the fractions of the fluxes of intercalation equal to δ = 0.45 ± 0.05 and diffusion $\delta_{Bi} = N_{dif}/N = 2{,}3\times10^{-3}$ bismuth atoms in the Re(1010)–C system. The amount of intercalated and diffused bismuth depends on the electrical field, i.e., on the positive potential in the Re(1010)–C system. It has been noted that a considerable diffusion of bismuth into rhenium started at 100 V and increased up to 3000 V. The activation energies for bismuth diffusion into and from rhenium were calculated to be E_{n1}= 5.95 ± 0.05 eV and E_{1n}= 6,1 ± 0.1 eV, respectively.

Keywords: Graphite Monolayer, Diffusion, Intercalation, Surface Ionization, Thermo electronic emission.

MONOKRİSTAL RENİUMA BİSMUT ATOMLARININ DİFFUZİYASI

XÜLASƏ

İlk dəfə termodesorbsiya spektroskopiyası metodu ilə göstərilmişdir ki,qrafit monotəbəqəsi ilə örtülmüş reniuma bismut atomları diffuziya edə bilıır. Re (1010) – C sistemində bismutun reniuma diffuziyası ən çox 1400 K <T <1600 K oblastına uyğun gəlr. İnterkalyasiya və diffuziya edən bismut atomlarının nisbi miqdarı üçün δ = 0,45 ± 0,05 və $\delta_{Bi} = N_{dif} / N = 2{,}3 \times 10^{-3}$ qiymətləri alınmışdı.Bu miqdarlar elektrik sahəsinin intensivliyindən,başqa sözlə tətbiq edilən gərginlikdən asılıdır.Müəyyən edilmişdir ki,diffuziya gərginliyin 100V qiymətindən başlayır və 3000V-a qədər artırdıqca duffuziya da artır. Bismutuun renima diffuziyasının və ondan əks diffuziyasının aktivləşmə erjiləri üçün uyğun olaraq E_{n1} = 5,95 ± 0,05 eV və E_{1n} = 6,1 ± 0,1 eV qiymətləri alınışdır.

Açar sözlər: qrafit monotəbəqəsi, diffuziya, interkalyasiya, səthi ionlaşma, termoelektron emissiyası.

ДИФФУЗИЯ АТОМОВ БИСМУТА В МОНОКРИСТАЛЛИЧЕСКИЙ РЕНИЙ

РЕЗЮМЕ

Впервые методами термодесорбционной спектроскопии показана, что атомы висмута диффундируют в рений покрытой монослоем графита.. В системе Re (1010) – С при 1400 K <T <1600 K наблюдается наиболее сильная диффузия висмута в рений. Установлено, что доля потоков интеркаляции в системе Re (1010) –С равна δ = 0,45 ± 0,05 и диффузии $\delta_{Bi} = N_{dif} / N = 2{,}3 \times 10^{-3}$. Количество интеркалированного и диффузионного висмута зависит от электрического поля, то есть от положительного потенциала в системе Re (1010) –С. Отмечено, что значительная диффузия висмута в рений началась при 100 В и увеличилась до 3000 В. Для энергии активации диффузии висмута в рений и из него были получены E_{n1} = 5,95 ± 0,05 эВ и E_{1n} = 6,1 ±. 0,1 эВ соответственно.

Ключевые слова: монослой графита, диффузия, интеркаляция, поверхностная ионизация, термоэлектронная эмиссия.

Introduction

The investigation of the diffusion of sodium, potassium, cesium, samarium, and barium atoms into rhenium via an intermediate graphite monolayer [1–6] demonstrates that the diffusion process depends both on the ionic state of atoms on the Re–C surface as well as the state of the external electronic shell and the valence of the element. Na, K, and Cs are the group

Manuscript receved 10.08.2018

I elements with the ground states of the valence electrons $3s^1$, $4s^1$, and $6s^1$, respectively. The ground state of the samarium external shell is $4f^6 6s^2$, and for Ba, the Group II element, $6s^2$. Bismuth is the Group V element with the ground state of the valence electron $4f^{14}5d^{10}6s^2 6p^3$; from the perspective of interaction with the Re(1010) and Re(1010)-C surfaces, it holds an intermediate position between K, Cs, and Ba. The ionization potential of bismuth is higher than that of Na and Ba. As a consequence, it is essential to study bismuth diffusion into rhenium upon the irradiation of the Re-C system by a flux of bismuth atoms. The main purpose of this work is to study the diffusion of bismuth atoms in the Re(1010)-C system, determination of the activation energy of bismuth diffusion into and from rhenium, as well as to determine the concentration of diffused atoms compared to other elements.

Experimental

The measuring was conducted in an ultrahighvacuum magnetic mass spectrometer of sector type with the angle of deflection of the ion trajectory equal to 90°ata residual pressure of 1.10^{-10} Torr. A detailed description of the experimental setup is presented elsewhere [1–7]. Rhenium was taken in the form of a thin textured tape 50 ×1.5 ×0.3 mm^3 with the major face (1010) with the work function $\varphi = 5{,}1eV$ [8]. The graphite monolayer was obtained by exposure of rhenium heated to 1750 K in benzene vapors at a partial pressure from 10^{-4} to 10^{-6} Torr. The benzene molecules C6H6 do not dissociate on the valence saturated surface of the graphite monolayer and, therefore, do not modify its thickness. Bismuth was sprayed onto the Re–C surface from a Knudsen cell, and its state in the adlayer was studied by the method of thermodesorption spectroscopy (TDS) in the flash thermodesorption mode with the mass spectrometric registration of the current of Bi ions. In order to revealintercalated bismuth, the flash was performed at the rate of 100 K/s up to 2300 K (lower than the melting point 2683 K of the rhenium tape) and then the current of Bi ions was recorded at a constant T. Every time at so high a temperature, graphite islands in the adlayer on rhenium become dissolved carbon flies away, and the freed intercalated and diffused atoms are desorbed in the form of Bi^+ ions. The neutral component of the flux desorbed during the flash was ionized in an electron impact source before the entrance into the mass analyzer. The data related to the thermionic emission and dissociation of CsCl molecules were also utilized for the surface analysis.

Results and Discussion

Fig. 1. Logarithm of the amount (number) N of intercalated bismuth atoms as a function of the logarithm of the flux of bismuth atoms, $\log(N \times 10^{-9}) = f(\log(\nu \times 10^{-9}))$.

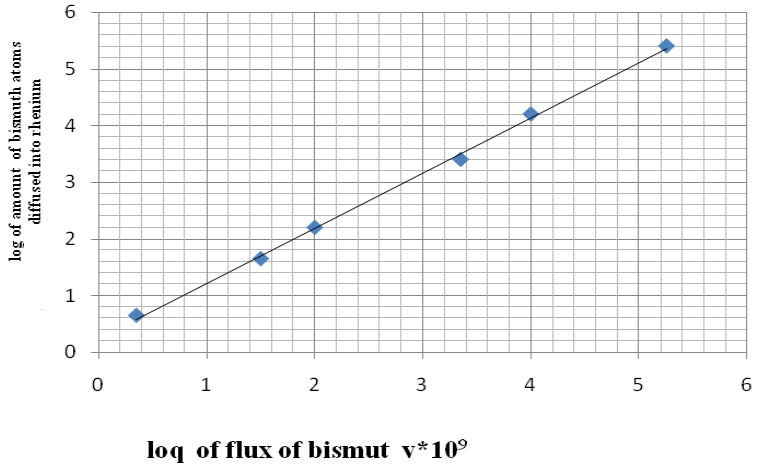

Over the process of irradiation of Re(1010)–C heated by a flux of bismuth atoms, with a flux density of ν= (10^{10}–10^{14}) sm^{-2} s^{-1}, to T ≤1800K, there was observed an intercalation of bismuth atoms into the graphite monolayer on rhenium and diffusion of bismuth into rhenium. As the flux increased from 10^{10} to 10^{14} sm^{-2} s^{-1}, the amount of intercalated bismuth increased linearly (Fig. 1). The amount of diffused bismuth increased strongly at high fluxes of ν= (10^{13}–10^{14}) sm^{-2} s^{-1} and sufficiently high temperatures of Re–C (T = 1400–1600 K). Upon irradiation of Re(1010)–C heated to T =1600 K by a flux of bismuth atoms with a high density of ν≈$10^{14}$$sm^{-2}$ s^{-1} in t = 5, 10, 15 min, etc., the amount of intercalated bismuth was hundreds times lower than that in the diffusion zone. The length of the diffusion phase was also significantly higher than that of the bismuth intercalation phase. The thermodesorption of Bi^+ ions from the Re(1010)–C system started at 1800 K, i.e., before the vaporization of the graphite monolayer. With an increase in the exposure temperature of Re–C from 1600 to 1800 K, the amount of diffused bismuth decreased. The most intensive diffusion of bismuth into rhenium occurred at T = 1400–1600 K in the Re(1010)–C system. From a comparison of the amount of bismuth atoms $N = \nu t$ incident onto the Re(1010)–C surface heated to T = 1600 K in a time t with the amount of bismuth diffusing from rhenium as determined by the TDS analysis of Bi^+ ions, we found that the fraction of the flux of bismuth atoms diffusing into rhenium is δ_{Bi} = ≈2 × 10–3. The fraction of the flux of bismuth atoms diffusing into rhenium was determined from the comparison of the Cs^+ and Bi^+ ions thermodesorbed from Re(1010)- C using the known value δ_{Cs}= 0.25 [2]. Under equal conditions of exposure of Re–C in the fluxes of bismuth and cesium atoms, the ratio of the amounts of diffusing atoms can be determined as the ratio of the fraction of the fluxes of Bi and Cs diffusing into rhenium: From the comparison of the areas under the TDS peaks of Bi^+ and Cs^+ ions, we found that γ_{Bi} ≈5.2 ×10^{-3}. Then, δ_{Bi}≈1.3 ×10^{-3}, which is in good agreement with the above mentioned estimate of δ_{Bi} into rhenium. From the TDS analysis of Bi^+ ions arising upon the electrons ionization of the flux of bismuth atoms desorbed from the rhenium surface and from the Re–C system, we determined the fraction in a flux of bismuth atoms characteristic of those atoms that pass into the intercalated state under the graphite monolayer on irridium at room temperature. To do this, we recorded the amount of Bi^+ ions thermodesorbed from the rhenium surface in a definite time of irradiation of the rhenium tape by the flux of bismuth atoms with a definite density. Then, under the same conditions, we irradiated Re(1010)-C and again recorded the amount of thermodesorbed bismuth ions. From the comparison of the area under the peak from the bismuth atoms thermodesorbed from the rhenium with the area under the peak corresponden to the intercalated atoms thermodesorbed from Re(1010)-C, we found the fraction of the flux of intercalated bismuth atoms in the Re(1010)-C system to be $\bar{\delta} = 0{,}45 \pm 0{,}05$. Thus, at room temperature from the flux of bismuth atoms falling onto Re(1010)–C only approximately one of three bismuth atoms becomes intercalated into the graphite monolayer. From the TDS analysis it follows that the amount of the bismuth atoms desorbed from the rhenium surface is equal to the sum of the bismuth atoms desorbed from the Re(1010)–C surface, on the one hand, and the bismuth atoms intercolated upon the preliminary irradiation of Re and Re(1010)–C by this flux within the same exposure time, on the other. This demonstrates that at room temperature it is possible to neglect the diffusion of bismuth atoms into rhenium. The TDS analysis of Bi^+ ions showed that at the irradiation of Re(1010)–C heated to T ≤1600 K by a flux of bismuth atoms with a density of ν≈$10^{14}$$sm^{-2}$ s^{-1} the amount of intercalated and diffused bismuthatoms depends on the positive potential of Re(1010)–C, i.e., on the electric field. The noticeable diffusion of bismuth into rhenium

started at 180 V and increased with increasing field up to 3000 V. For instance, as the voltage increased from 180 V to 3000 V the amount of intercalated bismuth increased by a factor of three, while the amount of diffused bismuth increased by a factor of 10^3. In another series of experiments aiming at the study of the possibility of using rhenium as a source of atoms and ions of bismuth, we performed the irradiation of Re(1010)–C heated to T = 1550 K by a flux of bismuth atoms with a density of $\nu \approx 10^{14}$ sm^{-2} s^{-1} in a time of up to t = 30 h. The values of the flux of bismuth atoms diffused from rhenium at T = 2100 K after the exposure of Re–C under aforementioned conditions for various exposure time periods are given in the table.

Table

t,h	**0,5**	**1**	**1,5**	**2**	**2,5**	**3**
$\nu \cdot 10^{-9}\, sm^{-2} s^{-1}$	**4,2**	**10,5**	**15,8**	**32,3**	**50,2**	**56**

Fig. 2. Logarithm of the ionic current of bismuth has a function of the reciprocal temperature, $\ln I^{+}_{Bi} = f(1/T)$.

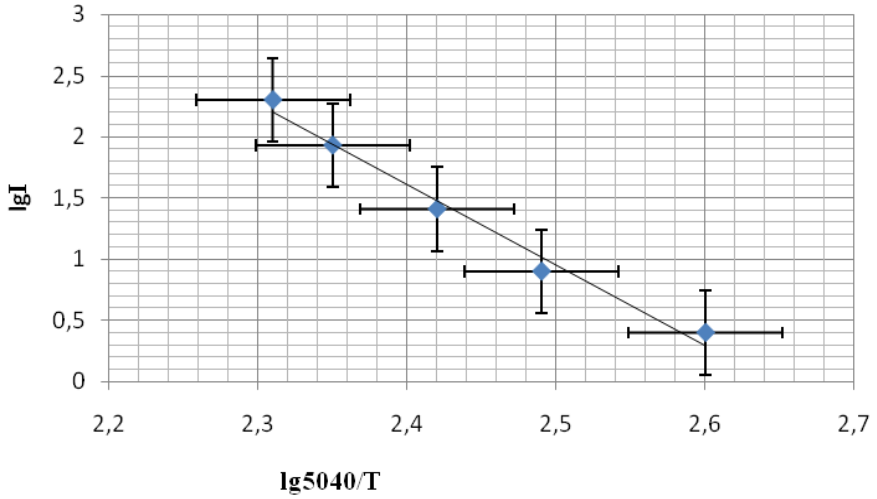

With the use the equation shown in [1–3, 6], the activation energy of the bismuth diffusion into rhenium was found to be E_{n1}= 5.95 ± 0.05 eV. The equation suggested in [1–3, 6] was also used to determine the activation energy of the bismuth diffusion from rhenium. Since $\varphi_{Re} \approx V_{Bi}$= 5.785 V, the coefficient of the surface ionization of bismuth atoms does not depend on temperature; hence, the $\ln I_{Bi^+} = f(5040/T)$ dependence is linear(Fig 2). By the slope of this dependence, the activation energy for bismuth diffusion from rhenium is E_{1n}= 6,1 ± 0.1 eV. The amount of the intercalated and the diffused bismuth as a function of the positive potential upon irradiation of Re(1010)–C heated to $T \leq 1800$ K demonstrated that the intercalation of the graphite monolayer at on rhenium is mainly performed by positive Bi^+ ions, which are formed on Re (1010)–C from the incident flux by the mechanism of surface ionization. This is also confirmed by the fact that the direct determination of the fraction of the bismuth flux δ_{Bi} diffused into rhenium upon the irradiation of Re(1010)–C by a flux of bismuth atoms coincides with the magnitude of δ_{Bi} determined from the comparison of the TDS data on the diffusion of bismuth and cesium into rhenium (on the Re(1010)-C surface, the cesium atoms are present in completely ionized state). The thermodesorption of Bi^+ ions from the Re(1010)-C system before the vaporization of the graphite monolayer may be explained bythe low radii of bismuth atoms and ions [9] (r_0 = 1.70 Å, r^+ = 0.74 Å(+5e) r^+ = 0,96 Å(+3e) compared with the atomic and ionic radius of potassium (r_0 = 2.31 Å, r^+ = 1.33 Å), cesium (r_0 = 2.62 Å, r^+ = 1.69 Å), samarium (r_0 = 1.8 Å, r^+ = 1 Å), and barium (r_0 = 2.17 Å, r^+ = 1.35 Å).

Conclusion

In result, the presented work displays a new phenomenon of high efficiency diffusion into rhenium of bismuth atoms adsorbed on the metal under a graphite monolayer. This phenomenon is used in practice as a method of active alloying with bismuth atoms of near surface layers of solid substances for the purpose of developing new materials which possess particular physicochemical characteristics of near surface zones.

REFERENCES

1. A.Y. Tontegode, F.K.Yusifov. Highly diffusion in rhenium atoms K adsorbed on graphite monolayer on iridiy. FTT 1993, T.35 №4, s.987-993.
2. A.Y. Tontegode, F.K.Yusifov. Intensive diffusion of Cs atoms in rhenium, stimulated by a monolayer of graphite on its poverhnosti.Poverhnost, 1994, №4, s.20-24
3. A.K. Orujov A.O. Dashdemirov, A.K. Elchieva. Diffusion samarium rhenium incident flux of atoms of samarium on rhenium covered with a monolayer of grafita.Fizika Metals and Metallography, 2010, volume 109, number 4, pp. 13
4. A.Ya.Tontegode, E.V.Rutkov.Interkalirovanie atoms of a two-dimensional graphite film on metallah.UFN, 1993, t.163, №11, s.57-74.
5. A.K.Orudzhov A.O.Dashdemirov diffusion of Na atoms in Ir when Ir-C irradiation flux of atoms Na. VII International Conference "solid-state chemistry and modern micro- and nanosystems." Russia, Kislovodsk, 2007. str.95-96.
6. OrudzhovA.K., DashdemirovA.O., AhmedovaA.T., Elchieva AK Determination of the activation energy and the activation energy of dissolution release atoms Ba, Sm, and In to rhenium. Proceedings of the International Conference "Physics - 2005", Baku, str.183-185.
7. A.K .Orudzhov, A.O.Dashdemirov. Adsorption and desorption samarium atoms on the surface of rhenium and rhenium-coated graphite monolayer // FMM.2009. T. 109. № 1. C. 53-57.
8. F.S.Fomenko emission properties of materials. Kiev, Naukova Dumka, 1981, s.338
9. Physical value. Directory of Moscow, Energoizdat 1991, s.1232

JOURNAL OF BAKU ENGINEERING UNIVERSITY - PHYSICS
2018. Volume 2, Number 2 *Pages 134-138*

UOT: 359.12; 537.8
PACS : 12.40.Yx, 12.40.Nn

PARTICLE NUMBER FLUCTUATIONS IN RELATIVISTIC NUCLEAR COLLISIONS

A. RUSTAMOV[1,2,3,4]

[1]Physikalisches Institut, Universität Heidelberg, Heidelberg, Germany

[2]GSI HelmholtzzentrumfürSchwerionenforschung, Darmstadt, Germany

[3]National Nuclear Research Center, Baku, Azerbaijan

[4]Baku State University, Baku, Azerbaijan

ABSTRACT

Several methods are discussed to account for non-dynamical contributions to experimentally measured distributions of net-particle numbers. Specifically, a detailed procedure is given for subtracting non-dynamical fluctuations such as those arising from fluctuations of participat nucleons. Moreover, modifications of dynamical fluctuations due to the overall baryon number conservation arecalculated. These modifications are to be accounted for before performing comparisons to the corresponding theoretical calculations.

Keywords: nuclear collisions, phase transitions, fluctuations.

1. Introduction

Phase transitions in strongly interacting matter can be addressed by investigating the response of the system to external perturbations via fluctuations of conserved charges. At LHC energies, for vanishing light quark masses (u and d quarks), there would be a temperature driven genuine phase transition of the second order between the hadron gas and the quark-gluon plasma [1, 2]. This transition, however, becomes a smooth cross over as soon as the quark masses are accounted for [1,2, 3]. On the other hand,due to their relatively small current masses one can still probe critical phenomena at vanishing baryon chemical potential as argued in [4]. Moreover, the pseudo-critical temperature, reported from LQCD, agrees with the chemical freeze-out temperature as extracted by fitting the Hadron Resonance Gas (HRG) model to the hadron multiplicities measured by the ALICE experiment [5, 6, 7, 8]. The latter implies that the strongly interacting matter, created in collisions of Pb nuclei at the ALICE energies, freezes-out near the chiral phase transition line. Hence, the singularities stemming from the second order phase transition can be captured by measuring fluctuations of conserved charges such as net-baryon numbers. Indeed, at the LHC energies, higher than second order net-baryon cumulants are predicted to significantly differ from the HRG baseline, while second order cumulants are still consistent with HRG, in which the multiplicity distribution of net-baryons follows the Skellam distribution.

Conserved quantities fluctuate only in the sub-region of the available total phase space of the reaction. In statistical mechanics they are hence predicted within the Grand Canonical Ensemble (GCE) formulation, where only the average values of net-baryons are conserved [9]. In order to compare theoretical calculations within the Grand Canonical Ensemble (GCE), such as HRG [7] and Lattice QCD (LQCD) [1], to experimental results, the requirements of GCE have to beachieved in experiments. This is typically done by analyzing the experimental data in a finite acceptance by imposing cuts on rapidity and/or transverse momentum of detectedpar-

Manuscript receved 06.07.2018

ticles. However, in experiments, in the full acceptance, the baryon number is conserved in each event, hence also in the selected acceptance its implications will be seen. Only in a very small acceptance one could completely ignore event-by-event baryon number conservation, which leads to misleading conclusions. Indeed, if the selected acceptance window is too small, the possible dynamical correlations we are after will also be strongly reduced [3, 10, 11] and consequently, net-baryons will be distributed according to the Skellam distribution. But the latter is only the artefact of the small acceptance and independent of any physics behind.

Recently this issue was addressed by treating net-baryon fluctuations in the Canonical Ensemble (CE) formulation of thermodynamics [12, 13]. In this approach, like in the experimental situation, the net-baryon fluctuations appear only in the finite acceptance.

2. Participant fluctuations

Within the Wounded Nucleon Model (WNM), we derived analytical formulae for non-dynamical event-by-event contributions stemming from fluctuations of participant nucleons (cf. [10] and references therein). In the WNM, both particles and antiparticles are produced from statistically independent wounded nucleons.

Figure 1. Left Panel: produced number of charged particles versus the impact parameter. Right Panel: produced number of charged particles versus the number of wounded nucleons.

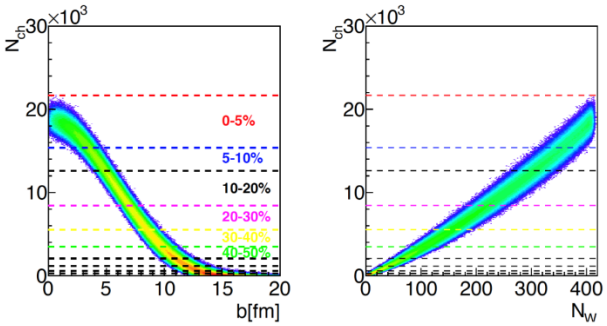

To proceed further we provide the following notations and definitions: (i) the net number of particles from a single wounded nucleon is denoted by Δn , while ΔN refers to the mean number of net-particles summed over all wounded nucleons; (ii) N_w represents the number of wounded nucleons; (iii) first four cumulants of $X = \Delta N$ are defined as:

$$k_1(X) = \langle X \rangle, \tag{1}$$

$$k_2(X) = \langle (X - \langle X \rangle)^2 \rangle, \tag{2}$$

$$k_3(X) = \langle (X - \langle X \rangle)^3 \rangle, \tag{3}$$

$$k_4(X) = \langle (X - \langle X \rangle)^4 \rangle - 3k_2(X)^2. \tag{4}$$

Due to their additive nature, the measured cumulants from all wounded nucleons can be easily calculated, $k_n(\Delta N) = N_w k_n(\Delta n)$. In realistic environments, however, the number of wounded nucleons is not a constant number, because it fluctuates from event-to-event. In fact, in experiments, the events are first classified into centrality classes, defined as percentiles of energy deposited in a zero-degree calorimeter, the multiplicity of charged particles produced in a given acceptance, etc. Moreover, fluctuations of wounded nucleons depend on both, centrality percentiles, as well as the methods (detectors) used for binning the data into centrality classes. For example, in Figure 1, the produced number of charged particles versus the impact

parameter and the number of wounded nucleons is presented. In doing so, the measured signal amplitudes in the two forward scintillator hodoscopes(V0) of the ALICE experiment are fitted with the Glauber Monte Carlo simulations. Figure 2 demonstrates the one-dimensional distributions of the number of wounded nucleons for 3 different centrality classes, selected by applying sharp cuts on the number of produced particles (cf. Right panel of Figure 1). As seen in Figure 2, in the all three centrality classes the wounded nucleons follow different distribution functions with finite widths and higher moments, i. e., the number of wounded nucleons fluctuate from event-to-event.

Figure 2. Distributions of the number of wounded nucleons for 3 different centrality classes selected by applying sharp cuts on the number of produced charged particles. The left panel corresponds to selections of 0–5%, the middle panel to 5–10% and the right panel 40–50% of the total inelastic cross section.

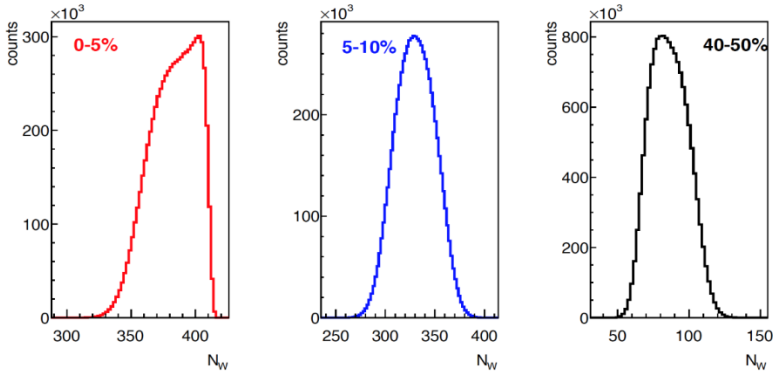

The non-dynamical contributions can be accounted for by using the following analytical formulae[10]:

$$\kappa_1(\Delta N) = \langle N_W \rangle \kappa_1(\Delta n), \tag{5}$$

$$\kappa_2(\Delta N) = \langle N_W \rangle \kappa_2(\Delta n) + \langle \Delta n \rangle^2 \kappa_2(N_w), \tag{6}$$

$$\kappa_3(\Delta N) = \langle N_W \rangle \kappa_3(\Delta n) + 3\langle \Delta n \rangle \kappa_2(\Delta n)\kappa_2(N_w) + \langle \Delta n \rangle^3 \kappa_3(N_w), \tag{7}$$

$$\kappa_4(\Delta N) = \langle N_W \rangle \kappa_4(\Delta n) + 4\langle \Delta n \rangle \kappa_3(\Delta n)\kappa_2(N_w) + 3\kappa_2^2(\Delta n)\kappa_2(N_w), \tag{8}$$

$$+ 6\langle \Delta n \rangle^2 \kappa_2(\Delta n)\kappa_3(N_w) + \langle \Delta n \rangle^4 \kappa_4(N_w).$$

Interestingly, for LHC energies, fluctuations of wounded nucleons are irrelevant for $\kappa_2(\Delta N)$ and $\kappa_3(\Delta N)$. This is because in Eqs. (6) and (7) theparticipant fluctuation part scales with the mean number of net-particles$\langle \Delta n \rangle$and its powers, which vanish for LHC energies at mid-rapidity. This, however, does not hold for$\kappa_4(\Delta N)$.

Using Eqs.(6-8) one can subtract contributions from fluctuations of wounded nucleons. The inputs to be used are experimentally measured mean numbers of particles and antiparticles and the distribution of Wounded Nucleons in nucleus-nucleus collisions of a given centrality. The latter is obtained by fitting the experimentally measured signals with the corresponding Glauber Monte Carlo simulations.

3. Conservation laws

As mentioned in the introduction, conserved quantities fluctuate only in sub-regions of the available total phase space of the reaction. In statistical mechanics they are hence predicted within the Grand Canonical Ensemble (GCE) formulation, where only the average values of net-baryons are conserved [9].

Figure 3. Normalized cumulants of net-baryons from 5×10^8 generated MC events in CE are presented with the black circles. The blue lines are calculated with Eqs. (10, 12), while the red dashed lines represent the GCE baseline.

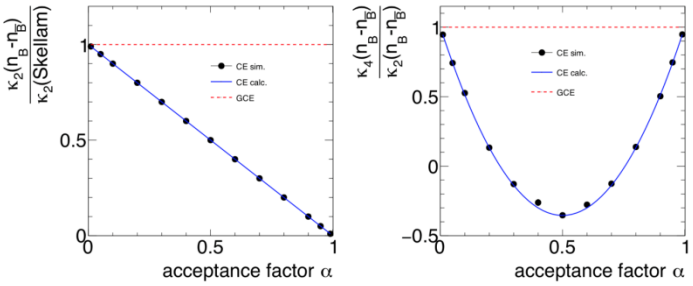

In a thermal system with an ideal gas EoS, composed of baryon/anti-baryon species with baryon numbers +1 and -1, GCE partition function yields the uncorrelated Poisson distributions for baryons and anti-baryons, hence the net-baryon distribution has the following cumulants [13]

$$\kappa_n(Skellam) = \langle n_B \rangle + (-1)^n \langle n_{\bar{B}} \rangle \tag{9}$$

where $\langle n_B \rangle$ and $\langle n_{\bar{B}} \rangle$ denote the first cumulants (mean numbers) of baryons and anti-baryons, respectively. Eq. (9) implies that ratios of even-to-even and odd-to-odd cumulants of net-baryons are always unity, while the ratios of odd-to-even cumulants depend on mean multiplicities. Hitherto, these conditions are used as baseline for net-baryon fluctuations. However, this can lead to misleading conclusions because, apart from dynamical fluctuations induced by critical phenomena, deviations from this baseline may be driven by non-dynamical contributions. In the previous section it was demonstrated that fluctuations of participating nucleons from event-to-event significantly distort measured event-by-event fluctuation signals. At low energies, participant fluctuations always increase the measured dynamical fluctuations up to the third cumulant of net-proton distributions. In contrast, starting from the fourth cumulant, they can in fact decrease the signal.

The exact baryon number conservation in the full phase space leads to the following modifications of cumulant ratios in the finite acceptance [12, 13]:

$$\left[\frac{\kappa_2(n_B - n_{\bar{B}})}{\kappa_2(Skellam)}\right]_{CE} = 1 - \alpha, \tag{10}$$

$$\left[\frac{\kappa_3(n_B - n_{\bar{B}})}{\kappa_2(n_B - n_{\bar{B}})}\right]_{CE} = \left[\frac{\langle n_B - n_{\bar{B}} \rangle}{\langle n_B + n_{\bar{B}} \rangle}\right]_{CE} (1 - 2\alpha), \tag{11}$$

$$\left[\frac{\kappa_4(n_B - n_{\bar{B}})}{\kappa_2(n_B - n_{\bar{B}})}\right]_{CE} = 1 - 6\alpha(1 - \alpha)F, \tag{12}$$

where α is the fraction of the baryons falling into the experimental acceptance,$\langle n_B \rangle$ and $\langle n_{\bar{B}} \rangle$ are mean numbers of baryons and anti-baryons inside the experimental acceptance and F is defined as:

$$F = 1 - 2\frac{\langle N_B \rangle_{CE} \langle N_{\bar{B}} \rangle_{CE}}{\langle N_B \rangle_{CE} + \langle N_{\bar{B}} \rangle_{CE}} \left(\frac{\langle N_B \rangle_{GCE} \langle N_{\bar{B}} \rangle_{GCE}}{\langle N_B \rangle_{CE} \langle N_{\bar{B}} \rangle_{CE}} - 1 \right), \tag{13}$$

with $\langle N_B \rangle$ and $\langle N_{\bar{B}} \rangle$ referring to baryons and anti-baryons in the full phase space.

The resultsfor the normalized values of κ_2 and $\kappa_4$of net-baryons, as a function of accepted fraction of baryonsα, arepresented in Fig. 3, where the lines are analyticalcalculations with Eqs (10, 12).

Eqs. (10-13) need to be used to correct experimentally measured ratios of cumulants before comparing them to theoretical calculations within GCE.

4. Summary

In summary, non-dynamical contributions to fluctuations of net-baryons, such as those arising from fluctuations of participant nucleons and overall global baryon number conservation are addressed. To this end analytic relations are provided between net-baryon and wounded nucleon cumulants. Furthermore, the study of the effects of global baryon number conservation laws on fluctuations of net-baryonsis presented. These results will be relevant for the research programs at facilitiessuch as LHC at CERN, FAIR at GSI and NICA at JINR. Near future challenges will be precision measurements of highermoments at RHIC and LHC and their connection to fundamental QCD predictions.

REFERENCES

[1] A. Bazavov et al., Phys. Rev. D85 (2012) 054503.

[2] S. Borsanyi, Z. Fodor, J. N. Guenther, S. K. Katz, K. K. Szabó, A. Pasztor, I. Portillo and C. Ratti, arXiv:1805.04445.

[3] V. Koch, in "Relativistic Heavy Ion Physics", R. Stock (ed.) (Springer, Heidelberg, 2010), (Landolt-Boernstein New Series I, v. 23) p. 626, arXiv:0810.2520v1.

[4] B. Friman, F. Karsch, K. Redlich, and V. Skokov, Eur. Phys. J. C71 (2011) 1964.

[5] F. Karsch, Nucl.Phys. A967 (2017) 461-464.

[6] O. Kaczmarek, Nucl.Phys. A967 (2017) 137-144.

[7] A. Andronic, P. Braun-Munzinger, K. Redlich, and J. Stachel, J.Phys.Conf.Ser. 779 (2017).

[8] K.Aamodt et al. (ALICECollab.), JINST3 (2008) S08002.

[9] L. D. Landau and E. M. Lifshitz, Statistical Physics, Pergamon Press, 1980.

[10] P. Braun-Munzinger, A. Rustamov, J. Stachel, Nucl. Phys. A960 (2017), 114.

[11] A. Rustamov for the ALICE Collaboration, Nucl.Phys. A967 (2017) 453-456.

[12] A. Bzdak, V. Koch, V. Skokov, Phys.Rev. C87 (2013) 014901

[13] P. Braun-Munzinger, A. Rustamov, J. Stachel, arXiv:1807.08927.

JOURNAL OF BAKU ENGINEERING UNIVERSITY - PHYSICS
2018. Volume 2, Number 2 *Pages 139-146*

UOT:531:530.145
PACS: 03.65.Ge

ANALYTICAL SOLUTIONS OF THE DIRAC EQUATION FOR HULTHÉN POTENTIAL

M. V. QOCAYEVA[1], S. M. ASLANOVA[2], A. I. AHMADOV[2]

[1]Institute of Physics, Azerbaijan National Academy of Sciences,
H.Javid Avenue,131, AZ-1143, Baku, Azerbaijan
E-mail:mefkureqocayeva@yahoo.com
[2]Baku State University,Z. Khalilov str.23, AZ-1148, Baku, Azerbaijan,
E-mail:ahmadovazar@yahoo.com

ABSTRACT

In this paper studied the analytical bound state solutions of the Dirac equation with the Hulthén potential for arbitrary spin–orbit coupling quantum number k are carried out by taking a properly approximate expansion for the spin–orbit coupling term. In the case of exact spin symmetry, and pseudospin symmetry the associated two-component spinor wave functions of the Dirac equation for arbitrary spin–orbit quantum number k are presented and the corresponding bound state energy equation is derived. The bound state energy eigenvalues and the corresponding spinors are obtained in the closed forms.

Key words: Hulthén potential, exact spin symmetry, pseudospin symmetry.

HÜLTEN POTENSİALI ÜÇÜN DIRAK TƏNLİYİNİN ANALİTİK HƏLLİ

XÜLASƏ

İşdə spin-orbital mərkəzəqaçma potensialına yeni yaxınlaşma tətbiq etməklə Hülten potensialı üçün modifiyə olunmuş radial Dirak tənliyinin spin-orbital kvant ədəinin ixtiyari k qiymətlərində əlaqəli hallar üçün analitik həlli tapılmışdır. Dəqiq spin və psevdospin simmetriya halları üçün iki komponentli spinor dalğa funksliyaları üçün Dirak tənliyinin analitik həlləri k spin-orbital kvant ədədi ilə ifadə edilmişdir. Əlaqəli halların enerjinin məxsusi qiymətləri və məxsusi funksiyaları üçün kompakt ifadələr tapılmışdlr.

Açar sözlər: Hülten potentialı, dəqiq spin simmetriyası, psevdospin simmetriyası.

АНАЛИТИЧЕСКИЕ РЕШЕНИЯ УРАВНЕНИЯ ДИРАКА ДЛЯ ПОТЕНЦИАЛА ХЮЛЬТЕНА

РЕЗЮМЕ

В данной работе изучаются аналитические решения в связанном состоянии уравнения Дирака с потенциалом Хюльтена для произвольного квантового числа k спин-орбитальной связи с применением нового подхода для центростримительного потенциала связянного с членом спин-орбитального взаимодействия. В случае точной спиновой и псевдоспиновой симметрии представлены связанные двухкомпонентные спинорные волновые функции уравнения Дирака для произвольного спин-орбитального квантового числа и получено соответствующее уравнение энергии связанного состояния. Собственные значения энергии связанного состояния и соответствующие спиноры получены в замкнутых формах.

Ключевые слова: потенциал Хюльтена, точная спиновая симметрия, псевдоспиновая симметрия.

1. Introduction

Since the early years of quantum mechanics (QM), the study of exactly solvable problems for some special potentials has aroused considerable interest in theoretical physics. In addition, since the wave function contains all necessary knowledge for the full description of a quantum system, so an analytical solution of the wave equations is of quite high significance in quantum mechanics [1,2].

Manuscript receved 12.08.2018

Since the exact solutions of the Klein-Fock-Gordon (KFG) and Dirac equations with any potential play an important role in relativistic quantum mechanics [1,2], there are many discussions about

the KFG and Dirac equations with physical potentials by using different methods.

Many methods were developed and has been used successfully in solving the non-relativistic and relativistic wave equations in the presence of some well known potentials. Such as supersymmetry (SUSY), factorization, Laplace transform approach and the path integral method, shifted 1/N expansion approach for solving radial and azimuthal part of the wave equations exactly or quasi-exactly for any orbital quantum numbers within different potentials. An other method known as the Nikiforov-Uvarov (NU) method [3] was proposed for solving the wave equations analytically. There are few potentials for which the Dirac equation are able solved exactly for any spin-orbit coupling quantum number k .

However, analytic solutions are possible only for a few simple quantum systems like the movement in the spherical simmetrical field and the linear harmonic oscillator. In general, many quantum systems can only be treated by approximation methods or numerical solutions.

As known, one of the main purpose in theoretical physics since the early years of quantum mechanics (QM) is to obtain an exact solution of the Dirac equation for some special potentials in physical interest. It would be interesting and an significant to solve the Dirac equation for the Hulthén potential any spin-orbit coupling quantum number k in cases exact spin and pseudospin symmetry. Hulthén potential for spin-orbit quantum number k since it has been extensively used to describe the bound and continuum states of the interacting systems. The pseudospin symmetry with the nuclear shell model has been introduced many years ago and it has been widely applied to explain and describing of phenomena in nuclear physics and related others areas.

It is very significant to notice that Dirac eduqtion for the Manning-Rosen and Hulthén potentials üithin asymptotic iteration method are studied in Refs. [4,5]. In Ref.[6] a complete solution of the problem of squaring the Dirac equation with arbitrary external electromagnetic field is expounded.

Therefore, it would be interesting and important to solve Dirac equation for the Hulthén potential since it has been extensively used to describe the bound and the continuum states of the interaction systems.

Thus, the main purpose of our investigation is the analytical solution of modified Dirac equation for the Hulthén potential for arbitrary spin–orbit quantum number k in the case of exact spin symmetry and pseudospin symmetry using Nikiforov-Uvarov (NU) method[3]. This method is based on solving the second-order linear differential equation by reducing to a generalized equation of hypergeometric-type which is a second-order type homogeneous differential equation with polynomials coefficients of degree not exceeding the corresponding order of differentiation.

The Hulthèn potential is defined by [7,8]

$$V_H(r) = -\frac{Ze^2\delta e^{-\delta r}}{(1-e^{-\delta r})}. \tag{1}$$

Here Z and δ are respectively the atomic number and the screening parameter, determining the range for the Hulthèn potential.

The Hulthèn potential is one of the important short-range potentials in physics, extensively using to describe the bound and continuum states of the interaction systems. It has been applied to the several research areas such as nuclear and particle physics, atomic physics, condensed matter and chemical physics, so the analyzing relativistic effects for a particle under this potential could become significant, especially for strong coupling. At small values of the radial coordinate r, the Hulthèn potential behaves like a Coulomb potential, whereas for large values of r it decreases exponentially so that its influence for bound state is smaller than, that of Coulomb potential. In contrast to the Hulthèn potential, the Coulomb potential is analytically solvable for any l angular momentum. Take into account of this point will be very interesting and important solving Dirac equation for the Hulthèn potential for arbitrary spin–orbit coupling quantum number k within ordinary quantum mechanics.

2. Bound states of the Hulthèn potential with arbitrary k

The Dirac equation of a nucleon with mass M moving in an attractive scalar potential $S(r)$ and a repulsive vector potential $V(r)$ can be written as ($\hbar = c = 1$):

$$[\vec{\alpha}\vec{p} + \beta(M + S(r))]\psi(r) = [E - V(r)]\psi(r) \tag{2}$$

where E is the relativistic energy of the system, and α and β are the Dirac matrices.

For spherical symmetrical nuclei, the total angular momentum of the nucleon J and spin–orbit matrix $\hat{K} = -\beta(\hat{\sigma}\cdot\hat{L} + 1)$ commute with the Dirac Hamiltonian $[\hat{H}^D, \hat{K}] = 0$, where L is the orbital angular momentum. The eigenvalues of K are $k = \pm(j + 1/2)$, where $k = -(j + 1/2) < 0$ is for the aligned spin $j = l + 1/2 (s_{1/2}, p_{3/2}, ets)$ and $k = (j + 1/2) > 0$ is for the unaligned spin $j = l - 1/2 (p_{1/2}, d_{3/2}, ets)$. For fully investigation of the quantum system the complete set of the conservative quantities can be taken as (H, K, J^2, J_z) and the spinor wave functions can be classified according to their angular momentum j,k and the radial quantum number n. The spherically symmetric Dirac spinor wave functions can be written as

$$\psi_{nk} = \frac{1}{r}\begin{bmatrix} F_{nk}(r) & Y^l_{jm}(\theta,\varphi) \\ iG_{nk}(r) & Y^{\tilde{l}}_{jm}(\theta,\varphi) \end{bmatrix} \tag{3}$$

where the upper and lower components $F_{nk}(r)$ and $G_{nk}(r)$ are real square-integral functions, $Y^l_{jm}(\theta,\varphi)$ and $Y^{\tilde{l}}_{jm}(\theta,\varphi)$ are the spherical harmonic functions, and m is the projection of the total angular momentum on the third axis, and $l(l+1) = k(k+1),\ \tilde{l}(\tilde{l}+1) = k(k-1)$

The substitution of Eq. (3) into (2) then we obtain two coupled differential equations as follows:

$$\left(\frac{d}{dr} + \frac{k}{r}\right)F_{nk}(r) = [M + E_{nk} + S(r) - V(r)]G_{nk}(r), \tag{4}$$

$$\left(\frac{d}{dr} - \frac{k}{r}\right)G_{nk}(r) = [M - E_{nk} + S(r) + V(r)]F_{nk}(r). \tag{5}$$

By eliminating $G_{nk}(r)$ in Eq. (4) and $F_{nk}(r)$ in Eq. (5), one is able to obtain two second-order differential equations for the upper $F_{nk}(r)$ and lower $G_{nk}(r)$ components as follows:

$$\left\{\frac{d^2}{dr^2}-\frac{k(k+1)}{r^2}-[M+E_{nk}-\Delta(r)][M-E_{nk}+\Sigma(r)]++\frac{\frac{d\Delta(r)}{dr}\left(\frac{d}{dr}+\frac{k}{r}\right)}{M+E_{nk}-\Delta(r)}\right\}F_{nk}(r)=0, \tag{6}$$

$$\left\{\frac{d^2}{dr^2}-\frac{k(k-1)}{r^2}-[M+E_{nk}-\Delta(r)][M-E_{nk}+\Sigma(r)]+\frac{\frac{d\Sigma(r)}{dr}\left(\frac{d}{dr}-\frac{k}{r}\right)}{M-E_{nk}+\Sigma(r)}\right\}G_{nk}(r)=0\ , \tag{7}$$

here $\Delta(r)=V(r)-S(r)$ and $\Sigma(r)=V(r)+S(r)$, respectively.

Now, let us consider the exact spin symmetry, in this case $d\Delta/dr=0$ then $\Delta=const$. In this work we take $\Sigma(r)$ as the Hulthén potential, $\Sigma(\mathrm{r})=\mathrm{V_H(r)}$

$$\Sigma(r)=-\frac{Ze^2\delta e^{-\delta r}}{1-e^{-\delta r}}. \tag{8}$$

Substituting Eq. (8) into Eq. (6) then we obtain:

$$\left\{\frac{d^2}{dr^2}-\frac{k(k+1)}{r^2}-[M+E_{nk}-c]\Sigma(r)+\left[E_{nk}^2-M^2+c(M-E_{nk})\right]\right\}F_{nk}(r)=0 \tag{9}$$

This equation cannot be solved analytically except for *s*-wave $k=-1$ case due to the spin–orbit coupling term $\mathrm{k(k+1)/r^2}\to 0$. Thus, for the solving this problem in this work we apply a new approximate scheme to the centrifugal term [9-11]

$$\frac{1}{r^2}\approx\delta^2\left(C_0+\frac{e^{-\delta r}}{(1-e^{-\delta r})^2}\right). \tag{10}$$

where the parameter $\mathrm{C_0=1/12}$ [12], is a dimensionless constant. However, when $\mathrm{C_0=0}$, the approximation scheme becomes the convectional approximation scheme suggested by Greene and Aldrich [13].

Substituting expression (10) into (9) then we obtain:

$$\left[\frac{d^2}{dr^2}-[M+E_{nk}-c]\Sigma(r)+\left[E_{nk}^2-M^2+c(M-E_{nk})\right]-k(k+1)\delta^2\left(C_0+\frac{e^{-\delta r}}{(1-e^{-\delta r})^2}\right)\right]F_{nk}(r)=0\cdot \tag{11}$$

Main aim to transform Eq. (11) the equation of the generalized hypergeometric type which is in the form:

$$\chi''(x)+\frac{\tilde{\tau}}{\sigma}\chi'(x)+\frac{\tilde{\sigma}}{\sigma^2}\chi(x)=0. \tag{12}$$

The Eq.(11) can be further simplified using a new variable $s=e^{-\delta r}$. Taking into account, that here $\mathrm{r}\in[0,1]$ and $\mathrm{s}\in[1,0]$, then we obtain:

$$\frac{d^2F_{nk}(s)}{ds^2}+\frac{1}{s}\frac{dF_{nk}(s)}{ds}+\left[\frac{Ze^2}{\delta s(1-s)}[M+E_{nk}-c]+\frac{1}{s^2\delta^2}\left[E_{nk}^2-M^2+c(M-E_{nk})\right]-\right.$$

$$\left.-\frac{k(k+1)}{s^2}\left[C_0+\frac{s}{(1-s)^2}\right]\right]F_{nk}(s)=0. \tag{13}$$

Here we use following ansats in order to make the differential equation more compact,

$$\alpha^2 = \frac{Ze^2(M + E_{nk} - c)}{\delta} \text{ and } \beta^2 = \frac{M^2 - E_{nk}^2 - c(M - E_{nk})}{\delta^2} \ . \tag{14}$$

Now, NU method can be successfully applied to define the eigenvalues of energy. By comparing Eq.(13) with Eq.(12) and applying Nikiforov-Uvarov metod after this a long and cumbersome calculations for energy spectrum we find:

$$\beta^2 = \left[\frac{\alpha^2 - (k+n+1)^2}{2(k+n+1)}\right]^2 - k(k+1)C_0 \tag{15}$$

Take into account (14) into (15), then for energy spectrum we obtain:

$$M^2 - E_{nk}^2 - c(M - E_{nk}) = \delta^2\left[\frac{Ze^2(M + E_{nk} - c)}{2\delta(k+n+1)} - \frac{k+n+1}{2}\right]^2 - k(k+1)C_0\delta^2 \tag{16}$$

If in the Eq.(16) we take $C_0 = 0$ then we directly obtain result [5].

If we take the following factorization

$$F_{nk}(s) = \phi(s)y(s) \tag{17}$$

for the appropriate function $\phi(s)$, Eq.(13) takes the form of the well-known hypergeometric-type equation. The appropriate $\phi(s)$ function has to satisfy the following condition:

$$\frac{\phi'(s)}{\phi(s)} = \frac{\pi(s)}{\sigma(s)} \ , \tag{18}$$

where function $\pi(s)$ is defined as

$$\pi(s) = \frac{\sigma' - \bar{\tau}}{2} \pm \sqrt{\left(\frac{\sigma' - \bar{\tau}}{2}\right)^2 - \bar{\sigma} + k\sigma} \ . \tag{19}$$

Finally for $\pi(s)$ we found:

$$\pi(s) = -\frac{s}{2} \pm \begin{cases} \left(\sqrt{c} - \sqrt{c+a-b}\right)s - \sqrt{c} \ , \ k = (b-2c) + 2\sqrt{c^2 + c(a-b)} \\ \left(\sqrt{c} + \sqrt{c+a-b}\right)s - \sqrt{c} \ , \ k = (b-2c) - 2\sqrt{c^2 + c(a-b)} \end{cases} \ . \tag{20}$$

Solving the Eq.(18) then for $\phi(s)$ we found:

$$\phi(s) = s^{\sqrt{c}}(1-s)^K \ . \tag{21}$$

Here, $K = k+1$, and $\sqrt{c} = \sqrt{\beta^2 + k(k+1)}$. Then for $\phi(s)$ finally we obtain:

$$\phi(s) = s^{\sqrt{\beta^2 + k(k+1)}} \ . \tag{22}$$

Furthermore, the other part of the wave function $y(s)$ is the hypergeometric-type function whose polynomial; solutions are given by Rodrigues relation

$$y_n(s) = \frac{C_n}{\rho(s)}\frac{d^n}{ds}\left[\sigma^n(s)\rho(s)\right] \tag{23}$$

where C_n is a normalizing constant and $\rho(s)$ is the weight function which is the solution of the Pearson differential equation. The Pearson differential equation and $\rho(s)$ for our problem is given as

$$(\sigma\rho)' = \tau\rho . \tag{24}$$

It is easy to find the second part of the wave function from the definition of weight function. Thus, solving the Eq.(24) very easy we found the second part of the wave function in this form:

$$\rho(s) = (1-s)^{2K-1} s^{2\sqrt{c}} . \tag{25}$$

Substituting Eq.(25) in Eq.(23), we get

$$y_n(s) = C_n (1-s)^{1-2K} s^{2\sqrt{c}} \frac{d^n}{ds^n}\left[s^{2\sqrt{c}+n} \cdot (1-s)^{2K-1+n} \right] = C_n P_n^{(2\sqrt{c},2K-1)}(1-2s) . \tag{26}$$

Finally substituting ϕ(s) and $y(s)$ into Eq.(17), then for the $F_{nk}(s)$ eigenfunctions we obtain:

$$F_{nk}(s) = C_n s^{\sqrt{c}} (1-s)^K P_n^{(2\sqrt{c},2K-1)}(1-2s) \tag{27}$$

After simple calculations, we obtain normalization constant as

$$C_n = \sqrt{\frac{n!2\sqrt{c}(n+K+\sqrt{c})\Gamma((2K+\sqrt{c})+n)}{(n+K)\Gamma(n+2\sqrt{c}+1)\Gamma(n+2K)}} . \tag{28}$$

In the case of exact pseudospin symmetry in Eq. (7) we take $d\Sigma(r)/dr = 0,$ and $\Sigma(r) = c = const$, then Eq.(7) we can write in this form:

$$\left[\frac{d^2}{dr^2} - \frac{k(k-1)}{r^2} - [M + E_{nk} - \Delta(r)][M - E_{nk} + c] \right] G_{nk}(r) = 0 \tag{27}$$

here $k = -\tilde{l}$ for $k < 0$ and $k = \tilde{l} + 1$ for $k > 0$, $\Delta(r)$ is the Hulthèn potential. The energy eigenvalues depend on n and $\tilde{l}$, $E_{nk} = E(n, \tilde{l}\,(\tilde{l}+1)$. The eigenstates with $j = \tilde{l} \pm 1/2$ are degenerate for $\tilde{l} \neq 0$ which is well known as the exact pseudospin symmetry. Here, also as above Eq. (16) cannot be solved exactly for the Hulthén potential for $k \neq 0$ by using the standard methods. Therefore, the solving this problem we apply a new approximate scheme to the centrifugal term presented in Eq.(27).

Thus, solving Eq.(27) by NU method for the energy eigenvalues obtain:

$$\beta^2 = \left[\frac{\alpha^2}{2(n+1-k)} - \frac{n+1-k}{2} \right]^2 - k(k-1)C_0 \tag{28}$$

To take into account in the case exact pseudospin symmetry β^2 defined in this form:

$$\beta^2 = \frac{M^2 - E_{nk}^2 + c(M + E_{nk})}{\delta^2} . \tag{29}$$

Substituting expression (29) into (28) then we obtain:

$$(M + E_{nk})(M - E_{nk} + c) = \delta^2 \left[-\frac{Ze^2(M - E_{nk} + c)}{2\delta(n+1-k)} - \frac{n+1-k}{2} \right]^2 - k(k-1)C_0\delta^2 \tag{30}$$

Also here if in the Eq.(30) we take $C_0 = 0$ then we directly obtain result [5].

For arbitrary spin–orbit coupling quantum number $k \neq 0$ in the exact pseudospin symmetry case $G_{nk}(s)$ eigenfunctions of this potential defined in this form:

$$G_{nk}(s) = C_n s^{\sqrt{c}} (1-s)^{\widetilde{K}} P_n^{(2\sqrt{c}, 2\widetilde{K}-1)}(1-2s). \tag{31}$$

Where $\widetilde{K} = k$

As is seen from Eqs.(16,27) and (30,31) energy spectrum and eigen functions very sensitive the choosing spin–orbit coupling quantum number k .

3. Conclusion

In this work, we have presented the bound state solutions of the Dirac equation for the Hulthén potential within the framework by using the developed scheme to overcome the centrifugal part.

For arbitrary spin–orbit coupling quantum $k \neq 0$ state, we have obtained the energy eigenvalues and Dirac spinors in the closed form for the case of the exact spin symmetry and exact pseudospin symmetry cases. The analytical formulas, given by Eqs. (16, 27, 30, 31) may have interesting applications in nuclear and particle physics and related areas. Regarding the method presented in this study, we should point out that it is a systematic one and it is very efficient and practical in solving the exact spin and pseudospin symmetric systems for any spin–orbit coupling quantum $k \neq 0$ state.

A closed form of the normalization constant of the wave functions is also found. The energy eigenvalues and corresponding eigenfunctions are obtained for arbitrary $\mathrm{k} \neq 0$ spin–orbit coupling quantum number and n_r radial quantum numbers.

It is worth to mention that the Hulthén potential is one of the important exponential potential, and it is a subject of interest in many fields of physics and chemistry. The main results of this paper are the explicit and closed form expressions for the energy eigenvalues, eigenfunctions and the normalized wave functions. The method presented in this study is a systematic one and in many cases it is one of the most concrete works in this area.

Consequently, studying of analytical solution of the modified Dirac equation is obtained for the Hulthén potential within the framework quantum mechanics could provide important information on the dynamics at nuclear, atomic and molecule physics and opens new window for futher investigation.

We can conclude that our analytical results of this study are expected to enable new possibilities for pure theoretical and experimental physicist, because the results are exact and more general.

REFERENCES

1. W. Grenier, Quantum Mechanics An Itroduction, Fourth ed. Springer, Berlin, 2000.
2. V. G. Bagrov, D. M. Gitman, Exact Solutions of Relativistic Wave Equations (Kluwer Academic Publishers, Dordrecht, 1990).
3. A.F. Nikiforov and V.B. Uvarov, Special Functions of Mathematical Physics, Birkhäuser, Basel 1988.
4. Gao-Feng Wei, Shi-Hai Dong, *Approximately analytical solutions of the Manning–Rosen potential with the spin–orbit coupling term and spin symmetry*, Physics Letters A **373**, 49 (2008).

5. A. Soylu, O Bayrak and I. Boztosun, *An approximate solution of Dirac-Hulthén problem with pseudospin and spin symmetry for any k state*, Journal of Mathematical Physics **48**, 082302 (2007).
6. V.G.Bagrov, *Squaring the Dirac equations*,Russian Physical Journal **61**, 403-411 (2018).
7. L. Hulthèn, *Uber die eigenlosunger der Schrodinger-gleiching ded deuterons,* Ark. Mat. Astron. Fys. A**28,** 5, 1942.
8. L. Hulthen, *On the virtual state of the deutron*. Ark. Mat. Astron. Fys. B**29,** 1, 1942.
9. Wen-Chao Qiang, Shi-Hai Dong, *Arbitrary l-state solutions of the rotating Morse potential through the exact quantization rule method,* Physics Letters A **363**, 169 (2007).
10. Gao-Feng Wei, Shi-Hai Dong, *Approximately analytical solutions of the Manning–Rosen potential with the spin–orbit coupling term and spin symmetry*, Physics Letters A **373**, 49 (2008).
11. Wen-Chao Qiang, Shi-Hai Dong,*The Manning–Rosen potential studied by a new approximate scheme to the centrifugal term*,Physica Scripta 79, 045004 (2009).
12. C.S. Jia, T. Chen and L. G. Cui,*Approximate Analytical Solutions of the Dirac Equation with the Generalized Pöschl-Teller Potential Including the Pseudo-Centrifugal Term,* Physics Letters A **373**, 1621 (2009).
13. R.L. Greene and C. Aldrich, Variational wave functions for a screened Coulomb potential, Physical Reveiw A 14, 2363 (1976).

INSTRUCTIONS FOR AUTHORS

1. "The Baku Engineering University Journal-Physics" accepts original unpublished articles and reviews in the research field of the author.
2. Articles are accepted in English.
3. File format should be compatible with **Microsoft Word** and must be sent to the electronic mail (**journal@beu.edu.az**) of the Journal. The submitted article should follow the following format:

- Article title, author's name and surname
- The name of workplace
- Mail address
- Abstract and key words

4. The title of the article should be in each of the three languages of the abstract and should be centred on the page and in bold capitals before each summary.
5. **The abstract** should be written in **9 point** type size, between **100** and **150** words. The abstract should be written in the language of the text and in two more languages given above. The abstracts of the article written in each of the three languages should correspond to one another. The keywords should be written in two more languages besides the language of the article and should be at least three words.
6. . **UDC** and **PACS** index should be used in the article.
7. The article must consist of the followings:

- Introduction
- Research method and research
- Discussion of research method and its results
- In case the reference is in Russian it must be given in the Latin alphabet with the original language shown in brackets.

8. **Figures, pictures, graphics and tables** must be of publishing quality and inside the text. Figures, pictures and graphics should be captioned underneath, tables should be captioned above.
9. **References** should be given in square brackets in the text and listed according to the order inside the text at the end of the article. In order to cite the same reference twice or more, the appropriate pages should be given while keeping the numerical order. For example: [7, p.15].

Information about each of the given references should be full, clear and accurate. The bibliographic description of the reference should be cited according to its type (monograph, textbook, scientific research paper and etc.) While citing to scientific research articles, materials of symposiums, conferences and other popular scientific events, the name of the article, lecture or paper should be given.

Samples:

a) ***Article:*** Demukhamedova S.D., Aliyeva İ.N., Godjayev N.M.. *Spatial and electronic structure af monomerrik and dimeric conapeetes of carnosine üith zinc,* Journal of structural Chemistry, Vol.51, No.5, p.824-832, 2010

b) ***Book:*** Christie ohn Geankoplis. *Transport Processes and Separation Process Principles.* Fourth Edition, Prentice Hall, p.386-398, 2002

c) ***Conference paper:*** Sadychov F.S., Aydın C., Ahmedov A.İ.. Appligation of Information – Commu-nication Technologies in Science and education. II International Conference."*Higher Twist Effects In Photon- Proton Collisions", Bakı, 01-03 Noyabr, 2007, ss 384-391*

References should be in 9-point type size.

10. The margins sizes of the page: - Top 2.8 cm. bottom 2.8 cm. left 2.5 cm, right 2.5 cm. The article main text should be written in Palatino Linotype 11 point type size single-spaced. Paragraph spacing should be 6 point.
11. The maximum number of pages for an article should not exceed 15 pages
12. The decision to publish a given article is made through the following procedures:

- The article is sent to at least to experts.
- The article is sent back to the author to make amendments upon the recommendations of referees.
- After author makes amendments upon the recommendations of referees the article can be sent for the publication by the Editorial Board of the journal.

YAZI VƏ NƏŞR QAYDALARI

1. "Journal of Baku Engineering University" Fizika- əvvəllər nəşr olunmamış orijinal əsərləri və müəllifin tədqiqat sahəsi üzrə yazılmış icmal məqalələri qəbul edir.
2. Məqalələr İngilis dilində qəbul edilir.
3. Yazılar **Microsoft Word** yazı proqramında, (**journal@beu.edu.az**) ünvanına göndərilməlidir. Göndərilən məqalələrdə aşağıdakılara nəzərə alınmalıdır:

- Məqalənin başlığı, müəllifin adı, soyadı,
- İş yeri,
- Elektron ünvanı,
- Xülasə və açar sözlər.

4. **Məqalədə başlıq hər xülasədən əvvəl** ortada, qara və böyük hərflə xülasələrin yazıldığı hər üç dildə olmalıdır.
5. **Xülasə** 100-150 söz aralığında olmaqla, 9 punto yazı tipi böyüklüyündə, məqalənin yazıldığı dildə və bundan əlavə yuxarıda göstərilən iki dildə olmalıdır. Məqalənin hər üç dildə yazılmış xülasəsi bir-birinin eyni olmalıdır. Açar sözlər uyğun xülasələrin sonunda onun yazıldığı dildə verilməklə ən azı üç sözdən ibarət olmalıdır.
6. Məqalədə UOT və PACS kodları göstərilməlidir.
7. Məqalə aşağıdakılardan ibarət olmalıdır:

- Giriş,
- Tədqiqat metodu
- Tədqiqat işinin müzakirəsi və onun nəticələri,
- İstinad ədəbiyyatı rus dilində olduğu halda orjinal dili mötərzə içərisində göstərməklə yalnız Latın əlifbası ilə verilməlidir.

8. **Şəkil**, **rəsm**, **grafik** və **cədvəllər** çapda düzgün, aydın çıxacaq vəziyyətdə və mətn içərisində olmalıdır. Şəkil, rəsm və grafiklərin yazıları onların altında yazılmalıdır. Cədvəllərdə başlıq cədvəlin üstündə yazılmalıdır.
9. **Mənbələr** mətn içərisində kvadrat mötərizə daxilində göstərilməklə məqalənin sonunda mətn daxilindəki sıra ilə düzülməlidir. Eyni mənbəyə iki və daha cox istinad edildikdə əvvəlki sıra sayı saxlanmaqla müvafiq səhifələr göstərilməlidir. Məsələn: [7,səh.15].

Ədəbiyyat siyahısında verilən hər bir istinad haqqında məlumat tam və dəqiq olmalıdır. İstinad olunan mənbənin biblioqrafik təsviri onun növündən (monoqrafiya, dərslik, elmi məqalə və s.) asılı olaraq verilməlidir. Elmi məqalələrə, simpozium, konfrans, və digər nüfuzlu elmi tədbirlərin materiallarına və ya tezislərinə istinad edərkən məqalənin, məruzənin və ya tezisin adı göstərilməlidir.

Nümunələr:

a) ***Məqalə:*** Demukhamedova S.D., Aliyeva İ.N., Godjayev N.M.. *Spatial and electronic structure af monomeric and dimeric complexes of carnosine with zinc,* Journal of structural Chemistry, Vol.51, No.5, p.824-832, 2010

b) ***Kitab:*** Christie ohn Geankoplis. *Transport Processes and Separation Process Principles*. Fourth Edition, Prentice Hall, 2002

c) ***Konfrans:*** Sadychov F.S., Aydın C., Ahmedov A.İ.. Appligation of Information-Communication Technologies in Science and education. II International Conference. "*Higher Twist Effects In Photon- Proton Collisions", Bakı, 01-03 Noyabr, 2007, ss 384-391*

Mənbələr 9 punto yazı tipi böyüklüyündə olmalıdır.

10. **Səhifə ölçüləri:** üstdən 2.8 sm, altdan 2.8 sm, soldan 2.5 sm və sağdan 2.5 sm olmalıdır. Mətn 11 punto yazı tipi böyüklüyündə, **Palatino Linotype** yazı tipi ilə və tək simvol aralığında yazılmalıdır. Paraqraflar arasında 6 punto yazı tipi aralığında məsafə olmalıdır.
11. Orijinal tədqiqat əsərlərinin tam mətni bir qayda olaraq 15 səhifədən artıq olmamalıdır.
12. Məqalənin nəşrə təqdimi aşağıdakı qaydada aparılır:

- Hər məqallə ən azı iki ekspertə göndərilir.
- Ekspertlərin tövsiyələrini nəzərə almaq üçün məqalə müəllifə göndərilir.
- Məqalə, ekspertlərin tənqidi qeydləri müəllif tərəfindən nəzərə alındıqdan sonra Jurnalın Redaksiya Heyəti tərəfindən çapa təqdim oluna bilər.

YAZIM KURALLARI

1. "Journal of Baku Engineering University-Physics" önceler yayımlanmamış orijinal çalışmaları ve yazarın kendi araştırma alanın-da yazılmış derleme makaleleri kabul etmektedir.
2. Makaleler İngilizce kabul edilir.
3. Makaleler Microsoft Word yazı programında, (**journal@beu.edu.az**) adresine gönderilmelidir. Gönderilen makalelerde şunlar dikkate alınmalıdır:

- Makalenin başlığı, yazarın adı, soyadı,
- İş yeri,
- E-posta adresi,
- Özet ve anahtar kelimeler.

4. **Özet** 100-150 kelime arasında olup 9 font büyüklüğünde, makalenin yazıldığı dilde ve yukarıda belirtilen iki dilde olmalıdır. Makalenin her üç dilde yazılmış özeti birbirinin aynı olmalıdır. Anahtar kelimeler uygun özetin sonunda onun yazıldığı dilde verilmekle en az üç sözcükten oluşmalıdır.
5. Makalede UOT ve PACS tipli kodlar gösterilmelidir.
6. Makale şunlardan oluşmalıdır:

- Giriş,
- Araştırma yöntemi
- Araştırma
- Tartışma ve sonuçlar,
- İstinat Edebiyatı Rusça olduğu halde orjinal dili parantez içerisinde göstermekle yalnız Latin alfabesi ile verilmelidir.

7. **Şekil, Resim, Grafik** ve **Tablolar** baskıda düzgün çıkacak nitelikte ve metin içerisinde olmalıdır. Şekil, Resim ve grafiklerin yazıları onların alt kısımda yer almalıdır. Tablolarda ise başlık, tablonun üst kısmında bulunmalıdır.
8. **Kullanılan kaynaklar**, metin dâhilinde köşeli parantez içerisinde numaralandırılmalı, aynı sırayla metin sonunda gösterilmelidir. Aynı kaynaklara tekrar başvurulduğunda sıra muhafaza edilmelidir. Örneğin: [7,seh.15].

Referans verilen her bir kaynağın künyesi tam ve kesin olmalıdır. Referans gösterilen kaynağın türü de eserin türüne (monografi, derslik, ilmî makale vs.) uygun olarak verilmelidir. İlmi makalelere, sempozyum, ve konferanslara müracaat ederken makalenin, bildirinin veya bildiri özetlerinin adı da gösterilmelidir.

Örnekler:

a) ***Makale:*** Demukhamedova S.D., Aliyeva İ.N., Godjayev N.M.. *Spatial and Electronic Structure of Monomerik and Dimeric Conapeetes of Carnosine Üith Zinc,* Journal of Structural Chemistry, Vol.51, No.5, p.824-832, 2010

b) ***Kitap:*** Christie ohn Geankoplis. *Transport Processes and Separation Process Principles.* Fourth Edition, Prentice Hall, p.386-398, 2002

c) ***Kongre:*** Sadychov F.S., Aydın C., Ahmedov A.İ. Appligation of Information-Communication Technologies in Science and education. II International Conference. "*Higher Twist Effects In Photon- Proton Collisions", Bakı, 01-03 Noyabr, 2007, ss 384-391*

Kaynakların büyüklüğü 9 punto olmalıdır.

9. **Sayfa ölçüleri**; üst: 2.8 cm, alt: 2.8 cm, sol: 2.5 cm, sağ: 2.5 cm şeklinde olmalıdır. Metin 11 punto büyüklükte **Palatino Linotype** fontu ile ve tek aralıkta yazılmalıdır. Paragraflar arasında 6 puntoluk yazı mesafesinde olmalıdır.
10. Orijinal araştırma eserlerinin tam metni 15 sayfadan fazla olmamalıdır.
11. Makaleler dergi editör kurulunun kararı ile yayımlanır. Editörler makaleyi düzeltme için yazara geri gönderilebilir.
12. Makalenin yayına sunuşu aşağıdaki şekilde yapılır:

- Her makale en az iki uzmana gönderilir.
- Uzmanların tavsiyelerini dikkate almak için makale yazara gönderilir.
- Makale, uzmanların eleştirel notları yazar tarafından dikkate alındıktan sonra Derginin Yayın Kurulu tarafından yayına sunulabilir.

13. Azerbaycan dışından gönderilen ve yayımlanacak olan makaleler için,(derginin kendilerine gonderilmesi zamani posta karşılığı) 30 ABD Doları veya karşılığı TL, T.C. Ziraat Bankası/Üsküdar-İstanbul 0403 0050 5917 No'lu hesaba yatırılmalı ve makbuzu üniversitemize fakslanmalıdır.

ПРАВИЛА ДЛЯ АВТОРОВ

1. «Journal of Baku Engineering University» - Физика публикует оригинальные, научные статьи из области исследования автора и ранее не опубликованные.
2. Статьи принимаются на английском языке.
3. Рукописи должны быть набраны согласно программы **Microsoft Word** и отправлены на электронный адрес **(journal@beu.edu.az)**. Отправляемые статьи должны учитывать следующие правила:

- Название статьи, имя и фамилия авторов
- Место работы
- Электронный адрес
- Аннотация и ключевые слова

4. **Заглавие статьи** пишется для каждой аннотации заглавными буквами, жирными буквами и располагается по центру. Заглавие и аннотации должны быть представлены на трех языках.
5. **Аннотация**, написанная на языке представленной статьи, должна содержать 100-150 слов, набранных шрифтом 9 punto. Кроме того, представляются аннотации на двух других выше указанных языках, перевод которых соответствует содержанию оригинала. Ключевые слова должны быть представлены после каждой аннотации на его языке и содержать не менее 3-х слов.
6. В статье должны быть указаны коды UOT и PACS.
7. Представленные статьи должны содержать:

- Введение
- Метод исследования
- Обсуждение результатов исследования и выводов.
- Если ссылаются на работу на русском языке, тогда оригинальный язык указывается в скобках, а ссылка дается только на латинском алфавите.

8. **Рисунки, картинки, графики и таблицы** должны быть четко выполнены и размещены внутри статьи. Подписи к рисункам размещаются под рисунком, картинкой или графиком. Название таблицы пишется над таблицей.
9. **Ссылки** на источники даются в тексте цифрой в квадратных скобках и располагаются в конце статьи в порядке цитирования в тексте. Если на один и тот же источник ссылаются два и более раз, необходимо указать соответствующую страницу, сохраняя порядковый номер цитирования. Например: [7, стр.15]. Библиографическое описание ссылаемой литературы должно быть проведено с учетом типа источника (монография, учебник, научная статья и др.). При ссылке на научную статью, материалы симпозиума, конференции или других значимых научных мероприятий должны быть указаны название статьи, доклада или тезиса.

Например:

a) ***Статья:*** Demukhamedova S.D., Aliyeva I.N., Godjayev N.M. *Spatial and electronic structure of monomeric and dimeric complexes of carnosine with zinc,* Journal of Structural Chemistry, Vol.51, No.5, p.824-832, 2010

b) ***Книга:*** Christie on Geankoplis. *Transport Processes and Separation Process Principles.* Fourth Edition, Prentice Hall, 2002

c) ***Конференция:*** Sadychov F.S, Fydin C,Ahmedov A.I. Appligation of Information-Communication Nechnologies in Science and education. II International Conference. *"Higher Twist Effects In Photon-Proton Collision",* Bakı,01-03 Noyabr, 2007, ss.384-391

Список цитированной литературы набирается шрифтом 9 punto.

10. **Размеры страницы:** сверху 2.8 см, снизу 2.8 см, слева 2.5 и справа 2.5. Текст печатается шрифтом **Palatino Linotype**, размер шрифта 11 punto, интервал-одинарный. Параграфы должны быть разделены расстоянием, соответствующим интервалу 6 punto.
11. Полный объем оригинальной статьи, как правило, не должен превышать 15 страниц.
12. Представление статьи к печати производится в ниже указанном порядке:

- Каждая статья посылается не менее двум экспертам.
- Статья посылается автору для учета замечаний экспертов.
- Статья, после того, как автор учел замечания экспертов, редакционной коллегией журнала может быть рекомендована к печати.